University of Naples Federico II

Department of Chemical, Materials and Production Engineering

Ph.D. thesis in
INDUSTRIAL PRODUCT AND PROCESS ENGINEERING
XXXI cycle

IMPACT OF BIOPOLYMER MATRICES ON RELAXOMETRIC PROPERTIES OF MRI CONTRAST AGENTS AND THEIR APPLICATION TO NANOTECHNOLOGY

Supervisors:

Paolo Antonio Netti
Professor of Biomaterials and Tissue Engineering

Enza Torino
Researcher in Bioengineering

Candidate:

Alfonso Maria Ponsiglione
MSc in Biomedical Engineering

Ph.D. program coordinator:

Giuseppe Mensitieri
Professor of Materials Science and Engineering

IMPACT OF BIOPOLYMER MATRICES ON RELAXOMETRIC PROPERTIES OF MRI CONTRAST AGENTS AND THEIR APPLICATION TO NANOTECHNOLOGY

TABLE OF CONTENTS

FIGURES LIST

TABLES LIST

ABSTRACT

Magnetic Resonance Imaging (MRI) represents the first-line diagnostic imaging modality for numerous indications. It is a clinically well-established, non-invasive technique providing three dimensional whole body anatomical and functional imaging. It takes advantage of the magnetic properties of water protons present in the body and their tissue-dependent behaviour. High magnetic fields (1.5 T and above) are clinically favoured because of their higher signal-to-noise ratio, capability for MR spectroscopy, and other forms of functional MRI, high speed imaging, and high resolution imaging.

Signal intensity in MRI is related to the relaxation rate of in vivo water protons and can be enhanced by the administration of a contrast agent (CA) prior to scanning. These CAs utilize paramagnetic metal ions and enhance the contrast in an MR image by positively influencing the relaxation rates of water protons in the immediate surroundings of the tissue in which they localize. Among different CAs, Gadolinium contrast medium is used in up to 30% of MRI scans and the most clinically-used MRI. However, Gadolinium (Gd), like most of the clinically-used CAs, is characterized by a relaxivity well below its theoretical limit, lacks in tissue specificity and, in addition, it causes heavy allergic effects and serious nephrotoxicity.

In this framework, Port et al. have reported that the rigidification of MRI CAs, obtained through covalent or non-covalent binding to macromolecules, could be favourable to an increase in relaxivity of the metal-chelate. Later, Decuzzi et al. have proved that it is possible to modify through the geometrical confinement the magnetic properties of MRI CAs by controlling their characteristic correlation times without the chemical modification of the chelate structure. Furthermore, Courant et al. have highlighted the capability of combined hydrogels to boost the relaxivity of Gd-based CAs.

Despite several experimental studies addressed in this field, a comprehensive knowledge of the mechanisms involved in the relaxation enhancement due to the entrapment of CAs in polymer-based architectures is still missing. In particular, the role played by the water at the interface between polymer chains and MRI CAs has not been fully investigated and could lead to the availability of tailored models that accurately describe these novel complex systems.

In this work, we aim to demonstrate that a more in-depth knowledge about the interference between macromolecules and MRI CAs and an understanding of their physicochemical properties can significantly to impact in the design strategies of the nanostructures and, consequently, to overcome the limitations of clinically used MRI CAs, particularly linked to the low relaxivity. In this perspective, it is of primary importance to study the main phenomena involved in the formation of polymer matrices and how their properties can influence the relaxivity of MRI CAs.

For this reason, we proposed a general strategy based on formation of nanostructures for boosting the efficacy of commercial Gd-based CAs by using FDA approved biopolymers, providing also tissue specificity and reduced nephrotoxicity. Indeed, we want to take advantage not only by the use of nanotechnologies for enhanced MRI but only by their capability to reach a specific target and to accumulate only in the site of interest.

The implemented strategy has consisted in the control of the relaxometric properties by tuning the water dynamics, the physicochemical interactions and, therefore, the polymer conformation.

Effectively, we primary investigated, in bulk, the impact of hydrogel solutions on the relaxometric properties of commercial CAs, highlighting the key role of hydrogel structural parameters (mesh size and crosslink density) in the relaxation enhancement. In this part, chemical and thermodynamic interactions involved in the complexation between biopolymers and CAs have been investigated through Isothermal Titration Calorimetry. Furthermore, characterizations of water dynamics and mobility and measurement of the relaxometric properties in hydrogel solutions containing CAs have been carried out by NMR and Time-Domain relaxometer.

The main outputs were summarized in a concept called *Hydrodenticity* and defined as the equilibrium between the water osmotic pressure, the elastodynamic forces of the polymer chains and the hydration degree of the CA which is able to increase the relaxivity of the CA itself. Indeed, hydrogel nanostructures made of hydrophilic polymer chains held together by chemical or physical crosslinking, have the ability to swell in water, forming elastic gels that retain a large quantity of fluid in their mesh-like structures. The presence of hydrophilic polymer interfaces and the control of water behaviour in hydrogels play a fundamental role in the relaxation enhancement of the Gadolinium-based CAs by influencing the characteristic correlation times defined by the theory of Solomon and Bloembergen.

Then, starting from the acquired knowledge, we moved to observe the role of *Hydrodenticity* in the design of biopolymer nanostructures for enhanced MRI.

For the nanostructures' synthesis, we used two different processing techniques: (1) High Pressure Homogenization; (2) Microfluidic Flow Focusing. These techniques were selected because of their ability to control process parameters enabling the tuning of the interaction between the biopolymers and the CA. Indeed, by easily adjusting concentrations, pressure of the Homogenizer and/or flow rates of the Microfluidic platform, we can modulate the crosslinking degree of the nanostructures and tune their hydrophilicity, size, shape and surface charge, impacting on the relaxometric properties.

These approaches allow us to load MRI CAs into functional nanostructures and obtain nanocarries with tunable relaxometric properties.

The powerful aspect and the novelty of our approach lies in the definition of Hydrodenticity and in its application to several architectures, biopolymers, lipids and mixture of them., preserving the main properties of nanoparticles for drug delivery. As future perspective, the nanostructures can also be engineered to carry more than one agent, accumulate in specific tissues or to act as probes for simultaneous diagnosis and therapy (theranostic or multimodal imaging agents), thereby facilitating targeted treatments and precision medicine.

STRUCTURE OF THE THESIS AND IMPLEMENTATION STRATEGY

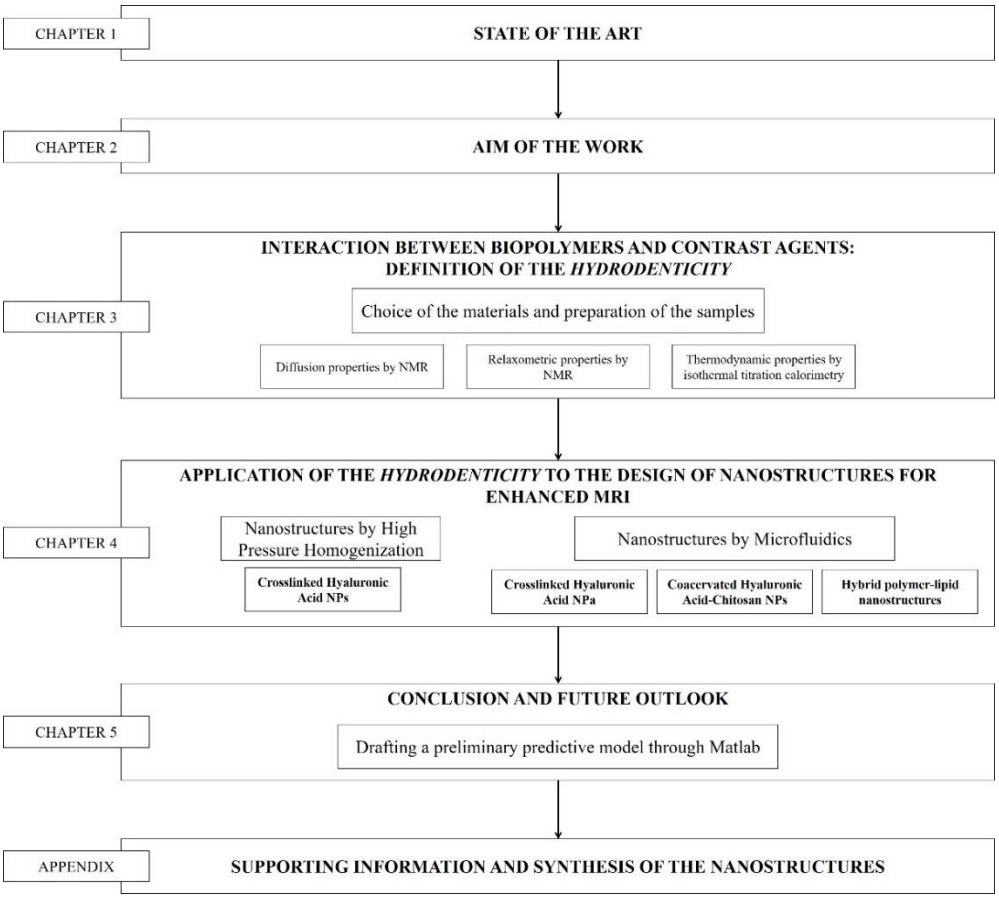

The PhD Thesis is structured as follows:

1. **CHAPTER 1: State of the Art.** We examined the literature about contrast agents for MRI with specific focus on their mechanisms of action, on their efficacy, i.e. the relaxivity, and on the strategies currently used by researchers and industries to improve the performances of the already used contrast agents. In this perspective, the crucial role of hydrogel matrices in enhancing the relaxometric properties of Gd-based CAs has been widely recognised. However, despite the considerable efforts made towards the improvement of GdCAs through macromolecules and hydrogel nanostructures, a fundamental understanding of the energetic and thermodynamic contribution capable to boost the efficacy of the CAs by using hydrogels, which could potentially become advanced nanostructure for MRI, is still missing. Besides, only few strategies to produce biocompatible nanostructures with enhanced relaxivity using biopolymers are available.

2. **CHAPTER 2: Aim of the Work.** In this section, the aim of the Thesis is presented and contextualized in light of the already presented State of the Art.

3. **CHAPTER 3: Interaction between biopolymers and contrast agents: definition of the Hydrodenticity.** In this section, we investigate changes in the relaxivity of Gd-DTPA in different biopolymer solutions (hyaluronic acid was chosen as a model biopolymer) by varying both the polymer concentration used and the structure of the polymer matrix (crosslinked and non-crosslinked). We show isothermal calorimetry and NMR measurements performed to characterize the thermodynamic properties and diffusion behaviour of the polymer/Gd-DTPA solutions. We identify the best conditions that boost CAs' relaxivity and understand how to tune polymer structures to reach these favourable conditions. We point out that the balanced water-mediated interplay between hydrophilic biopolymers

and CAs is significant in determining both the arrangement of the polymer chains in solution and the CA's relaxivity. On the basis of this theoretical considerations, the concept of *Hydrodenticity*, defined as the equilibrium between elastodynamic forces of the hydrogel network and the water osmotic pressure and hydration degree of the CA responsible for the relaxivity enhancement, is introduced and discussed. The fundamental thermodynamic concepts here highlighted can be transferred to the nano-scale and applied to develop high effective MRI nanoprobes.

4. **CHAPTER 4: Application of the Hydrodenticity to the design of nanostructures for enhanced MRI.**

    a. **Nanostructures by High Pressure Homogenization.** Using the acquired knowledge on the interactions between biopolymers and MRI CAs, we bring it to the nano-scale. We use the high pressure homogenization to synthetize crosslinked hyaluronic acid nanoparticles entrapping the Gd-DTPA. The obtained formulation showed an increase in the relaxivity far higher than what was expected from the experiments in bulk systems. The structure-function relationships nanoparticles is studied through the Inductively coupled plasma mass spectrometry (ICP-MS) to test the loading capability and through the Fast Field Cycling NMR relaxometry to measure the nuclear magnetic relaxation dispersion (NMRD) profiles and test the relaxivity of the nanostructures in the high magnetic field region. Scanning and Transmission Electron Microscopy (SEM and TEM) along with Dynamic Light Scattering (DLS) are also used to carry out the morphological and structural characterization.

    b. **Nanostructures by Microfluidics.** To better tune the nanostructure's characteristics, a microfluidic platform is used to produce the nanoparticles. Three different types of nanostructures are designed and synthesized: (1) crosslinked HA nanohydrogels; (2) HA-CS coacervated nanoparticles; (3) hybrid polymer-lipid

nanostructures. We show that by varying the composition of the nanostructures and its structural properties it is possible to tune the relaxivity of the overall system. The microfluidic platform allows a fine and continuous control over the nanostructures' characteristics by changing the process parameters. NMR and ICP-MS are used to test the relaxometric properties of the nanoparticles. Scanning and Transmission Electron Microscopy (SEM and TEM) along with Dynamic Light Scattering (DLS) are also used to carry out the morphological and structural characterization.

5. **CHAPTER 5: Conclusion and future outlook.** The achieved results demonstrate that the relaxivity of Gd-based CAs varies in presence of polymer matrices. The relaxivity can be tuned by controlling the concentration, composition and structural properties polymer networks. This capability is enhanced at the nano-scale. Therefore, Gd-loaded nanoarchitectures can perform differently in terms of relaxivity by tailoring their structural parameters. A draft of a preliminary predictive model that describes the polymer-CA systems is implemented and it is today under development. Such a model could provide a versatile and helpful tool to study, control and properly design new structures obtained through the combination of polymers and metal-chelates, paving the way to the implementation of a library containing different biopolymer-CAs combinations with improved relaxometric properties and potentially leading to a new generation of nanostructured CAs.

6. **APPENDIX: Supporting Information and Synthesis of the nanostructures.** In this section, the materials and methods adopted to synthesize the nanostructures presented in Chapter 4 are presented. In addition, all the supporting figures, tables and data are also available in this section.

Chapter 1.

STATE OF THE ART

1.1. NANOMEDICINE

In the field of material science, the prefix *"nano"* is used to describe materials that have structural components smaller than 1 μm in at least one dimension. At the nanometer scale, materials are comparable to atoms and molecules. The creation and utilization of these materials in the biotechnology take the name of *nanobiotechnology* and its application to the medicine field is called *nanomedicine* [1]. Nanomaterials for medicine have a number of applications in several disciplines, such as oncology, cardiology and neurology, because pathological and physiological processes occur at level of cells [1,2].

In particular, nanoparticles (NPs) have proved to be new promising nano-scaled structures for improved detection, treatment and prevention of several diseases. Indeed, NPs have novel physicochemical properties with a considerable impact on delivery of drugs and agent, from the molecular to the systemic level. NPs' properties influence their behaviour *in vivo* and consequently their therapeutic and/or diagnostic efficacy. For this reason, it is crucial in the design of NPs to know what the main characteristics of a NP are:

- Size
- Surface properties (charge and functionalization)
- Shape

- Composition
- Purity
- Stability
- Biological environment (for example pH) where NPs need to be applied.

Surface charge and shape of nanoparticles are crucial in extravasation, in interstitial transport and in targeting, while size affects circulation time in bloodstream, in renal clearance and can be optimized for each tumour. All these properties play an active role from determining circulation of NPs in the bloodstream to modulating cellular responses [3].

NPs' design and production present some issues that still need to be overcome. The first problem concerns the size distribution of the NPs; indeed, high polydispersity can compromise the pharmacokinetics and the efficacy of the treatment. Furthermore, NPs need to be biocompatible and low toxic *in vivo*. In addition, sterility conditions must be preserved through all the production process [4].

To understand better NPs' advantages, it is important to know those differences between tumour and normal tissues that can influence the delivery of diagnostic or therapeutic agents. In fact, during their travel toward the target, NPs flow in the bloodstream, overcome vessel walls and penetrate through interstitial space to reach target cells.

In tumour tissues, these aspects become abnormal: tortuous and leaky vessels, heterogeneous blood flow, lack of functional lymphatic vessels, vascular hyperpermeability owing to vessel walls irregular structure, a uniformly elevated interstitial fluid pressure (IFP) that reduces pressure gradients across vessel wall and so convective transport, a dense ECM with high collagen-fibres concentration that hinders diffusion (Figure 2.1) All these issues can be resolved using engineered nanoparticles [5,6].

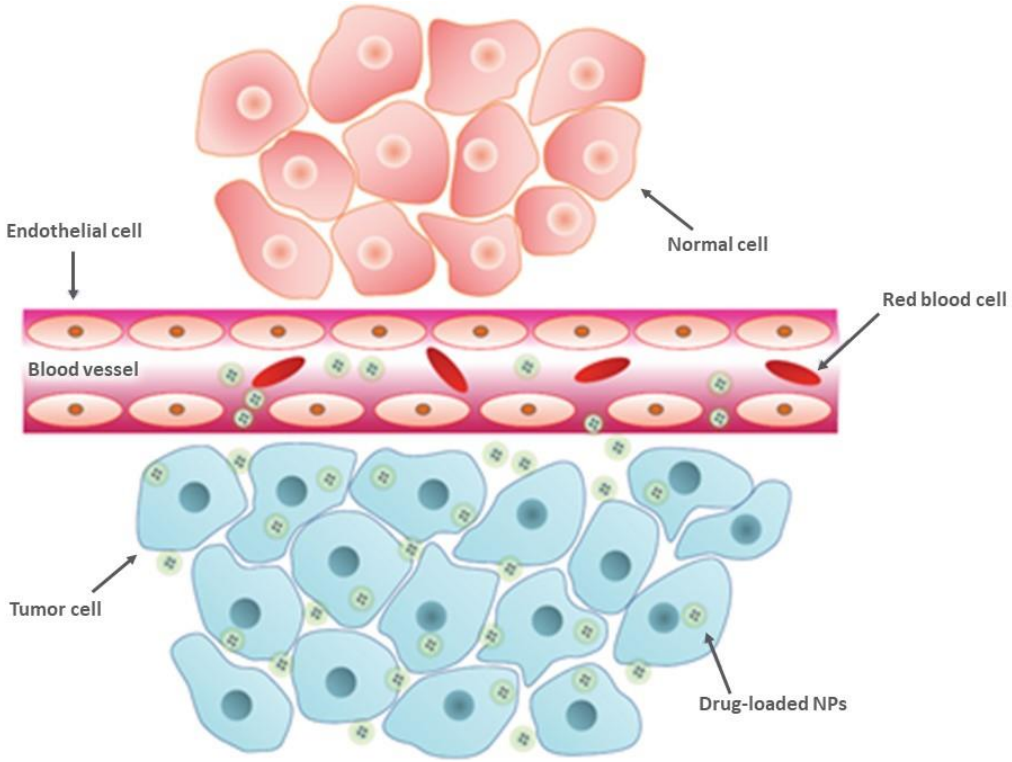

Figure 1.1 Schematic illustration of EPR effect. Image adapted from [4]: Yu, X.; Trase, I.; Ren, M.; Duval, K.; Guo, X.; Chen, Z., *Design of Nanoparticle-Based Carriers for Targeted Drug Delivery*. 2016; Vol. 2016, p 1-15.

To obtain a desirable effect, it is necessary the overpassing a series of obstacles which can reduce bioavailability and therapeutic or diagnostic efficacy. Macrophages and monocytes of the reticuloendothelial system (RES) are highly efficient at removing NPs through opsonization. Digestive enzymes and low pH contribute to the rapid degradation of NPs, while renal system rapidly filter NPs with diameter under 10 nm. Therefore, it is important to understand all factor affecting biodistribution to develop successful nanostructured drug delivery systems.

1.1.1. NANOPARTICLES FOR THERAPY

Therapeutic NPs are used for different goals: among them, targeting and adhesion into atherosclerotic lesions within the cardiovascular system, heart therapy thanks to

target antigen characteristic of infarcted myocardium, treatments of lung diseases through the circulation and/or respiratory tract and many others but the main and most widespread applications are related to cancer therapy [7]. In fact, cancer cells can through a genetic mutation that lead them to grow uncontrollably. The aim of therapeutic agents is to bring a sufficient drug payload to kill cancer cells but, at the same time, preserve normal tissues [5,6]. Current treatments like radiotherapy or chemotherapy are not able to damage specifically only target cancer cells and lead to undesirable side effects.

Many chemotherapeutic drugs, such as paclitaxel or doxorubicin, can be loaded into NPs and it is possible to modify NPs' properties to use them through three different targeting modalities:

- *Passive targeting*: use natural properties and processes to drive therapeutic agents to the target site. The most used is EPR effect that is influenced mainly by the size. Increased permeability and insufficient lymphatic drainage lead to therapeutic accumulation. Passive targeting requires a NPs circulation time of at least 6 hours NPs between 100-200 nm accumulate in tumour target through leaky tumour vessels. The surface charge of the NPs is another fundamental property. Negative charged NPs circulate longer in the bloodstream but they are less taken up by cancer cells compared to positively charged NPs [4,8–10].
- *Active Targeting*: receptor-specific ligands on NPs surface can promote drug delivery toward diseased cells or tissue. High accumulation at the diseased site and uptake selectivity can be achieved using ligands that bind with overexpressed molecules on cancer cell. Antibodies are most employed because of their high specificity and availability; small molecules like folic acid can be used for their small size, stability and reproducibility [4,8–10].
- *Physical Targeting*: external stimuli like magnetic fields, temperature or radiation can be used to drive NPs until target cancer cells. It is even possible the use NPs as means to convert external energy to heat and so kill cancer cells [4].

To understand and predict how the dynamics and behaviour of NPs vary according to their physicochemical properties during their route through the bloodstream,

theoretical and mathematical models can be used (continuum, molecular and stochastic modelling) [4,8–10].

1.1.2. NANOPARTICLES FOR DIAGNOSTICS

Diagnostic agents allow obtaining images about a specific investigated body area to achieve information on tissues' condition.

The goal of using NPs to deliver diagnostic agents is the increase of specificity, i.e. the ability to concentrate the agent only in the target site, preserving surrounding tissues and allowing better diagnosis.

Some of the main diagnostic modalities are examined in the following paragraphs. A special attention will be given to the Magnetic Resonance Imaging (MRI), which is the main focus of this thesis.

1.1.2.1. Optical imaging

Optical imaging uses visible light as vehicle for medical investigation. It mainly uses photons and their interaction with matter to obtain detailed images of organs and tissues.

Optical imaging significantly reduces patient exposure to radiation by using non-ionizing radiation, which includes visible, ultraviolet, and infrared light. It is particularly effective for soft tissue and permits to investigate different properties using different light colors.

Near-infrared imaging (NIR) is highly used because NIR light penetrates deeper into and out tissues than other wavelengths of visible spectrum. NIR used contrast agents as organic agents suffer from rapid photobleaching, instability, biological and chemical degradation and tend to aggregate.

These aspects lead to reduce emission signals and often confined agents in untargeted tissues. NP-based agents have strong stable signal in the NIR region, increased lifetime, lower degradation and cytotoxic effect.

Examples of NPs for NIR imaging are semiconductor quantum dots, gold nanoshells and dye encapsulating nanoparticles [11].

1.1.2.2. PET

Positron emission tomography (PET) is a nuclear medicine technique that provides functional information through positron emitting radionuclides employment. Positron is a particle with the same mass and charge of electron but different sign. Collision between positron and electron causes a reaction called "annihilation" that leads to formation of two 511 kV gamma radiations with an angle of 180° between them. In a narrow temporal window around 10 nanoseconds, PET scintillation crystals measure line that link two detectors including in coincidence event.

This line is called Line of Response (LOR) and identify annihilation. PET permits tracer distribution visualization in body but limitation is given by absence of anatomical information. Employed radionuclides are natural radioactive isotopes as carbon-11, oxygen-15 or fluorine-18 like elements that constitute biological matter. Therefore, they can be bound to molecules to form radioactive tracer and to study directly biological and physiological processes.

Advantages of using NPs for PET lie in the possibility to use targeting ligands, alter pharmacokinetics and increase PET radionuclides quantity and type [12].

1.2. MAGNETIC RESONANCE IMAGING

The Magnetic Resonance Imaging (MRI) represents the first-line diagnostic imaging modality for numerous indications. During the past 30 years, it has emerged as an established technique for preclinical imaging and clinical diagnosis [13–15].

It is a clinically well-established, non-invasive technique providing three-dimensional whole body anatomical and functional imaging [16,17] by using the magnetic properties of water protons present in the body and their tissue-dependent behavior. High magnetic fields (1.5 T and above) are clinically favoured because of their higher signal-to-noise ratio, capability for MR spectroscopy [18], and other forms of functional MRI, high-speed imaging, and high-resolution imaging.

Although MRI enables visualization of tissues at high spatial resolution without using ionizing radiation or invasive procedures [19], it is largely limited because it lacks the proper sensitivity, which is significantly lower than other imaging modalities, such as PET/SPECT [20–23]. Performances of MRI examinations can be improved by

using Contrast Agents (CAs), which allow differentiating tissue types that would otherwise be indistinct [24–26].

1.3. CONTRAST AGENTS FOR MRI

1.3.1. ADVANTAGES IN USING CONTRAST AGENTS

MRI Performances of the CAs are well-described by the " relaxivity", defined as the rate of change in longitudinal or transverse relaxation times of the water protons per mM concentration of metal ions and determining the enhancement of the image contrast [27].

The presence of the CA causes a significant increase in the relaxation rate of the water proton nearby paramagnetic ions, thereby adding details to the anatomical resolution. Thanks to its very high magnetic moment, Gadolinium (Gd) is the most frequently used metal ion for MRI.

However, owing to the toxicity of free Gd ions [21], which can induce nephrogenic system fibrosis (NSF), Gd-chelates, such as Gd-DTPA (Magnevist, Schering AG) [28], are commonly used in contrast-enhanced examinations [20,26,29].

1.3.2. PHYSICS OF CONTRAST AGENTS

Starting from the Solomon–Bloembergen–Morgan (SBM) theory [30], the physics of CAs is described by a set of physicochemical parameters characterizing the fluctuating magnetic dipole created by the paramagnetic ion. In detail, according to the SBM model, the metal complex can be viewed as having separate coordination spheres [31]: the Inner Sphere (IS), which consists of water molecules directly coordinated to the metal ion, and the Outer Sphere (OS), which is a less organized structure consisting of bulk water molecules diffusing in the near environment of the metal complex.

In some cases, a Second Sphere (SS) contribution is taken into account, which is related to water molecules hydrogen bonded to the metal complex [32]. Each of the coordination mentioned above spheres has its characteristic parameters. IS parameters include the number of labile water molecules coordinated to the metal

ion (q), the residence time of the coordinated water molecule (τ_M), which in turn determines the rate of the coordinated water molecule exchanging with the bulk, and the rotational correlation time (τ_R), which is how quickly the contrast agent is tumbling in solution. Conversely, OS parameters include the translational diffusional time (τ_D), which represent the diffusion of water molecules in the bulk near to the Gd complex.

1.3.3. CONTRAST AGENTS LIMITATIONS

Currently, more than 35% of all clinical MRI scans utilize the injection of clinically approved Gd-based CAs (GdCAs) intravenously [19,20].

Despite this widespread use, most of the clinically-used CAs are characterized by poor effectiveness in the high magnetic fields region (3 T and above), mainly limited by their concentration (mM) and relaxivity (r_1, $mM^{-1}s^{-1}$), which is clinically favored because of its higher signal-to-noise ratio and high-resolution imaging. MRI CAs also lack of tissue specificity and can cause heavy allergic effects, serious nephrotoxicity [33–35].

Some concerns arise also from long scan time and rapid renal clearance, which significantly reduce the time window for clinical imaging acquisitions [34,36,37]. Furthermore, McDonald et al. [38] have recently reported results about intracranial Gd deposition after repeated intravenous administration of CAs even if these signal intensity changes are not specific and can be seen with several other pathologic conditions.

In these perspectives, the possibility to have a CAs that could work at low concentration but without giving over its signal intensity and, therefore, positive contrast effect is of great interest.

Furthermore, the poor relaxivity of commercially available CAs, much below its theoretically maximal value required to obtain an accurate diagnosis at safe administration dosage [39] has led to to a growing interest in studying different types of Gd derivatives and to the development of novel macromolecules conjugating CAs [13,40–47].

1.4. POLYMERS AND CONTRAST AGENTS

1.4.1. ADVANTAGES IN COMBINING POLYMERS AND CONTRAST AGENTS

As previously reported in the SBM theory, characteristic parameters of the metal chelate can be physically or chemically tuned and are of primary importance in the design of new CAs [48]. In particular, the Gd-chelator determines the number of coordinated water molecules (q) and the water exchange rate (k_{ex}), which is the inverse of the residence time τ_M. Moreover, decreased τ_D and τ_R, which can be obtained, for instance, through the binding of the metal chelate with large macromolecules, generally yield increased relaxation rates at low magnetic fields (<1.5 T) [35].

It is already known that molecular motion, size, rigidity and possible binding between Gd-chelates and other macromolecules may induce changes in relaxivity [34]. Furthermore, polymer architecture and properties can strongly affect the MRI enhancement [49–51]. Among them, crosslinked hydrophilic biopolymers networks (hydrogels) have been investigated because of their biocompatibility, biodegradability, low immunogenicity, low toxicity, prolonged circulation time [52] and, not least, high affinity to water and swelling properties [50,53–56].

Several studies, indeed, have demonstrated that the polymer architecture plays a crucial role on different parameters, such as the water exchange time and the rotational correlation time, thereby influencing the CA's relaxivity [49]. In particular, polymer properties, such as the rigidity, strongly affects the MRI enhancement [50]. Internal rigidification, obtained for example by ionic interactions [57,58], can retard rotational motion of the complex and enhance the relaxivity more than flexible polymers [52,59].

Crosslinked polymers, like nanogels and hydrogels, have significant applicability to the design of switchable CAs, because an increasing of the crosslinking degree can induce relaxivity enhancement by restricting molecular tumbling while maintaining the switching property [60] and allowing facile access of water throughout the structure, which is a key feature in the development of MRI contrast agents [61,62]. In details, hydrogels [53,56,63,64] show these three-dimensional networks, made of hydrophilic polymer chains held together by chemical or physical crosslinking, they are glassy in the dry state but have the ability to swell in water, forming elastic gels

that retain a large quantity of fluid in their mesh-like structures [65]. The presence of hydrophilic polymer interfaces and the control of water behaviour in hydrogels play a fundamental role in the relaxation enhancement of the Gadolinium-based contrast agents by influencing the characteristic correlation times defined by the theory of Solomon and Bloembergen [30].

1.4.2. LITERATURE OVERVIEW

The extensive research on nano-engineered systems and polymer-based nanocomposites [54,55,66–74] has led to significant advances also in the field of MRI [50,52,72,75–77]. In particular, some recent studies have shown that nanoconstructs can improve CAs' relaxivity and many efforts have been devoted to the development of polymer-based carriers for MRI CAs with particular reference to Gadolinium (Gd) chelates, which are the most commonly clinically used agents [49,75,78–82].

As reported by Port et al. [51], rigidification of Gd-based CAs would be favourable to an increase in the relaxivity of the metal chelate since the presence of the ligand around the Gd ion induces a shortening of the residence lifetime of the inner-sphere water molecules (τ_M) [51,83,84]. In addition, they hypothesized that the presence of a rigid coordination cage of a chelate should limit its intramolecular conformational motions, which distorts the ligand field at the metal centre due to solvent molecules collisions, thus influencing the electronic relaxation times (τ_{S1} and τ_{S2}) [51]. To assess the rigidification strategy, Port synthetized a constrained derivative of Gd-PCTA12, Gd-cyclo-PCTA12, in which one ethylene bridge connecting two nitrogen atoms of the triamine block is replaced by a cyclohexylene bridge, and the impact of rigidification was studied by comparing the physicochemical and relaxometric properties of both gadolinium MRI contrast agents, Gd-PCTA12 and Gd-cyclo-PCTA12.

Other experimental approaches studied by Decuzzi et al. [27,85,86] proved that geometrical confinement could limit the mobility of water molecules and thereby enhance the relaxation response of Gd-based CAs without its chemical modification. In particular, they observed that nanometric pores of silica microparticles increase the rotational correlation time (τ_R) of Gd-DTPA (inner-sphere effect), which cannot tumble freely being adsorbed on the walls of the 100 nm pores. At the same time, it

also increases the diffusion correlation time (τ_D) for water molecules (outer-sphere effect), which are geometrically confined and forced to interact longer with Gd-DTPA adsorbed to the inner pore surface [27]. Through the confinement strategy, a poor increment of the relaxivity can be obtained without modifying the chemical structure of the CA.

As advancement of the geometrical confinement, in some more recent works, Courant et al. [80] and Callewaert et al. [87], showed that biocompatible hydrophilic hydrogels can be exploited to produce high water content nanoparticles (NPs) encapsulating the metal chelate. Inside the hydrogel, which creates a favourable aqueous environment for Gd-based CAs [52,75,88–90], the rotational motion of the encapsulated CA (Gd-DOTP, Gd-DOTA and Gd-DTPA) is restricted and its magnetic properties are amplified.

Courant et al. [80] developed a polymeric system based on the integration of Gd-chelates (Gd-DOTA) into nanoparticles to improve the relaxivity for MRI applications. Because of its hydrophilic nature, the encapsulation of (Gd-DOTA) was made in a hydrophilic and biocompatible polymer matrix obtained by interaction of chitosan (CH) [89] and hyaluronic acid (HA) [52,75,88] that forms a favourable aqueous environment for Gd-based CAs. Furthermore, inside the hydrogel, CA rotational motion is restricted and the magnetic properties of the encapsulated CA are amplified, without modification of chemical structure of chelate.

Callewaert et al. [87] showed that Gd-loaded CH nanohydrogel relaxivities can be tuned according to the Gd-based CA and the hydrogel matrix composition. They observed that, since the crosslinking degree could limit water access and mobility inside the nanogels, this can be counterbalanced by the association of a second hydrophilic polymer (HA) to constitute high-water content nanoparticles.

In our recently published works [90,91], we have initially analysed the impact that hydrophilic biopolymer networks have on the relaxivity of Gd-based CAs and explained the role of the water in the interaction between polymers and metal chelates. This concept, called "*Hydrodenticity*", has been the subject of further investigations as reported by Russo et al. [92]. In a still previous work published by Russo and co-worker [93], crosslinked Hyaluronic Acid NanoParticles (cHANPs) containing a Gd chelate (Gd-DTPA), are synthesized through a microfluidic platform

that allows a high degree of control over particle synthesis, enabling the production of monodisperse particles as small as 35 nm for MRI applications. The relaxivity (r1) achieved with the cHANPs is 12-times higher than Gd-DTPA. Within cHANPs, the properties of *Hydrodenticity* can be modulated to obtain desired mesh size, crosslink density, hydrophilicity and loading capability, as reported by Russo et al. [92,94]. Moreover, they proved that an increase of the crosslinking degree of biopolymer can induce the enhancement of relaxivity by restricting molecular tumbling while maintaining the switching property and allowing easy access of water throughout the structure, which is a key feature in MRI CAs.

The possibility to adopt a unique platform to tune the hydrogel structural parameters and, consequently, increase the relaxivity of a metal chelate without any chemical modification, could have a great impact on the clinical outcome. In fact, thanks to their improved relaxometric properties, cHANPs could ensure a brighter contrast with a lower amount of metal chelate, thus enabling the potential reduction of the administration dosage as approved for clinical use.

In a further work [95], we reported an efficient way to produce Hybrid Core-Shell (HyCoS) NPs composed of a Chitosan core and a shell of Hyaluronic Acid (HA) with improved relaxometric properties (up to 5-times than the commercial CA). Subsequently, the same nanosystem is used to develop a new nanoprobe for simultaneous Positron Emission Tomagraphy (PET)/MRI acquisitions as reported in our more recent publication [96].

Based on the above reported works, it has been finally demonstrated that the polymer architecture affects some characteristic parameters of the metal chelate and tunes its relaxometric properties [30,49,80,81,85,92].

Moreover, it is clear that crosslinked biopolymers can have a significant role to overcome the limitations of clinically relevant CAs without their chemical modification and as a compound in the design of advanced nanostructures with improved safety profile and switchable relaxometric properties.

Indeed, it is known that the functional properties as well as the swelling behaviour of hydrogels are influenced by the hydration degree, which can be likely modulated by changing the chemical composition of the system [50,53–56,97,98].

1.5. THE NEED FOR NEW POLYMER-BASED CONTRAST AGENTS

In this perspective, we believe that a more in-depth knowledge about the interference between macromolecules and MRI CAs and an understanding of their physicochemical properties is necessary to impact in the design strategies of the nanostructures and, consequently, to overcome the limitations of clinically used MRI CAs, particularly linked to the low relaxivity. To this aim, it is crucial to study the main phenomena involved in the formation of polymer matrices and how their properties can influence the relaxivity of MRI CAs is performed.

1.6. CHAPTER 1 REFERENCES

1. Jain, K. K. Nanomedicine: application of nanobiotechnology in medical practice. Med. Princ. Pract. Int. J. Kuwait Univ. Health Sci. Cent. 17, 89–101 (2008).
2. Buzea, C., Pacheco, I. I. & Robbie, K. Nanomaterials and nanoparticles: sources and toxicity. Biointerphases 2, MR17-71 (2007).
3. Lin, P.-C., Lin, S., Wang, P. C. & Sridhar, R. Techniques for physicochemical characterization of nanomaterials. Biotechnol. Adv. 32, 711–726 (2014).
4. Yu, X. et al. Design of Nanoparticle-Based Carriers for Targeted Drug Delivery. Journal of Nanomaterials (2016). doi:10.1155/2016/1087250
5. Jain, R. K. & Stylianopoulos, T. Delivering nanomedicine to solid tumors. Nat. Rev. Clin. Oncol. 7, 653–664 (2010).
6. Blanco, E., Shen, H. & Ferrari, M. Principles of nanoparticle design for overcoming biological barriers to drug delivery. Nat. Biotechnol. 33, 941–951 (2015).
7. Torchilin, V. P. Drug targeting. Eur. J. Pharm. Sci. 11, S81–S91 (2000).
8. Liechty, W. B. & Peppas, N. A. Expert opinion: Responsive polymer nanoparticles in cancer therapy. Eur. J. Pharm. Biopharm. Off. J. Arbeitsgemeinschaft Pharm. Verfahrenstechnik EV 80, 241–246 (2012).
9. Phillips, M. A., Gran, M. L. & Peppas, N. A. Targeted nanodelivery of drugs and diagnostics. Nano Today 5, 143–159 (2010).
10. Steichen, S. D., Caldorera-Moore, M. & Peppas, N. A. A review of current nanoparticle and targeting moieties for the delivery of cancer therapeutics. Eur. J. Pharm. Sci. Off. J. Eur. Fed. Pharm. Sci. 48, 416–427 (2013).
11. Altinoğlu, E. I. & Adair, J. H. Near infrared imaging with nanoparticles. Wiley Interdiscip. Rev. Nanomed. Nanobiotechnol. 2, 461–477 (2010).
12. Muehllehner, G. & Karp, J. S. Positron emission tomography. Phys. Med. Biol. 51, R117-37 (2006).

13. Holbrook, R. J. et al. Gd(III)-Dithiolane Gold Nanoparticles for T1-Weighted Magnetic Resonance Imaging of the Pancreas. Nano Lett. 16, 3202–3209 (2016).

14. Chang, Y., Lee, G. H., Kim, T.-J. & Chae, K.-S. Toxicity of magnetic resonance imaging agents: small molecule and nanoparticle. Curr. Top. Med. Chem. 13, 434–445 (2013).

15. Ni, Y. MR Contrast Agents for Cardiac Imaging. in Clinical Cardiac MRI (eds. Bogaert, J., Dymarkowski, S., Taylor, A. M. & Muthurangu, V.) 31–51 (Springer Berlin Heidelberg, 2011). doi:10.1007/174_2011_360

16. Caravan, P., Ellison, J. J., McMurry, T. J. & Lauffer, R. B. Gadolinium(III) Chelates as MRI Contrast Agents: Structure, Dynamics, and Applications. Chem. Rev. 99, 2293–2352 (1999).

17. Mansfield, P. Snapshot magnetic resonance imaging (Nobel lecture). Angew. Chem. Int. Ed Engl. 43, 5456–5464 (2004).

18. Rutt, B. K. & Lee, D. H. The impact of field strength on image quality in MRI. J. Magn. Reson. Imaging JMRI 6, 57–62 (1996).

19. Frias, J. C., Ma, Y., Williams, K. J., Fayad, Z. A. & Fisher, E. A. Properties of a versatile nanoparticle platform contrast agent to image and characterize atherosclerotic plaques by magnetic resonance imaging. Nano Lett. 6, 2220–2224 (2006).

20. Xue, S., Qiao, J., Pu, F., Cameron, M. & Yang, J. J. Design of a novel class of protein-based magnetic resonance imaging contrast agents for the molecular imaging of cancer biomarkers. Wiley Interdiscip. Rev. Nanomed. Nanobiotechnol. 5, 163–179 (2013).

21. Lee, N. et al. Iron Oxide Based Nanoparticles for Multimodal Imaging and Magnetoresponsive Therapy. Chem. Rev. 115, 10637–10689 (2015).

22. Iagaru, A. et al. Simultaneous whole-body time-of-flight 18F-FDG PET/MRI: a pilot study comparing SUVmax with PET/CT and assessment of MR image quality. Clin. Nucl. Med. 40, 1–8 (2015).

23. Sampath, S. C. et al. Detection of osseous metastasis by 18F-NaF/18F-FDG PET/CT versus CT alone. Clin. Nucl. Med. 40, e173-177 (2015).

24. Do, C., Barnes, J. L., Tan, C. & Wagner, B. Type of MRI contrast, tissue gadolinium, and fibrosis. Am. J. Physiol. Renal Physiol. 307, F844-855 (2014).

25. Guglielmo, F. F., Mitchell, D. G. & Gupta, S. Gadolinium contrast agent selection and optimal use for body MR imaging. Radiol. Clin. North Am. 52, 637–656 (2014).

26. Strijkers, G. J., Mulder, W. J. M., van Tilborg, G. A. F. & Nicolay, K. MRI contrast agents: current status and future perspectives. Anticancer Agents Med. Chem. 7, 291–305 (2007).

27. Sethi, R. et al. Enhanced relaxivity of Gd3+-based contrast agents geometrically confined within porous nanoconstructs. Contrast Media Mol. Imaging 7, (2012).

28. Wang, Y.-X. J. Superparamagnetic iron oxide based MRI contrast agents: Current status of clinical application. Quant. Imaging Med. Surg. 1, 35–40 (2011).

29. Weidman, E. K. et al. MRI safety: a report of current practice and advancements in patient preparation and screening. Clin. Imaging 39, 935–937 (2015).

30. Wood, M. L. & Hardy, P. A. Proton relaxation enhancement. J. Magn. Reson. Imaging JMRI 3, 149–156 (1993).

31. Caravan, P., Farrar, C. T., Frullano, L. & Uppal, R. Influence of molecular parameters and increasing magnetic field strength on relaxivity of gadolinium- and manganese-based T1 contrast agents. Contrast Media Mol. Imaging 4, 89–100 (2009).

32. Debroye, E. & Parac-Vogt, T. N. Towards polymetallic lanthanide complexes as dual contrast agents for magnetic resonance and optical imaging. Chem. Soc. Rev. 43, 8178–8192 (2014).

33. Zhou, Z. & Lu, Z.-R. Gadolinium-based contrast agents for magnetic resonance cancer imaging. Wiley Interdiscip. Rev. Nanomed. Nanobiotechnol. 5, 1–18 (2013).

34. Caravan, P. Strategies for increasing the sensitivity of gadolinium based MRI contrast agents. Chem. Soc. Rev. 35, 512–523 (2006).

35. Bruckman, M. A., Yu, X. & Steinmetz, N. F. Engineering Gd-loaded nanoparticles to enhance MRI sensitivity via T(1) shortening. Nanotechnology 24, 462001 (2013).

36. Penfield, J. G. & Reilly, R. F. What nephrologists need to know about gadolinium. Nat. Clin. Pract. Nephrol. 3, 654–668 (2007).

37. Shetty, A. N. et al. A liposomal Gd contrast agent does not cross the mouse placental barrier. Sci. Rep. 6, (2016).

38. McDonald, R. J. et al. Intracranial Gadolinium Deposition after Contrast-enhanced MR Imaging. Radiology 275, 772–782 (2015).

39. Yang, J. J. et al. Rational design of protein-based MRI contrast agents. J. Am. Chem. Soc. 130, 9260–9267 (2008).

40. Liepold, L. O. et al. Supramolecular protein cage composite MR contrast agents with extremely efficient relaxivity properties. Nano Lett. 9, 4520–4526 (2009).

41. Frangville, C. et al. Assembly of Double-Hydrophilic Block Copolymers Triggered by Gadolinium Ions: New Colloidal MRI Contrast Agents. Nano Lett. 16, 4069–4073 (2016).

42. Lesniak, W. G. et al. Salicylic Acid Conjugated Dendrimers Are a Tunable, High Performance CEST MRI NanoPlatform. Nano Lett. 16, 2248–2253 (2016).

43. Manus, L. M. et al. Gd(III)-Nanodiamond Conjugates for MRI Contrast Enhancement. Nano Lett. 10, 484–489 (2010).

44. Stuckey, D. J. et al. Magnetic resonance imaging evaluation of remodeling by cardiac elastomeric tissue scaffold biomaterials in a rat model of myocardial infarction. Tissue Eng. Part A 16, 3395–3402 (2010).

45. Hachani, R. et al. Polyol synthesis, functionalisation, and biocompatibility studies of superparamagnetic iron oxide nanoparticles as potential MRI contrast agents. Nanoscale 8, 3278–3287 (2016).

46. Ni, K. et al. Geometrically confined ultrasmall gadolinium oxide nanoparticles boost the T1 contrast ability. Nanoscale 8, 3768–3774 (2016).

47. Zhang, L. et al. The evolution of gadolinium based contrast agents: from single-modality to multi-modality. Nanoscale 8, 10491–10510 (2016).

48. Hermann, P., Kotek, J., Kubícek, V. & Lukes, I. Gadolinium(III) complexes as MRI contrast agents: ligand design and properties of the complexes. Dalton Trans. Camb. Engl. 2003 3027–3047 (2008). doi:10.1039/b719704g

49. Li, Y. et al. Macromolecular Ligands for Gadolinium MRI Contrast Agents. Macromolecules 45, 4196–4204 (2012).

50. Davies, G.-L., Kramberger, I. & Davis, J. J. Environmentally responsive MRI contrast agents. Chem. Commun. 49, 9704–9721 (2013).

51. Port, M. et al. Impact of rigidification on relaxometric properties of a tricyclic tetraazatriacetic gadolinium chelate. Contrast Media Mol. Imaging 1, 121–127 (2006).

52. Guérard, F., Ray, G. L. & Brechbiel, M. W. MRI with Gadolinium-Based Nanoparticles. in Nanotechnology for Biomedical Imaging and Diagnostics 223–262 (Wiley-Blackwell, 2015). doi:10.1002/9781118873151.ch8

53. Pasqui, D. et al. Polysaccharide-Based Hydrogels: The Key Role of Water in Affecting Mechanical Properties. Polymers 4, 1517–1534 (2012).

54. Sierra-Martin, B. & Fernandez-Barbero, A. Multifunctional hybrid nanogels for theranostic applications. Soft Matter 11, 8205–8216 (2015).

55. Raemdonck, K., Demeester, J. & De Smedt, S. Advanced nanogel engineering for drug delivery. Soft Matter 5, 707–715 (2009).

56. Pal, K., Banthia, A. K. & Majumdar, D. K. Polymeric Hydrogels: Characterization and Biomedical Applications. Des. Monomers Polym. 12, 197–220 (2009).

57. Rudovský, J., Hermann, P., Botta, M., Aime, S. & Lukeš, I. Dendrimeric Gd(III) complex of a monophosphinated DOTA analogue: optimizing relaxivity by reducing internal motion. Chem. Commun. 0, 2390–2392 (2005).

58. Rudovský, J. et al. PAMAM dendrimeric conjugates with a Gd-DOTA phosphinate derivative and their adducts with polyaminoacids: the interplay of global motion, internal rotation, and fast water exchange. Bioconjug. Chem. 17, 975–987 (2006).

59. Tang, J., Sheng, Y., Hu, H. & Shen, Y. Macromolecular MRI contrast agents: Structures, properties and applications. Prog. Polym. Sci. 38, 462–502 (2013).

60. Okada, S., Mizukami, S. & Kikuchi, K. Switchable MRI contrast agents based on morphological changes of pH-responsive polymers. Bioorg. Med. Chem. 20, 769–774 (2012).

61. Lux, J. et al. Metal Chelating Crosslinkers Form Nanogels with High Chelation Stability. J. Mater. Chem. B Mater. Biol. Med. 1, 6359–6364 (2013).

62. Lux, J., White, A. G., Chan, M., Anderson, C. J. & Almutairi, A. Nanogels from metal-chelating crosslinkers as versatile platforms applied to copper-64 PET imaging of tumors and metastases. Theranostics 5, 277–288 (2015).

63. Oliveira, R. N. et al. Mechanical properties and in vitro characterization of polyvinyl alcohol-nano-silver hydrogel wound dressings. Interface Focus 4, 20130049 (2014).

64. Manetti, C., Casciani, L. & Pescosolido, N. Diffusive contribution to permeation of hydrogel contact lenses: theoretical model and experimental evaluation by nuclear magnetic resonance techniques. Polymer 43, 87–92 (2002).

65. Omidian, H. & Park, K. Swelling agents and devices in oral drug delivery. J. Drug Deliv. Sci. Technol. 18, 83–93 (2008).

66. Netti, P. A. Nano-engineered bioactive interfaces. Interface Focus 4, 20130065–20130065 (2013).

67. Wang, X., He, J., Wang, Y. & Cui, F.-Z. Hyaluronic acid-based scaffold for central neural tissue engineering. Interface Focus 2, 278–291 (2012).

68. Wu, C. & Chang, J. Mesoporous bioactive glasses: structure characteristics, drug/growth factor delivery and bone regeneration application. Interface Focus 2, 292–306 (2012).

69. Ahearne, M. Introduction to cell-hydrogel mechanosensing. Interface Focus 4, 20130038 (2014).

70. Fadeeva, E., Deiwick, A., Chichkov, B. & Schlie-Wolter, S. Impact of laser-structured biomaterial interfaces on guided cell responses. Interface Focus 4, 20130048 (2014).

71. Bhowmik, D., Margret, R., Tripathi, K. K. & Kumar, K. P. S. NANOMEDICINE-AN OVERVIEW. 9

72. Lacroix, L.-M., Delpech, F., Nayral, C., Lachaize, S. & Chaudret, B. New generation of magnetic and luminescent nanoparticles for in vivo real-time imaging. Interface Focus 3, (2013).

73. Li, H., LaBean, T. H. & Leong, K. W. Nucleic acid-based nanoengineering: novel structures for biomedical applications. Interface Focus 1, 702–724 (2011).

74. Shen, Y. et al. Antisense peptide nucleic acid-functionalized cationic nanocomplex for in vivo mRNA detection. Interface Focus 3, 20120059 (2013).

75. Zhu, W. & Artemov, D. Biocompatible blood pool MRI contrast agents based on hyaluronan. Contrast Media Mol. Imaging 6, 61–68 (2011).

76. Masotti, A. et al. Synthesis and characterization of polyethylenimine-based iron oxide composites as novel contrast agents for MRI. Magma N. Y. N 22, 77–87 (2009).

77. Corti, M. et al. Magnetic and relaxometric properties of polyethylenimine-coated superparamagnetic MRI contrast agents. J. Magn. Magn. Mater. 320, (2008).

78. Xiao, Y., Xue, R., You, T., Li, X. & Pei, F. A new biodegradable and biocompatible gadolinium (III) -polymer for liver magnetic resonance imaging contrast agent. Magn. Reson. Imaging 33, 822–828 (2015).

79. Jeong, S. Y. et al. Biocompatible Polyhydroxyethylaspartamide-based Micelles with Gadolinium for MRI Contrast Agents. Nanoscale Res. Lett. 5, 1970–1976 (2010).

80. Courant, T. et al. Hydrogels Incorporating GdDOTA: Towards Highly Efficient Dual T1/T2 MRI Contrast Agents. Angew. Chem. Int. Ed. 51, 9119–9122 (2012).

81. Courant, T. et al. Biocompatible nanoparticles and gadolinium complexes for MRI applications. Comptes Rendus Chim. 16, 531–539 (2013).

82. Arosio, P. et al. Hybrid iron oxide-copolymer micelles and vesicles as contrast agents for MRI: impact of the nanostructure on the relaxometric properties. J. Mater. Chem. B 1, 5317–5328 (2013).

83. Jászberényi, Z., Sour, A., Tóth, É., Benmelouka, M. & Merbach, A. E. Fine-tuning water exchange on GdIII poly(amino carboxylates) by modulation of steric crowding. Dalton Trans. 0, 2713–2719 (2005).

84. Ruloff, R. et al. Accelerating water exchange for GdIII chelates by steric compression around the water binding site. Chem. Commun. 0, 2630–2631 (2002).

85. Ananta, J. S. et al. Geometrical confinement of gadolinium-based contrast agents in nanoporous particles enhances T1 contrast. Nat. Nanotechnol. 5, 815–821 (2010).

86. Gizzatov, A. et al. Geometrical confinement of Gd(DOTA) molecules within mesoporous silicon nanoconstructs for MR imaging of cancer. Cancer Lett. 352, 97–101 (2014).

87. Callewaert, M. et al. Tuning the composition of biocompatible Gd nanohydrogels to achieve hypersensitive dual T1/T2 MRI contrast agents. J. Mater. Chem. B 2, 6397–6405 (2014).

88. Necas, J., Bartosikova, L., Brauner, P. & Kolar, J. Hyaluronic acid (hyaluronan): a review. Vet. Med. (Praha) 2008

89. Dash, M., Chiellini, F., Ottenbrite, R. M. & Chiellini, E. Chitosan—A versatile semi-synthetic polymer in biomedical applications. Prog. Polym. Sci. 36, 981–1014 (2011).

90. Russo, M., Bevilacqua, P., Netti, P. A. & Torino, E. Commentary on "A Microfluidic Platform to Design Crosslinked Hyaluronic Acid Nanoparticles (cHANPs) for Enhanced MRI". Mol. Imaging 16, (2017).

91. Ponsiglione, A. M., Russo, M., Netti, P. A. & Torino, E. Impact of biopolymer matrices on relaxometric properties of contrast agents. Interface Focus 6, (2016).

92. Russo, M., Ponsiglione, A. M., Forte, E., Netti, P. A. & Torino, E. Hydrodenticity to enhance relaxivity of gadolinium-DTPA within crosslinked hyaluronic acid nanoparticles. Nanomed. 12, 2199–2210 (2017).

93. Russo, M., Bevilacqua, P., Netti, P. A. & Torino, E. A Microfluidic Platform to design crosslinked Hyaluronic Acid Nanoparticles (cHANPs) for enhanced MRI. Sci. Rep. 6, 37906 (2016).

94. Russo, M. et al. PEGylated crosslinked hyaluronic acid nanoparticles designed through a microfluidic platform for nanomedicine. Nanomed. 12, 2211–2222 (2017).

95. Vecchione, D. et al. Hybrid Core-Shell (HyCoS) Nanoparticles produced by Complex Coacervation for Multimodal Applications. Sci. Rep. 7, 45121 (2017).

96. Vecchione, D. et al. Hybrid core shell nanoparticles entrapping Gd-DTPA and 18F-FDG for simultaneous PET/MRI acquisitions. Nanomed. 12, 2223–2231 (2017).

97. Panagopoulou, A. et al. Glass Transition and Water Dynamics in Hyaluronic Acid Hydrogels. Food Biophys. 8, 192–202 (2013).

98. Vázquez, B., San Roman, J., Peniche, C. & Cohen, M. E. Polymeric Hydrophilic Hydrogels with Flexible Hydrophobic Chains. Control of the Hydration and Interactions with Water Molecules. Macromolecules 30, 8440–8446 (1997).

Chapter 2.

AIM OF THE WORK

2.1. AIM

Magnetic Resonance Imaging (MRI) is a promising technology in biomedical research and clinical diagnosis and provides high spatial resolution without the use of ionizing radiation [16,17]. Contrast Agents (CAs) are metal ions injected prior MRI scanning in the human body to enhance the signal intensity and improve the contrast between healthy and pathological tissues [26,34,99,100]. Among them, the most extensively used CAs in the clinical practice are paramagnetic gadolinium (Gd) chelates [101]. Despite their widespread use, these Gd-based CAs are limited by low sensitivity [49,91,93]; therefore, large amount of these paramagnetic agents need to be used in order to obtain an appropriate diagnostic contrast [31,102]. In many cases, the exposure to Gd-based MRI CAs in patients with compromised renal function is associated with Nephrogenic Systemic Fibrosis (NSF) [103], a systemic disease that can lead to death [104–106]. Moreover, recent studies in humans conducted by McDonald, Kanda and coworkers [38,107] have revealed that these compounds are retained in some tissues (i.e. kidneys, bone, skin and brain) also in healthy subjects.

In this framework, the opportunity to develop a safer and more effective probe for MRI [108,109] starting by clinical approved CAs is a significant and valuable challenge [110–112].

Despite several experimental studies addressed in the field of MRI CAs, a comprehensive knowledge of the mechanisms involved in the relaxation enhancement due to the entrapment of CAs in polymer-based architectures is still

missing. In particular, the role played by the water at the interface between polymer chains and MRI CAs has not been fully investigated and could lead to the availability of tailored models that accurately describe these novel complex systems.

The Thesis presents a study of the interactions involved in polymer-hydrogel-based CAs' solutions, aiming at understanding the key role of the water as mediating agent that acts at the interface between the polymer and the metal-chelate and determines both the polymer conformation and the relaxation enhancement.

The first aim is to investigate the thermodynamic properties of different combinations of hydrogels and Cas for Magnetic Resonance Imaging (MRI), to understand how the polymer structure can impact on the relaxometric properties of the metal chelate. As result of the study, we introduced the novel concept of *Hyrodenticity*, describing the equilibrium, occurring in hydrogel entrapping Gd-based CAs, between water osmotic pressure, elastodynamic of polymer chains and hydration degree of the CA able to enhance its relaxivity.

Then, we applied the concept of *Hydrodenticity* to design nanostructures and investigate the impact of different nano-architectures on the efficacy of CAs for MRI highlighting the key role of hydrogel structural parameters (mesh size and crosslink density) in the enhancement of the relaxometric properties of the CAs.

The nanostructures are made of biocompatible and natural polymers, like hyaluronic acid (HA) and chitosan (CS), also combined with lipids in the form of liposomes, and are formulated together with with FDA-approved and clinically used CAs for MRI without inducing chemical modifications to the CAs.

Two different processes have been implemented to design the nanostructures: (1) High Pressure Homogenization; (2) Microfluidic Flow Focusing.

Three main goals have been achieved:

- Definition of the *Hydrodenticity*: the concept of *Hydrodenticity* has been proposed to describe the complex equilibrium formed by elastic stretches of polymer chains, water osmotic pressure and hydration degree of Gadolinium-based CAs able to boost the relaxivity of the CAs;
- Application of the *Hydrodenticity* to nanostructures: three types of Gd-loaded nanostructures with increased relaxivity have been obtained

without chemically modifying the CA's structure and biocompatibility: (1) crosslinked HA nanohydrogels; (2) HA-CS coacervated nanoparticles; (3) hybrid polymer-lipid nanostructures;

- Development of a preliminary predictive model to describe nanostructured CAs based on *Hydrodenticity*: a preliminary model has been implemented in Matlab to fit relaxometric data of different nanostructured CAs.

2.2. CHAPTER 2 REFERENCES

1. Mansfield, P. Snapshot magnetic resonance imaging (Nobel lecture). Angew. Chem. Int. Ed Engl. 43, 5456–5464 (2004).
2. Caravan, P., Ellison, J. J., McMurry, T. J. & Lauffer, R. B. Gadolinium(III) Chelates as MRI Contrast Agents: Structure, Dynamics, and Applications. Chem. Rev. 99, 2293–2352 (1999).
3. Lauffer, R. B. Paramagnetic metal complexes as water proton relaxation agents for NMR imaging: theory and design. Chem. Rev. 87, 901–927 (1987).
4. Caravan, P. Strategies for increasing the sensitivity of gadolinium based MRI contrast agents. Chem. Soc. Rev. 35, 512–523 (2006).
5. Strijkers, G. J., Mulder, W. J. M., van Tilborg, G. A. F. & Nicolay, K. MRI contrast agents: current status and future perspectives. Anticancer Agents Med. Chem. 7, 291–305 (2007).
6. Huang, H. & Lovell, J. F. Advanced Functional Nanomaterials for Theranostics. Adv. Funct. Mater. 27, (2017).
7. Shokrollahi, H. Contrast agents for MRI. Mater. Sci. Eng. C Mater. Biol. Appl. 33, 4485–4497 (2013).
8. Li, Y. et al. Macromolecular Ligands for Gadolinium MRI Contrast Agents. Macromolecules 45, 4196–4204 (2012).
9. Ponsiglione, A. M., Russo, M., Netti, P. A. & Torino, E. Impact of biopolymer matrices on relaxometric properties of contrast agents. Interface Focus 6, (2016).
10. Russo, M., Bevilacqua, P., Netti, P. A. & Torino, E. A Microfluidic Platform to design crosslinked Hyaluronic Acid Nanoparticles (cHANPs) for enhanced MRI. Sci. Rep. 6, 37906 (2016).
11. Caravan, P. Protein-targeted gadolinium-based magnetic resonance imaging (MRI) contrast agents: design and mechanism of action. Acc. Chem. Res. 42, 851–862 (2009).
12. Caravan, P., Farrar, C. T., Frullano, L. & Uppal, R. Influence of molecular parameters and increasing magnetic field strength on relaxivity of gadolinium- and manganese-based T1 contrast agents. Contrast Media Mol. Imaging 4, 89–100 (2009).

13. Klemm, P. J., Floyd, W. C., Smiles, D. E., Fréchet, J. M. J. & Raymond, K. N. Improving T1 and T2 magnetic resonance imaging (MRI) contrast agents through the conjugation of an esteramide dendrimer to high water coordination Gd(III) hydroxypyridinone (HOPO) complexes. Contrast Media Mol. Imaging 7, 95–99 (2012).

14. Sieber, M. A. et al. A preclinical study to investigate the development of nephrogenic systemic fibrosis: a possible role for gadolinium-based contrast media. Invest. Radiol. 43, 65–75 (2008).

15. Thomsen, H. S. et al. Nephrogenic systemic fibrosis and gadolinium-based contrast media: updated ESUR Contrast Medium Safety Committee guidelines. Eur. Radiol. 23, 307–318 (2013).

16. Yuan, H. et al. Well-Defined Protein-Based Supramolecular Nanoparticles with Excellent MRI Abilities for Multifunctional Delivery Systems. Adv. Funct. Mater. 26, 2855–2865 (2016).

17. Kanda, T., Ishii, K., Kawaguchi, H., Kitajima, K. & Takenaka, D. High signal intensity in the dentate nucleus and globus pallidus on unenhanced T1-weighted MR images: relationship with increasing cumulative dose of a gadolinium-based contrast material. Radiology 270, 834–841 (2014).

18. McDonald, R. J. et al. Intracranial Gadolinium Deposition after Contrast-enhanced MR Imaging. Radiology 275, 772–782 (2015).

19. Huang, J., Zhong, X., Wang, L., Yang, L. & Mao, H. Improving the Magnetic Resonance Imaging Contrast and Detection Methods with Engineered Magnetic Nanoparticles. Theranostics 2, 86–102 (2012).

20. Zhang, W. et al. Surface impact on nanoparticle-based magnetic resonance imaging contrast agents. Theranostics 8, 2521–2548 (2018).

21. Kotb, S. et al. Gadolinium-Based Nanoparticles and Radiation Therapy for Multiple Brain Melanoma Metastases: Proof of Concept before Phase I Trial. Theranostics 6, 418–427 (2016).

22. Benachour, H. et al. Multifunctional Peptide-Conjugated Hybrid Silica Nanoparticles for Photodynamic Therapy and MRI. Theranostics 2, 889–904 (2012).

23. Bloembergen, N. & Morgan, L. O. Proton Relaxation Times in Paramagnetic Solutions. Effects of Electron Spin Relaxation. J. Chem. Phys. 34, 842–850 (1961).

Chapter 3.

IMPACT OF BIOPOLYMERS ON RELAXOMETRIC PROPERTIES OF CONTRAST AGENTS: DEFINITION OF HYDRODENTICITY

3.1. SUMMARY OF THE CHAPTER

Properties of water molecules at the interface between Contrast Agents (CAs) for Magnetic Resonance Imaging (MRI) and macromolecules could have a valuable impact on the effectiveness of metal chelates. Recent studies, indeed, demonstrated that polymer architectures could influence CAs' relaxivity by modifying the correlation times of the metal chelate.

However, an understanding of the physicochemical properties of polymer/CA systems is necessary to improve the efficiency of clinically used CAs, still exhibiting low relaxivity.

In this context, we investigate the impact of Hyaluronic Acid (HA) hydrogels on the relaxometric properties of Gd-DTPA, a clinically-used CA, to understand better the determining role of the water, which is crucial for both the relaxation enhancement and the polymer conformation. To this aim, water self-diffusion coefficients, thermodynamic interactions and relaxometric properties of HA/Gd-

DTPA solutions are studied through Time-Domain NMR Relaxometry and Isothermal Titration Calorimetry.

We observed that the presence of Gd-DTPA could alter the polymer conformation and the behaviour of water molecules at the HA/Gd-DTPA interface, thus modulating the relaxivity of the system.The effect of the hydration of the hydrogel structure on the relaxometric properties of Gd-DTPA is explained for the first time and called *Hydrodenticity*.

3.2. INTRODUCTION

Investigation of water molecules at the interface between relevant clinical Contrast Agents (CAs) for Magnetic Resonance Imaging (MRI) and macromolecules can be of great interest to increase the performances of metal chelates. Indeed, most of the clinically-used CAs are characterized by poor effectiveness in the high magnetic fields region (3 T and above), which is clinically favored because of its higher signal-to-noise ratio and high-resolution imaging. MRI CAs also lack of tissue specificity and can cause heavy allergic effects, serious nephrotoxicity [33–35] and intracranial deposition of metal ion after repeated intravenous administration [38].

The extensive research on nano-engineered systems and polymer-based nanocomposites [54,55,66–74] has led to significant advances also in the field of MRI [50,52,72,75–77]. In particular, some recent studies have shown that nanoconstructs can improve CAs' relaxivity and many efforts have been devoted to the development of polymer-based carriers for MRI CAs with particular reference to Gadolinium (Gd) chelates, which are the most commonly clinically used agents [49,75,78–82].

In this chapter, we investigate the impact of and hydrogel-CA systems on the relaxometric properties of metal chelates to understand better the clear role of the water, which mediates interactions and could be responsible for their behaviour in solution. Indeed, water is crucial both in the relaxation process and in the polymer conformation. On one hand, the magnetic properties of the water protons surrounding the CA are fundamental to enhance the CA's relaxivity. On the other, the presence of water molecules can induce changes in the polymer structure through polar interactions, hydrogen bonding and osmotic pressure.

Among different biopolymer, Hyaluronic Acid (HA) [88] is chosen as model polymer due to its hydrophilic nature and established biocompatibility and biodegradability. Commercially available Gd-DTPA is selected as the CA due to its widespread use in clinical practice [113]. It is worth highlighting that both the selected polymer and CA are FDA approved and clinically used products [33,114,115].

First experiments are focused on determining the water self-diffusion coefficients in polymer and CA solutions through Time-Domain NMR Relaxometry to observe changes in water mobility in the presence of both HA and Gd-DTPA. Self-diffusion measurements have already proved especially successful for probing interfacial water structure and dynamics near various biological and polymer surfaces [116]. Intramolecular interactions, as well as entropy costs, can alter the mobility of solvent molecules within polymer matrices or in confined environments, with a slowing effect on the diffusion [117–119]. Moreover, since the relaxation efficiency is mediated by translational and rotational diffusion [116], a variation of the water diffusion behaviour at the interface between polymer chains and MRI CAs could impact on the τ_D of the complex, thereby influencing the relaxometric properties of the metal chelate.

Isothermal Titration Calorimetry (ITC) is employed after that to investigate thermodynamic interactions involved in the mixing of HA with Gd-DTPA. As already reported elsewhere [120], molecular interactions are accompanied by some level of heat exchange between the interacting system and its surrounding medium, which can be evaluated at a constant temperature through the ITC technique. Therefore, to investigate interactions between HA and Gd-DTPA, titration experiments were performed using a Nano ITC Low Volume calorimeter (TA Instruments). Basic principles of ITC measurements have been widely discussed elsewhere [120–122].

Relaxometric properties of HA/Gd-DTPA solutions are investigated by means of time-domain NMR relaxometry. The characterization of these systems, obtained through the combination of commercial MRI CAs and hydrophilic biopolymers, could give an insight into the development of novel hydrogel-based CAs without modifying the chemical structure or altering the biocompatibility of the original CA.

In this theoretical framework, the peculiar effect of *Hydrodenticity* on the polymer conformation and the formation of the stable water compartments responsible for the enhancement of the MRI signal is introduced and discussed.

3.3. MATERIALS AND METHODS

3.3.1. MATERIALS

HA (Bohus Biotech, Sweden) with an average molecular weight of 420000 Da is used for the polymer matrix because of its biocompatibility, biodegradability and swelling properties. Commercially available Gd-DTPA (Sigma-Aldrich) with a molecular weight of 547.57 Da is used since it is a well-known, low-risk CA. Divinyl Sulfone (DVS) (Sigma Aldrich) with a molecular weight of 118.15 Da is used as crosslinking agent. Milli-Q water is systematically used for sample preparation and analysis.

3.3.2. SAMPLE PREPARATION

Non-crosslinked hydrogel-CA solutions are prepared by dispersing both the HA and the Gd-DTPA powders in distilled deionized water and then mixing using magnetic stirrer. Different HA concentrations, ranging from 0.1 to 5 % w/v, is utilized for the experimentation. For each fixed concentration of HA, Gd-DTPA concentration is varied between 0 and 0.2 mM.

Crosslinked hydrogel-CA solutions are prepared by adding Divinyl Sulfone (DVS) to the above-described solutions to crosslink the polymer network chemically. Hydrogels are prepared at different HA: DVS ratios (from 1:1 to 1:16). The biocompatibility of HA–DVS hydrogels is already confirmed in the literature [123].

3.3.3. ISOTHERMAL TITRATION CALORIMETRY

Isothermal Titration Calorimetry (ITC) measurements are conducted by filling the sample cell (0.7 mL in volume) with an aqueous solution of HA at different concentrations (from 0.1 to 0.7 % w/v) and the 50 μL syringe with an aqueous

solution of Gd-DTPA at 1.5 mM. Measurements are performed at 25 °C and fixed stirring rate of 200 rpm. Fifty injections, each of 1 μL of Gd-DTPA, are delivered in intervals of 500 s. Data analysis and processing to provide ITC and enthalpy change, ΔH, profiles are carried out using the NanoAnalyze (TA instruments) and the Origin Pro 9.1 SRO software (OriginLab Corporation, USA).

3.3.4. RELAXOMETRIC MEASUREMENT

Relaxation times are measured on a Bruker Minispec (mq 60) bench-top relaxometer operating at 60 MHz for protons (magnetic field strength: 1.41 T). The acquisitions are performed at 37°C, and before each measurement, the sample is placed into the NMR probe for about 15 min for thermal equilibration. Longitudinal relaxation times, T_1, are determined by both saturation (SR) and inversion recovery (IR) pulse sequences. The relaxation recovery curves are fitted using a multi-exponential model.The solid line represents the linear regression and relaxivity values, r_1, are calculated from its slope. The longitudinal relaxation rate values, R_1, defined as the inverse of the longitudinal relaxation time, $R_1 = 1/T_1, s^{-1}$, are plotted versus each concentration of CA, measured in mM. Data are treated by a least-squares method using Origin Pro 9.1 SRO software (OriginLab Corporation, USA). Furthermore, the relaxation time distribution is obtained by CONTIN Algorithm. The relaxation spectrum is normalized with respect to the CONTIN processing parameters. Therefore, the integral of a peak corresponds to the contribution of the species exhibiting this peculiar relaxation to the relaxation time spectrum.

3.3.1. NMR SPECTROSCOPY

^{1}H NMR spectra are recorded at 25 °C with Varian Agilent NMR spectrometer operating at 600 MHz to observe chemical interactions between polymer and chelating agent (DTPA). The NMR samples consisted of water solution of HA-DTPA at different molar ratios (HA/DTPA ranging from 0 to 0.5), with 10% v/v D_2O.

Diffusion-ordered NMR Spectroscopy (DOSY) are also performed and the z-gradient strengths (Gz) is varied in 20 steps from 500 to 32500 G/cm (maximum

strength). The gradient pulse duration (δ) and the diffusion delay (Δ) are kept costant, 2 ms for δ and ranging from 7 to 1000 ms for Δ. After Fourier transformation and baseline correction, DOSY spectra are processed and analysed using Varian software VNMRJ (Varian by Agilent Technologies, Italy) in order to obtain the values of water self-diffusion coefficient.

3.3.1. Water Self-Diffusion Coefficient

Diffusion measurements of water molecules are carried out on a Bruker Minispec (mq 20) bench-top relaxometer operating at 20 MHz for protons (magnetic field strength: 0.47 T). A pulsed field gradient spin echo (PFG-SE) sequence [124], with two magnetic field gradient pulses of length δ and strength g, and with a delay Δ between the leading edges of them, is used to measure water self-diffusion coefficients. The self-diffusion coefficient, D, is derived by linear regression of signal attenuation ratio curve, a semi-logarithmic plot of the echo attenuation as a function of the tunable parameter of the sequence, $k = (\gamma g \delta)^2 * (\Delta - \delta/3)$.

3.3.2. Differential Scanning Calorimetry

For all measurements the HA/water solution (Mw = 42 kDa) is used. The aqueous solutions are prepared in a concentration range of polymer 0.3–0.7% w/v. Next, Gd-DTPA is added as CA at different molar ratio HA/Gd-DTPA (from 1:0.25 to 1:3) and stirred for 12 h. The hydrated polymer samples, with and without CA, are sealed at room temperature in a Tzero hermetic pans prior to analysis. DSC measurements are performed in a TA Instruments' Q20™ calorimeter on samples between 5 and 10 mg. The samples are cooled down from 25°C to -50°C followed by heating scan up to 25°C. The same heating and cooling rate are 10°C/min for all runs. Samples are tested in triplicate to ensure reproducibility. For DSC and ITC measurements, we used low molecular weight HA (42 kDa) to highlight better the energetic contributions of different components without exceeding the maximum scale of the instruments.

3.4. RESULTS

3.4.1. CHANGES IN POLYMER CONFORMATION INDUCED BY A GD-BASED CONTRAST AGENT

The polymer conformation can be modified by the affinity with the solvent solution [125,126]. Furthermore, the addition of a solute can still induce a change in the polymer conformation. In our previous work, we proved that the relaxivity of CAs can be modulated combining them with macromolecules or polymers [91]. Therefore, the understanding of the interaction between polymers and CAs in aqueous solution could be critical to tune the relaxometric properties of CAs. We aim to show how the presence of the Gd-DTPA in the aqueous solution can influence the behaviour of the polymer matrix and, on the other side, how these adjustments of the polymer conformation can govern the characteristic correlation times of the Gd-DTPA [91–93].

To investigate thermodynamic interactions between polymer and contrast agent, HA and Gd-DTPA respectively, are selected to be tested by Isothermal Titration Calorimetry (ITC). We aim to take advantage of the molecular interactions that are accompanied by some level of heat exchange between the interacting system and its surrounding medium; indeed, these interactions can be evaluated, at constant temperature, through the ITC. Basic principles of this technique have been widely discussed elsewhere [120,121]

Titration experiments are conducted injecting a solution of Gd-DTPA in the ITC cell containing the polymer solution. Different HA concentrations, ranging from 0.3 to 0.7% w/v, are tested and more representative results are reported in Figure 3.1 and 3.2 (peaks above the baseline represent exothermic phenomena while peaks below the baseline represent endothermic phenomena).

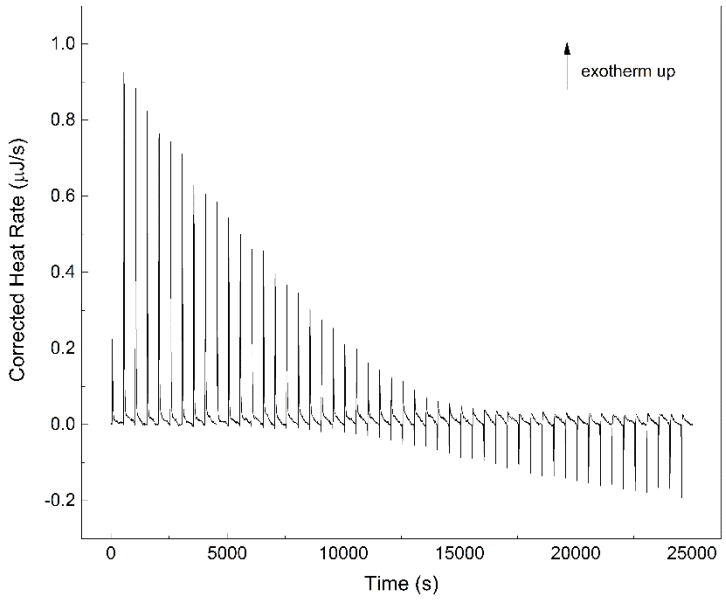

Figure 3.1 Thermograms (heat flow versus time) of Gd-DTPA into aqueous solution of HA at 0.6 % w/v. Temperature and stirring rate have been kept constant at 25 °C and 200 rpm, respectively, for each sample.

In our experiment, a simple dilution of Gd-DTPA in water or water in HA exhibits only small constant exothermic peaks (see Supporting Information). On the contrary, when Gd-DTPA is injected as titrant into the cell containing HA solution a change from exothermic to endothermic behaviour is clearly observed. This change occurs at an HA/Gd-DTPA molar ratio of 0.5 (Figure 3.2), i.e. when the molar concentration of Gd-DTPA in solution is twice the HA molar concentration. Starting from these observations, we hypothesize that at a certain HA/Gd-DTPA ratio, the enthalpy variations obtained in the binding experiment can be related to changes in the polymer structure, which in turn can be associated with the water-mediated interaction between the Gd-chelate and the polymer. The presence of Gd-DTPA, which has a high affinity for water molecules, may interfere with the polymer solution and induce peculiar arrangements in polymer chains' conformation.

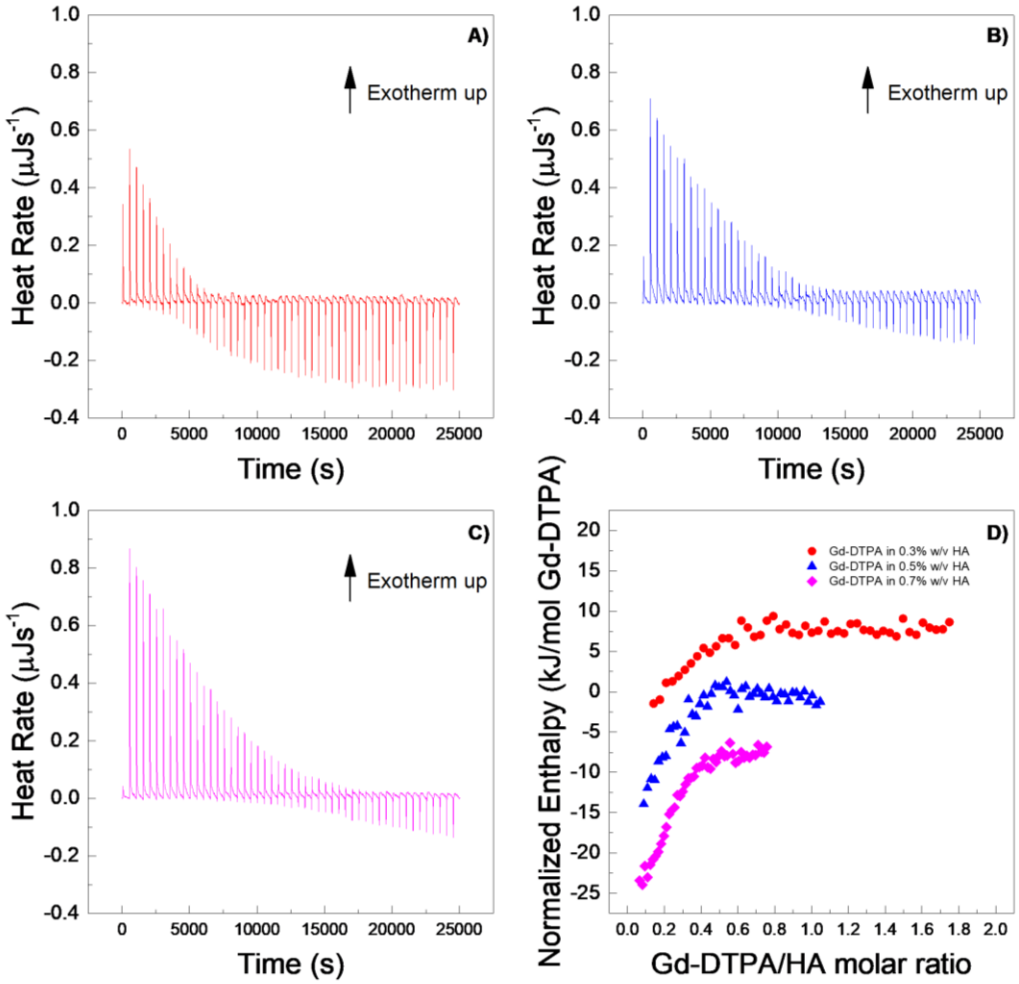

Figure 3.2 Titration curves of Gd-DTPA into aqueous polymer solutions at 25 °C. Calorimetric traces (heat flow against time) for (A) 0.3% w/v HA, (B) 0.5% w/v HA and (C) 0.7% w/v HA. In (D) it is reported the normalized enthalpy vs Gd-DTPA/HA molar ratio for Gd-DTPA in 0.3% w/v HA (red circles), in 0.5% w/v HA (blue triangles) and in 0.7% w/v HA (magenta diamonds). The curves were shifted vertically for clarity; y-offset were set at 2 (red circles), 0 (blue triangles) and -10 (magenta diamonds).

It is clear that significant enthalpy variations are obtained in the titration experiments (Figure 3.2A-C) and can be associated with the water-mediated interaction between the Gd-chelate and the polymer, which induces changes in

polymer chains' conformation. Since Figure 3.2A-C show ITC thermograms varying the HA concentration in the sample cell, a wide range of Gd-DTPA/HA molar ratios is examined and the relative energetic contribution and enthalpy values are calculated by integrating peaks of the experimental curves and are reported in Figure 3.2D. Simple dilution of Gd-DTPA in water exhibits only small constant exothermic peaks over the whole experiment.

In Figure 3.2, it is worth noting that the energetic contribution decreases as the Gd-DTPA/HA molar ratio increases; thus, the higher is the concentration of HA in the sample cell, the higher is the Gd-DTPA concentration needed to observe endothermic peaks. It can also be observed that the endothermic contribution exceeds the exothermic one at the recurrent Gd-DTPA/HA ratio approximatively equal to 0.5 through all the experiments at different HA concentrations in the sample cell. It means that a specific energetic contribution is needed to induce the adjustment of the polymer conformation. Then, when the Gd-DTPA/HA molar ratio equals 0.5, the endothermic peaks start slightly increasing until reaching a plateau, which corresponds to the thermodynamic equilibrium established within the ternary system (polymer-CA-water). The measured energetic variation reflects the conformational changes of polymer chains due to the presence of the CA in solution and leads to the formation of stable sub-domains in which a balanced exchange of water molecules occurs between the polymer, the CA and the bulk.

The attainment of this thermodynamic equilibrium derives from a water-mediated interaction occurring between HA and Gd-DTPA. As both hydrophilic components, HA and Gd-DTPA interact with the water by forming hydrogen bonds and by coordinating water molecules. This competitive behaviour generates a measurable heat that reflects the change in polymer chains conformation and the exchange of bound water molecules with the bulk, thereby, bringing the system to a more stable configuration. In our previous paper [92], we preliminary showed how this equilibrium is able to affect the relaxometric properties of the system, as an effect of the new concept of *Hydrodenticity*, which will be further explained in the following paragraphs.

3.4.2. NMR STUDY OF DTPA INTERACTIONS AND WATER MOBILITY IN POLYMER SOLUTION

Since previous ITC measurements reported by Gouin et al. [122] have shown no binding energy between free Gd^{3+} ions and HA, we hypothesize that polymer conformational changes are mainly induced by the presence of the chelating macromolecule, DTPA. NMR spectroscopy is used to confirm this hypothesis. NMR spectra are calculated for HA and DTPA solutions. We use only the DTPA without the metal ion since we are mostly interested in examining interactions between the polymer and the chelating macromolecule.

Considering the spectra of the only DTPA and HA (Figure 4.2A-B), whose characteristic peaks are circled in blue and red respectively, the observations of DTPA/HA solutions at different molar ratios are reported (Figure 4.2C-I). The molar ratio ranges from 2 to 100 and is obtained by decreasing the HA concentration from 150 to 10 μM.

In Figure 3.3, it can be observed that the characteristic DTPA peak at 3.50 ppm (s, 2 H, CH2–COOH) is influenced by the presence of HA in solution. In fact, it seems to shift and reduce its intensity far more than the other peaks by increasing the HA concentration. As an example, the shift is evident by comparing Figure 3.3I, where the DTPA peak is highlighted in blue, with Figure 3.3C, where the signal is dramatically reduced.

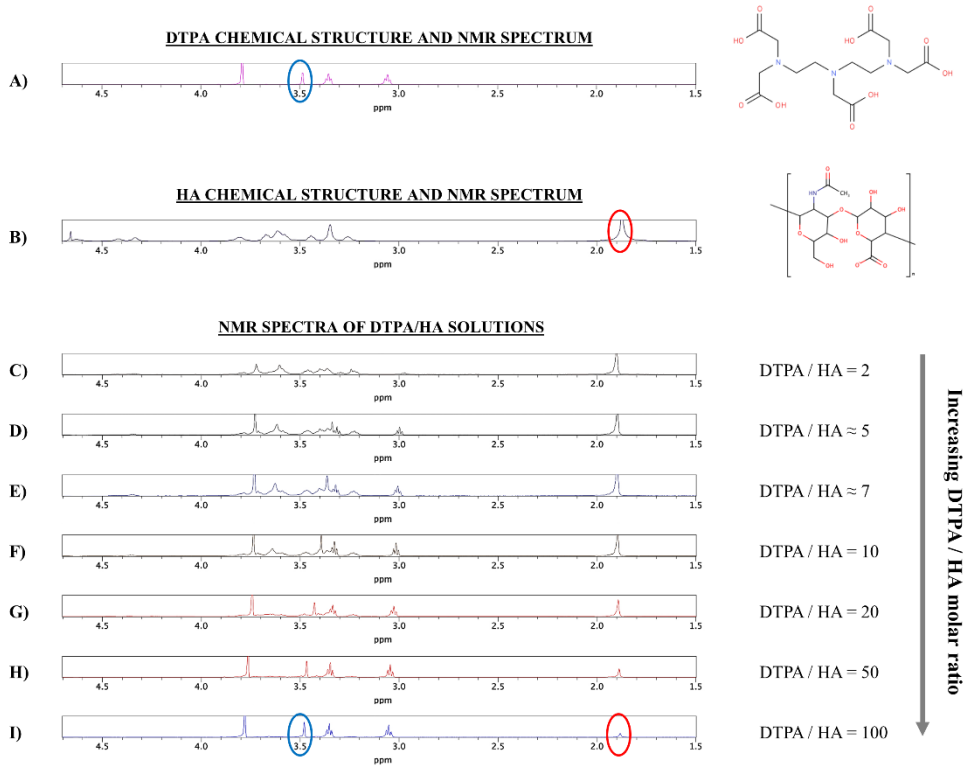

Figure 3.3 (A) ^{1}H NMR spectrum and chemical structure of DTPA; (B) ^{1}H NMR spectrum and chemical structure of DTPA; (C–I) ^{1}H NMR spectra of DTPA/HA solutions at different molar ratios, from DTPA/HA = 2 to DTPA/HA = 100. Characteristic peaks of DTPA and HA are highlighted in blue and red respectively.

It results that an interaction between the two components of the system exists and generates changes in the NMR spectrum of the solution.

Through NMR-DOSY, instead, we investigate how the presence of both HA and Gd-DTPA can affect the mobility of water molecules.

Figure 3.4 shows the normalized time-dependent self-diffusion coefficient of water in both polymer solutions (Figure 3.4A) and polymer-CA solutions (Figure 3.4B). For short diffusion delays, the measured self-diffusion coefficient D is nearly equal to the free self-diffusion coefficient D_0 of water at 25°C ($2.5 \cdot 10^{-9}$ m^2/s), since the molecules travel over a short distance and only few of them feel the surrounding

macromolecules. As the diffusion time increases, more water molecules go through these restrictions and the self-diffusion coefficient reaches a plateau value.

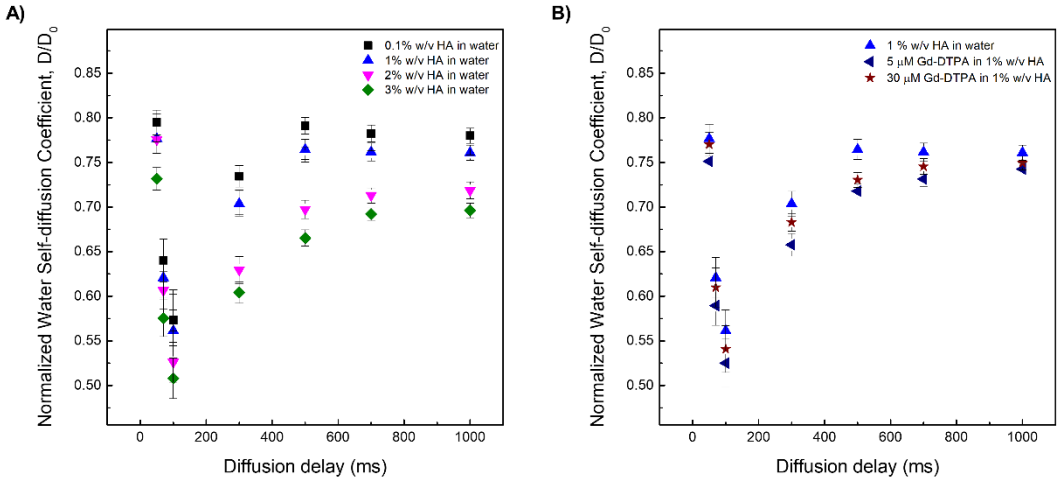

Figure 3.4 (A) Normalized time dependent water self-diffusion coefficient in 0.1% w/v HA (squares), 1% w/v HA (triangles), 2% w/v HA (flipped triangles), 3% w/v HA (diamonds). (B) Normalized time dependent water self-diffusion coefficient in 1% w/v HA (triangles), 5 μM Gd-DTPA in 1% w/v HA (flipped triangles) and 30 μM Gd-DTPA in 1% w/v HA (stars).

We can hypothesize that the presence of Gd-DTPA compete with those HA-molecular sites beared by water molecules and that are responsible for polymer hydration and hydrogel formation. As highlighted with ITC results, the polymer conformation can be modified by the presence of Gd-DTPA, which could interplay with the water molecules and with the formation of hydrogen bonding. NMR-DOSY measurements are carried out to assess these hypothesized changes in water mobility. It can be observed that, in the case of the ternary system, the diffusivity of water beyond decreases, suggesting that the polymer-CA combination affects the water mobility more than the polymer itself.

Figure 3.4A clearly shows that the water diffusion behaviour is affected by the polymer concentration. In particular, the diffusion coefficient decreases at increasing polymer concentration. Besides, Figure 3.4B shows the additional contribution of the CA to the water mobility. In fact, the presence of Gd-DTPA, even at relatively low concentrations (5 - 30 μM), can further reduce the value of the water self-diffusion coefficient for both short and long diffusion times.

It is worth noting that low Gd-DTPA concentrations are chosen (Figure 4.3B) because Gd-DTPA is highly paramagnetic and it can interfere with NMR measurements [127,128], while the HA concentrations (0.1 - 3% w/v) are slightly higher than those used in the ITC experiments to highlight and make more evident the differences in diffusion behaviour between samples. In particular, as illustrated in Figure 3.4B, a fixed polymer concentration of 1% w/v is selected to show the effect of CA on the diffusion of water molecules.

A data comparison between ITC and NMR spectra confirms the hypothesized fundamental properties behind the concept of *Hydrodenticity*: the ability of Gd-DTPA to induce changes in polymer conformation and in water mobility.

To further confirm the NMR results we also studied the diffusion in polymer matrices through time domain relaxometry. In our systems, we have observed that water mobility slightly changes with increasing network density induced by crosslinking reaction (Figure 3.5).

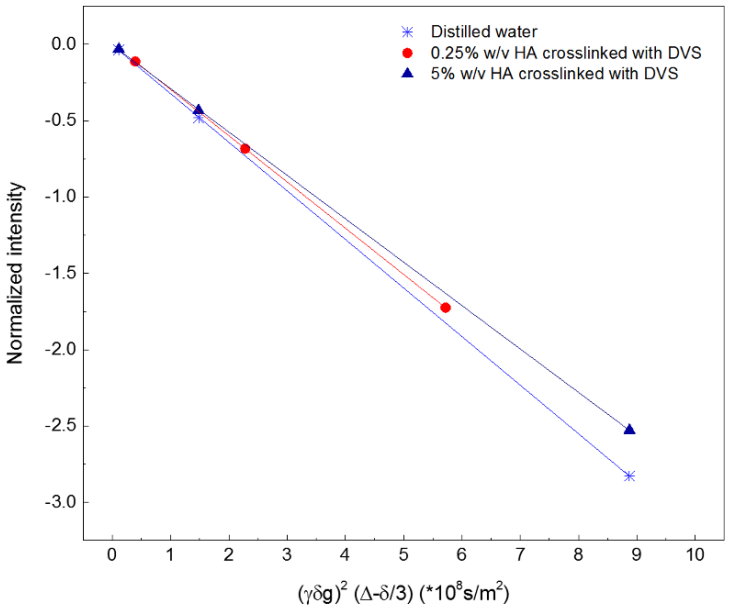

Figure 3.5 Stejskal Tanner Plot is used for calculating water self-diffusion coefficient of: (1) distilled water; (2) 0.25 % w/v HA solution with 5 µL DVS 8 hours after the crosslinking reaction; (3) 5 % w/v HA solution with 40 µL DVS 8 hours after the crosslinking reaction.

Besides, a more significant decrease in the water diffusion is observed in the presence of increasing polymer concentration rather than increasing CA concentration (Table 3.1).

Table 3.1 Range of water self-diffusion coefficients, D, measured for: (1) distilled water; (2) Gd-DTPA solutions at different Gd-DTPA concentrations; (3) 0.25 and 5 % w/v HA hydrogel solutions at varying crosslinking degrees, i.e. different DVS concentrations.

HA (% w/v)	DVS (μL)	Gd-DTPA (mM)	D[a] ($*10^{-9}$ m^2s^{-1})
0	0	0	3.19
0	0	0.05 ÷ 1	3.18 ÷ 3.09
0.25	0 ÷ 25	0	3.05 ÷ 2.90
5	5 ÷ 40	0	2.88 ÷ 2.83

[a] Values of the standard deviation for the measured diffusion coefficients are all below $0.4*10^{-12}$ m^2s^{-1}.

However, the study of the diffusion coefficient as a function of the crosslinking degree requires further investigation to understand its influence on the relaxometric properties. Further details on diffusion data are reported in the Supporting Information. Furthermore, results show that water mobility starts decreasing even at very low polymer concentration (0.25 % w/v HA). This dynamic can be attributed to the high molecular weight and hydrophilicity of the HA, which allows the formation of several hydrogen bonds at the surface of the polymer, thereby stabilizing the polymer structure and reducing water self-diffusion.

3.4.3. WATER DYNAMICS WITHIN HYDRATED POLYMER MATRIX CONTAINING GD-DTPA

To analyse further the role of water mobility in the *Hydrodenticity*, a study of the dynamics and behaviour of water molecules is needed. Within hydrated polymer matrices (hydrogels), containing metal chelates, water molecules mediate polymer-CA interactions and, therefore, play a dual role: on one hand, the amount of absorbed water [129,130] and its interaction with the hydrogel structure affects the chain motion of the hydrophilic polymer; on the other, the mobility of water molecules in the polymer matrix is responsible for the relaxometric properties of the CA.

We investigate the water dynamics in water-HA systems, with and without Gd-DTPA, using the Differential Scanning Calorimetry (DSC). We focus on the thermal effects that the polymer (Figure 3.6A) and the CA (Figure 3.6B) have on the water dynamics. According to the literature, indeed, the crystallization of water changes with the polymer concentration and with the hydration degree [97].

A)

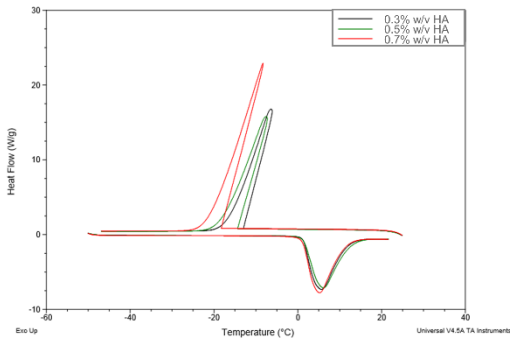

B)

Sample	Concentration	Tc (°C)	ΔH (J/g)	Tm (°C)	ΔH (J/g)
Gd-DTPA	60 µM	-7.47	218.7	5.37	249
	100 µM	-8.36	245.0	6.52	255
	140 µM	-8.00	239.7	5.36	266
	200 µM	-9.27	238.6	5.17	269.9
HA	0.3% w/v	-6.40	243	5.62	260.8
	0.5% w/v	-7.72	248.4	6.05	253.3
	0.7% w/v	-8.31	239.2	5.21	270
HA + Gd-DTPA	0.3% w/v + 60µM	-9.73	229.1	7.94	255.1
	0.5% w/v + 100µM	-7.88	244.9	6.47	273.0
	0.7% w/v + 140µM	-6.24	254.5	5.02	259.0

Figure 3.6 (A) DSC thermograms of HA at different concentrations (0.3, 0.5 and 0.7% w/v). (B) Melting (Tm) and crystallization (Tc) temperatures for free Gd-DTPA in water and HA solutions with and without CA.

In Figure 3.6A, thermograms of water-polymer systems at different HA concentrations (0.3 - 0.7% w/v) are displayed. We can observe that, during the cooling phase, the crystallization peaks shift to lower temperatures and lower enthalpy values. As expected, the enthalpy, given as the peak area, reaches its maximum value at the highest HA concentration (0.7% w/v).

Figure 3.6B shows a comparison of melting (T_m) and crystallization (T_c) temperatures between HA solutions with and without Gd-DTPA (concentration range: 60 - 200 µM). It can be noted that the transition properties remained unaffected in presence of the CA, suggesting that the influence of the polymer on the thermal behaviour of water is predominant with respect to the CA at the selected concentration.

3.4.4. Relaxation times, rates and relaxivity of the polymer matrix

Through Time-Domain Relaxometry, relationships between system formulation, polymer matrices and relaxivity enhancement are provided. Results show how the relaxivity could be varied by changing the structural parameters of the hydrogel, namely polymer concentration and crosslinking degree (DVS concentration). Figure 3.7 a) and b) display the longitudinal relaxation rate, R_1, and longitudinal relaxation time distribution for Gd-DTPA in distilled water and different crosslinked and non-crosslinked HA/Gd-DTPA solutions.

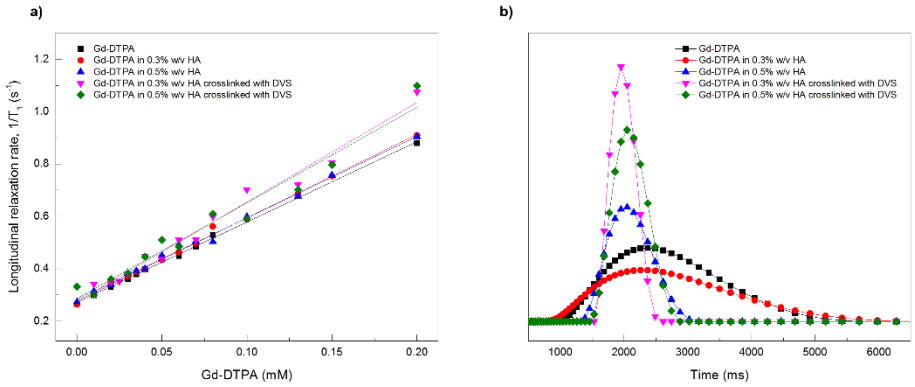

Figure 3.7 a) Longitudinal relaxation rate as a function of Gd-DTPA concentration and b) longitudinal relaxation time distribution for: (1) Gd-DTPA in distilled water; (2) Gd-DTPA in 0.3 % w/v HA solution; (3) Gd-DTPA in 0.5 % w/v HA solution; (4) Gd-DTPA in 0.3 % w/v HA crosslinked with DVS (HA:DVS = 1:8); (5) Gd-DTPA in 0.5 % w/v HA crosslinked with DVS (HA:DVS = 1:8). Linear regression is applied to each set of data reported in a).

In detail, Figure 3.7 a) demonstrates the variation of relaxation rates against the concentration of Gd-DTPA. As expected, R_1 rises linearly as Gd-DTPA concentration increases and surprisingly, the relaxivity, r_1, appears to be tuned mostly by the variation of hydrogel structure (polymer concentration and crosslinking degree). Therefore, we found out that could be possible to modulate the r_1 by changing the DVS concentration and to induce corresponding changes in the relaxation rates through the hydrogel matrix. Slopes of the regression lines in Figure 3.7 a), indicating each obtained relaxivity r_1 value, are reported in Table 3.2.

Table 3.2 Relaxivity enhancement for the investigated polymer/CA systems.

HA (% w/v)	DVS (% w/v)	r_1 ($mM^{-1}s^{-1}$)	r_1 increment (%)
0	0	3.07 ± 0.04	0
0.3	0	3.18 ± 0.05	3.6
0.3	2.4	3,81 ± 0.16	24,1
0.5	0	3,11 ± 0.06	1.3
0.5	4	3,65 ± 0.23	18,9
0.7	0	3,26 ± 0.06	6.2
0.7	5.6	3,41 ± 0.21	11.1

Figure 3.7 b) highlights through the relaxation time distribution the influence of hydrogel structure on the relaxation times as already discussed in Figure 3.7 a). In particular, it displays a narrower relaxation time distribution in the presence of crosslinking, thereby indicating an enhancement of the MRI signal.

As shown in Table 3.2, a slight increase in the relaxivity (from 1% to 6%) on the reference solution (Gd-DTPA in water) is observed for the non-crosslinked samples. Besides, for crosslinked hydrogel-CA systems, in the presence of a crosslinked network, the relaxivity increases to an even greater extent, ranging from 11% up to 25%. About this last result, it seems that the crosslinking degree is interfering more on the relaxivity of CAs than on the diffusivity of water, acting, therefore, more on the rigidification of the CAs than on the water mobility. However, this aspect is of crucial important and will require further investigations and comparison.

Percentages of increment in the relaxivity are calculated by dividing the difference between the relaxivity of the polymer/CA system and the reference (Gd-DTPA in water) by that of the reference solution, as follows:

$$r_1\ increment = \frac{\left.\frac{1}{T_1}\right|_{GdDTPA\ in\ HA} - \left.\frac{1}{T_1}\right|_{GdDTPA}}{\left.\frac{1}{T_1}\right|_{GdDTPA}} * 100$$

For further details on relaxometric data, please refer to the Supporting Information.

The existence of a water-mediated interaction between Gd-DTPA and HA, observed through ITC, NMR and DSC, and the effect of the polymer conformation on the characteristic correlation time of the metal chelate could explain the boosting of the relaxivity in the studied systems.

Relaxometric properties are investigated by means of time-domain relaxometry on two different systems: non-crosslinked and crosslinked polymer matrix (0.5% w/v HA) containing Gd-DTPA.

In the latter case, rheological and chemical-physical properties of polysaccharide can be modulated by changing the crosslinker (DVS) concentration, as known as crosslinking density. In fact, thanks to the presence of hydrophilic groups in the skeleton of HA, hydrogel is able to uptake a large amount of water. Under these conditions, water is in an abnormal aggregate state that influences the relaxivity of hydrated Gd-DTPA.

Figure 3.8 shows the results of relaxometric measurements for the hydrogel system (0.5% w/v HA) studied by loading different concentration of Gd-DTPA.

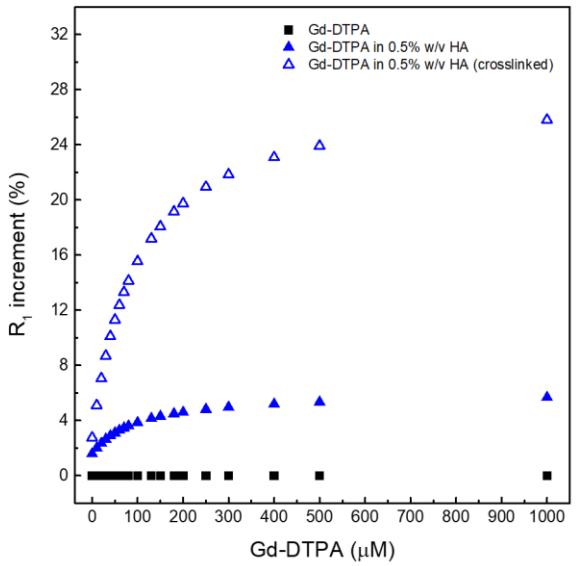

Figure 3.8 Increment in longitudinal relaxation rate, R1, at different contrast agent concentrations (from 0 to 1 mM) for: free Gd-DTPA in water (black squares); Gd-DTPA in 0.5% w/v HA solution (blue filled triangles); Gd-DTPA in 0.5% w/v HA crosslinked with DVS (blue empty triangles). The

R1 increment is calculated in percentage with respect to the corresponding R1 of Gd-DTPA in water. A fast increment in R1 is observed until a Gd-DTPA concentration equal to 300 µM. For higher Gd-DTPA concentrations, the R1 increment reaches a plateau.

The hydrogel system is analysed and compared to the free Gd-DTPA solution. In particular, we display the increment in percentage of the paramagnetic relaxation as a function of Gd-DTPA concentration. The increment in percentage of the relaxation enhancement has been calculated as follows (Equation 1):

$$Enhancement\ increment = \frac{\frac{1}{T_1}\Big|_{GdDTPA\ in\ HA} - \frac{1}{T_1}\Big|_{GdDTPA}}{\frac{1}{T_1}\Big|_{GdDTPA}} * 100 \qquad (1)$$

We find that the stronger the interaction is between Gd-DTPA and HA, the better is the MRI enhancement. Moreover, the crosslinked system is much more efficient than the non-crosslinked one. Indeed, in the crosslinked system, since the enhancement reaches a plateau at Gd-DTPA/HA molar ratio equal to 2.5 (i.e. at 300 µM of Gd-DTPA in 0.5% w/v HA water solution), it is not necessary to overload the system with Gd-DTPA in order to achieve higher relaxation. It is worth noting that, for both studies, with and without crosslinker, the Gd-DTPA concentration of 200 µM seems to represent a threshold for the maximum effect of the hydrogel on the Gd-DTPA relaxation mechanism.

Figure 3.9 displays a schematic representation of the hydrogel network formation, even in presence of the crosslinking agent, and its influence on the polymer conformation.

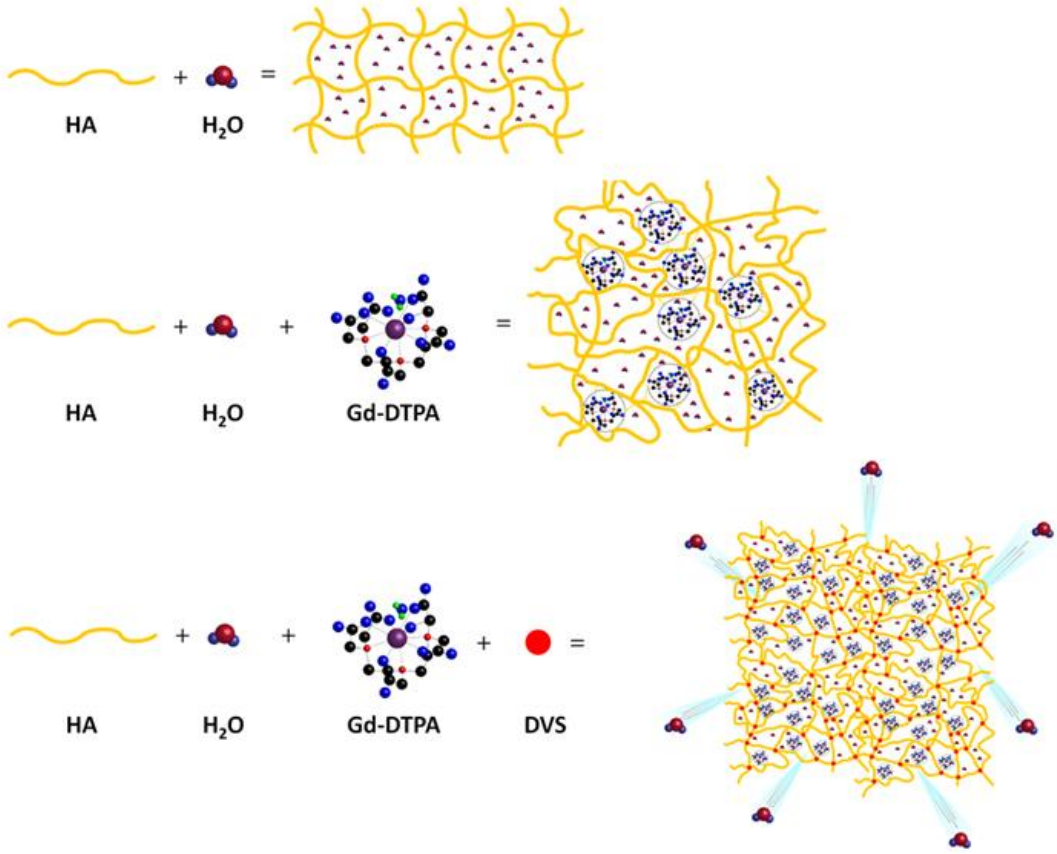

Figure 3.9 Formation mechanism affects hydrogel network structure: schematic representation of: formation of a hydrogel of hyaluronic acid in water (top); complex HA-Gd-DTPA structure (middle); crosslinked hydrogel network containing the contrast agent (bottom).

We hypothesize that the boosting of Gd-DTPA relaxivity in a hydrogel matrix is due to a proper complexation between the polymer and the CA in solution, mediated by the water and further amplified by the addition of a crosslinker. It is confirmed that the reached equilibrium among osmotic pressure and elastodynamic forces of the polymer meshes and hydration degree of the CA in the matrix are able to tune finely the relaxometric properties of the metal chelates in the ternary system. The overall ensemble of these phenomena is defined as *Hydrodenticity* [92].

3.5. THEORETICAL INTERPRETATION OF THE ENHANCED RELAXIVITY

Starting from the Solomon–Bloembergen–Morgan (SBM) theory [36], the physics of CAs is described by a set of physicochemical parameters characterizing the fluctuating magnetic dipole created by the paramagnetic ion. In detail, according to the SBM model, the metal complex can be viewed as having separate coordination spheres [31]: the Inner Sphere (IS), which consists of water molecules directly coordinated to the metal ion, and the Outer Sphere (OS), which is a less organized structure consisting of bulk water molecules diffusing in the near environment of the metal complex. In some cases, a Second Sphere (SS) contribution is taken into account, which is related to water molecules hydrogen bonded to the metal complex [32]. Each of the coordination mentioned above spheres has its characteristic parameters. IS parameters include the number of labile water molecules coordinated to the metal ion (q), the residence time of the coordinated water molecule (τ_M), which in turn determines the rate of the coordinated water molecule exchanging with the bulk, and the rotational correlation time (τ_R), which is how quickly the contrast agent is tumbling in solution. Conversely, OS parameters include the translational diffusional time (τ_D), which represent the diffusion of water molecules in the bulk near to the Gd complex.

It is already known that molecular motion, size, rigidity and possible binding between Gd-chelates and other macromolecules may induce changes in relaxivity [34]. Furthermore, polymer architecture and properties can strongly affect the MRI enhancement [49–51].

As previously reported in the SBM theory, characteristic parameters of the metal chelate can be physically or chemically tuned and are of primary importance in the design of new CAs [48]. In particular, the Gd-chelator determines the number of coordinated water molecules (q) and the water exchange rate (k_{ex}), which is the inverse of the residence time τ_M. Moreover, decreased τ_D and τ_R, which can be obtained, for instance, through the binding of the metal chelate with large macromolecules, generally yield increased relaxation rates at low magnetic fields (<1.5 T) [35].

Our findings report that the presence of a polymer network can significantly affect the relaxation enhancement since it influences the hydration mechanism of the CA, i.e. the number of water molecules in either the IS, SS or OS, their diffusion behaviour and exchange rate with the water molecule coordinated to the metal ion.

At first, as a result of the diffusion measurements, we can observe that thanks to the high hydrophilicity of the HA promoting the hydrogen bonds formation at the surface of the polymer, water mobility starts decreasing even at very low polymer concentrations. Secondly, ITC results suggest that the presence of Gd-DTPA induce considerable thermodynamic variations in the polymer/CA mixing process that can be related to changes in polymer conformation. Finally, taking into consideration the computed relaxivity values, we can hypothesize that the hydrogel structure, which is strictly dependent on the water content and its dynamics within the polymer matrix, can significantly impact on the relaxivity of the whole polymer/CA system.

As schematically represented in Figure 3.10, the obtained results suggest that changes in polymer conformation, induced by varying polymer/CA molar ratio, could be further exploited to improve the relaxivity of the CA.

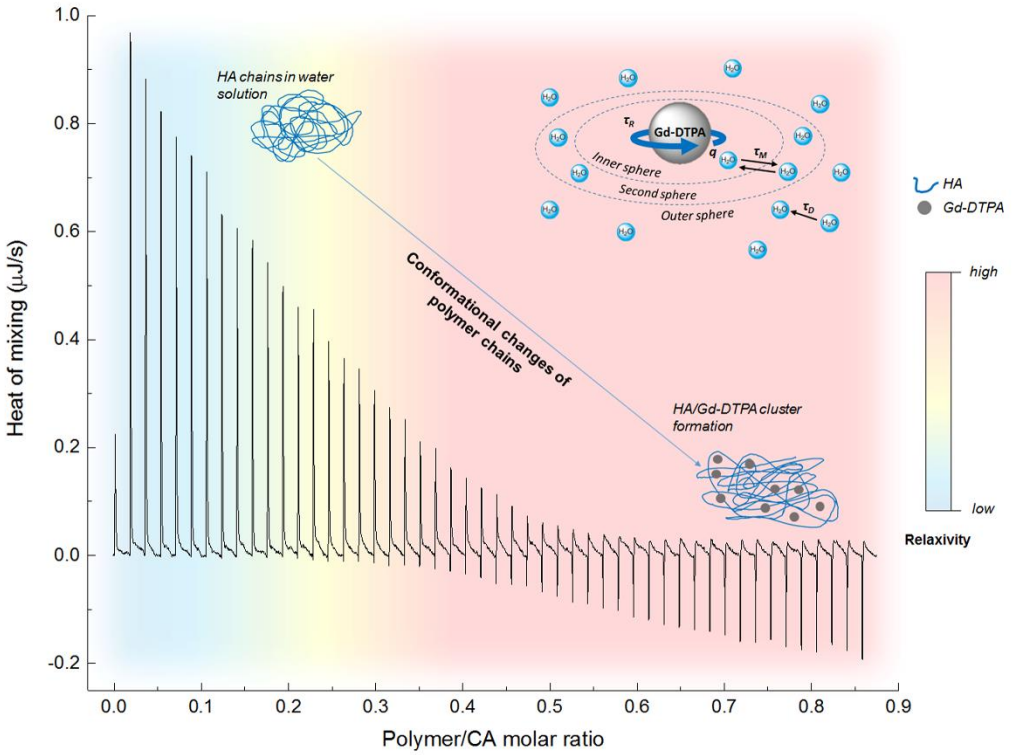

Figure 3.10 Relaxation enhancement induced by water-mediated HA/Gd-DTPA interactions.

Indeed, the altered behaviour of the water molecules at the HA/Gd-DTPA interface, exhibiting reduced mobility and strong interactions with the highly hydrophilic polymer surface, may have a considerable impact on the correlation times, especially τ_M and τ_D. In fact, the presence of polymer hydrophilic groups can change the access of bulk water molecules to the coordinated water molecule and, thus, alter the water exchange rate ($k_{ex} = 1/\tau_M$). Moreover, polymer chains can slightly reduce the mobility of the OS water molecules, with a consequent decreasing of τ_D. A simultaneous reduction of the CA's tumbling rate (τ_R) can also be hypothesized since the environment provided by the presence of the polymer chains as well as of the crosslinking degree may induce a slower rotation of the metal chelate.

3.6. THEORY OF THE GADO-MESH FORMATION

This work reports the use of polymer hydrogels for boosting the relaxivity of clinical relevant CAs.

Results show that a spontaneous complexation exists between HA and Gd-DTPA due to thermodynamic interactions as demonstrated by both calorimetric and NMR measurements. It is already known that, in an aqueous polymer solution, solvent affinity can alter polymer conformation by inducing a local solvation of the structure that influences the number of available conformations of the polymer chains. Moreover, the introduction of another soluble ionic component, such as Gd-DTPA, in the system can induce further changes in polymer conformation, detectable via diverse thermodynamic approaches [131–134]. Based on our findings, we prove for the first time that these conformational changes, induced by the metal chelate, contribute to an increase in CA's relaxivity.

In order to tune the MRI enhancement, we exploit the versatile structural characteristics of HA. In fact, the high porosity of the hydrogel, which shows a mesh-like structure, is controlled by varying the density of covalent crosslinking [135,136]. Moreover, the presence of negatively charged groups and the degree of crosslinking influence water adsorption capacity and, thus, the relaxometric properties of the ternary system [53].

Therefore, the presence of the hydrogel matrix can greatly amplify the magnetic properties of the encapsulated Gd-DTPA, suggesting a strong outer-sphere and second-sphere contribution to the relaxivity.

Based on these observations, we hypothesize that increased relaxivity is mainly related to the creation of water domains or clusters (water compartments) around the CA within the polymer matrix. In fact, biopolymer systems contain intermolecular cavities that can be considered as molecular nano-domains in which various self-assembly processes can be implemented in principle [137]. The formation of peculiar structures within these cavities can be associated with thermodynamic transitions and it is a characteristic of many metallopolymeric systems [138,139].

The sub-nanostructures, here defined "Gado-meshes", are generated from a three-way interaction between HA, Gd-DTPA and water. The entrapment of the CA inside

the hydrophilic matrix of HA results in a reduction of the rotational tumbling rate, due to an increase of the effective viscosity of the aqueous solution into the hydrogel matrix. At the same time, multiple CA-water interaction pathways occur between the exchangeable protons of the water molecules coordinated by the CA and the other water molecules freely moving within the hydrogel mesh or bonded to the polymer chains [27,81,140].

Our "Gado-mesh" consists of highly relaxing Gd-water compartments spontaneously generated within the hydrogel matrix by the combination of these multiple physico-chemical interactions. The so created nanostructure is composed of different water layers departing from the polymer chains that surround the Gd-molecules. It is known, in fact, that hydrated polysaccharides, such as HA, are characterized by the presence of multiple water layers, contiguous regions of variable water density within a polyelectrolyte solution [141], differing in their physical properties depending on the distance from the polysaccharide chain [142]. The hydration process of HA generates: the "bound water layer", which is the water fractions closely associated with the polymer matrix; the "unbound water layer", made by the water molecules which are not directly interacting with the polymer; and the "free water layer", which resembles dynamics of pure water. In addition, the developed polymer network can be dependent not only on the water layers organization but also on other solute species, such as Gd-DTPA, altering the bound water layer with non-negligible effect on the HA conformation and dynamic [143]. In the "Gado-mesh", Gd-DTPA has a competitive behaviour with the respect of HA, similar to the cation shielding of the HA due to the presence of salts [144], and interposes itself between the water molecules around the HA, altering the bound water layer and generating water compartments with high MRI enhancing properties. The "Gado-mesh" influences the τ_R, τ_D and τ_M times through the action of the *Hydrodenticity*, whose effect is magnified by the crosslinking. *Hydrodenticity*, hence, refers to the status of the hydrated Gd-DTPA with the coordination water subjected to osmotic pressure deriving from elastodynamics equilibrium of swollen gels [92,145–150].

We hypothesize that the attainment of this equilibrium is reached when the normal energetic stability of the meshes is compromised by the presence of the Gd-DTPA and evolves to a new spontaneous equilibrium involving the formation of

nanocompartments, so called “Gado-Meshes”, in which water is in an abnormal aggregate state that influences the relaxivity. Water molecules in the hydrogel matrix that are subjected to the effect of *Hydrodenticity*, are able to change their water dynamics and can mediate the hydrogel conformation and the physical and relaxometric properties of the metal chelate.

3.7. CONCLUSION

Here, a study of the interactions involved in polymer- hydrogel-based CA solutions has been presented, aiming at understanding the key role of the water as a mediating agent that acts at the interface between the polymer and the metal chelate and determines both the polymer conformation and the relaxation enhancement.

A multidisciplinary approach is used: changes in polymer conformation and thermodynamic interactions of CAs and polymers in aqueous solutions are detected by isothermal calorimetric (ITC) measurements and later, these interactions are investigated at molecular level using NMR to better understand the involved the phenomena. Water molecular dynamics of these systems is also studied by means of Differential Scanning Calorimetry (DSC). In order to observe relaxometric properties variations, we have monitored the MRI enhancement of the examined structures over all the experiments.

The systems have been investigated by mixing crosslinked or non-crosslinked HA with Gd-DTPA at specific polymer/CA molar ratios in aqueous solution without introducing chemical modifications of the CA. Water self-diffusion coefficients, as well as proton longitudinal relaxation curves for different HA/Gd-DTPA solutions, have been measured. A thermodynamic investigation of the mixing process between HA and Gd-DTPA in water has also been conducted.

We have observed that, in the presence of a crosslinked matrix, it is possible to modulate the water content of the system and, therefore, the hydration of the CA, by adjusting the crosslinking degree of the hydrogel structure. In these conditions, a more stable polymer network can be obtained, promoting more efficient water-polymer and water-CA interactions that boost the relaxivity to higher values. The

crosslinking degree is proposed as an advanced tool to modulate the hydrogel network and its properties, enabling the tuning of the relaxometric properties.

These findings could be useful to deepen the knowledge of hydrogel-CA systems and to achieve an advanced comprehension of the fundamental mechanisms that rule the interaction between MRI CAs and hydrogel matrices, and are responsible for the relaxation enhancement. Further characterization studies and computational simulations are necessary to insight the water behaviour within polymeric matrices in the presence of metal chelates and the potential impact that these structures can have on the relaxometric properties of clinically used CAs and, therefore, on the performance of MRI diagnosis. The knowledge of these complex systems could be scaled to nanoscale dimensions, inspiring the development of a new class of nanostructured MRI CAs with highly tunable relaxometric properties as well as the production of metallopolymer complexes or magnetic and conductive polymer-based materials with applications in areas such as sensors, memory devices, nanolithography and controlled release.

3.8. CHAPTER 3 REFERENCES

1. Zhou, Z. & Lu, Z.-R. Gadolinium-based contrast agents for magnetic resonance cancer imaging. Wiley Interdiscip. Rev. Nanomed. Nanobiotechnol. 5, 1–18 (2013).

2. Caravan, P. Strategies for increasing the sensitivity of gadolinium based MRI contrast agents. Chem. Soc. Rev. 35, 512–523 (2006).

3. Bruckman, M. A., Yu, X. & Steinmetz, N. F. Engineering Gd-loaded nanoparticles to enhance MRI sensitivity via T(1) shortening. Nanotechnology 24, 462001 (2013).

4. McDonald, R. J. et al. Intracranial Gadolinium Deposition after Contrast-enhanced MR Imaging. Radiology 275, 772–782 (2015).

5. Netti, P. A. Nano-engineered bioactive interfaces. Interface Focus 4, 20130065–20130065 (2013).

6. Wang, X., He, J., Wang, Y. & Cui, F.-Z. Hyaluronic acid-based scaffold for central neural tissue engineering. Interface Focus 2, 278–291 (2012).

7. Wu, C. & Chang, J. Mesoporous bioactive glasses: structure characteristics, drug/growth factor delivery and bone regeneration application. Interface Focus 2, 292–306 (2012).

8. Ahearne, M. Introduction to cell-hydrogel mechanosensing. Interface Focus 4, 20130038 (2014).

9. Fadeeva, E., Deiwick, A., Chichkov, B. & Schlie-Wolter, S. Impact of laser-structured biomaterial interfaces on guided cell responses. Interface Focus 4, 20130048 (2014).

10. Bhowmik, D., Margret, R., Tripathi, K. K. & Kumar, K. P. S. NANOMEDICINE-AN OVERVIEW. 9

11. Lacroix, L.-M., Delpech, F., Nayral, C., Lachaize, S. & Chaudret, B. New generation of magnetic and luminescent nanoparticles for in vivo real-time imaging. Interface Focus 3, (2013).

12. Li, H., LaBean, T. H. & Leong, K. W. Nucleic acid-based nanoengineering: novel structures for biomedical applications. Interface Focus 1, 702–724 (2011).

13. Shen, Y. et al. Antisense peptide nucleic acid-functionalized cationic nanocomplex for in vivo mRNA detection. Interface Focus 3, 20120059 (2013).

14. Sierra-Martin, B. & Fernandez-Barbero, A. Multifunctional hybrid nanogels for theranostic applications. Soft Matter 11, 8205–8216 (2015).

15. Raemdonck, K., Demeester, J. & De Smedt, S. Advanced nanogel engineering for drug delivery. Soft Matter 5, 707–715 (2009).

16. Zhu, W. & Artemov, D. Biocompatible blood pool MRI contrast agents based on hyaluronan. Contrast Media Mol. Imaging 6, 61–68 (2011).

17. Guérard, F., Ray, G. L. & Brechbiel, M. W. MRI with Gadolinium-Based Nanoparticles. in Nanotechnology for Biomedical Imaging and Diagnostics 223–262 (Wiley-Blackwell, 2015). doi:10.1002/9781118873151.ch8

18. Davies, G.-L., Kramberger, I. & Davis, J. J. Environmentally responsive MRI contrast agents. Chem. Commun. 49, 9704–9721 (2013).

19. Masotti, A. et al. Synthesis and characterization of polyethylenimine-based iron oxide composites as novel contrast agents for MRI. Magma N. Y. N 22, 77–87 (2009).

20. Corti, M. et al. Magnetic and relaxometric properties of polyethylenimine-coated superparamagnetic MRI contrast agents. J. Magn. Magn. Mater. 320, (2008).

21. Xiao, Y., Xue, R., You, T., Li, X. & Pei, F. A new biodegradable and biocompatible gadolinium (III) -polymer for liver magnetic resonance imaging contrast agent. Magn. Reson. Imaging 33, 822–828 (2015).

22. Jeong, S. Y. et al. Biocompatible Polyhydroxyethylaspartamide-based Micelles with Gadolinium for MRI Contrast Agents. Nanoscale Res. Lett. 5, 1970–1976 (2010).

23. Courant, T. et al. Hydrogels Incorporating GdDOTA: Towards Highly Efficient Dual T1/T2 MRI Contrast Agents. Angew. Chem. Int. Ed. 51, 9119–9122 (2012).

24. Li, Y. et al. Macromolecular Ligands for Gadolinium MRI Contrast Agents. Macromolecules 45, 4196–4204 (2012).

25. Courant, T. et al. Biocompatible nanoparticles and gadolinium complexes for MRI applications. Comptes Rendus Chim. 16, 531–539 (2013).

26. Arosio, P. et al. Hybrid iron oxide-copolymer micelles and vesicles as contrast agents for MRI: impact of the nanostructure on the relaxometric properties. J. Mater. Chem. B 1, 5317–5328 (2013).

27. Necas, J., Bartosikova, L., Brauner, P. & Kolar, J. Hyaluronic acid (hyaluronan): a review. Vet. Med. (Praha) 2008

28. Lu, Z.-R., Mohs, A. M., Zong, Y. & Feng, Y. Polydisulfide Gd(III) chelates as biodegradable macromolecular magnetic resonance imaging contrast agents. Int. J. Nanomedicine 1, 31–40 (2006).

29. Kasraie, N., Oviatt, H. W. & Clarke, G. D. On the Use of Molecular Weight Cutoff Cassettes to Measure Dynamic Relaxivity of Novel Gadolinium Contrast Agents: Example Using Hyaluronic Acid Polymer Complexes in Phosphate-Buffered Saline. Radiol. Res. Pract. 2011, (2011).

30. Huang, C.-H. & Tsourkas, A. Gd-based macromolecules and nanoparticles as magnetic resonance contrast agents for molecular imaging. Curr. Top. Med. Chem. 13, 411–421 (2013).

31. Yoo, H., Paranji, R. & Pollack, G. H. Impact of Hydrophilic Surfaces on Interfacial Water Dynamics Probed with NMR Spectroscopy. J. Phys. Chem. Lett. 2, 532–536 (2011).

32. Ori, G., Massobrio, C., Pradel, A., Ribes, M. & Coasne, B. Structure and Dynamics of Ionic Liquids Confined in Amorphous Porous Chalcogenides. Langmuir 31, 6742–6751 (2015).

33. Ori, G., Villemot, F., Viau, L., Vioux, A. & Coasne, B. Ionic liquid confined in silica nanopores: molecular dynamics in the isobaric–isothermal ensemble. Mol. Phys. 112, 1350–1361 (2014).

34. Chiessi, E., Cavalieri, F. & Paradossi, G. Water and polymer dynamics in chemically cross-linked hydrogels of poly(vinyl alcohol): a molecular dynamics simulation study. J. Phys. Chem. B 111, 2820–2827 (2007).

35. Kabiri, M. & Unsworth, L. D. Application of isothermal titration calorimetry for characterizing thermodynamic parameters of biomolecular interactions: peptide self-assembly and protein adsorption case studies. Biomacromolecules 15, 3463–3473 (2014).

36. Martinez, J. C., Murciano-Calles, J., Cobos, E. S., Iglesias-Bexiga, M. & Ruiz-Sanz, I. L. and J. Isothermal Titration Calorimetry: Thermodynamic Analysis of the Binding Thermograms of Molecular Recognition Events by Using Equilibrium Models. Appl. Calorim. Wide Context - Differ. Scanning Calorim. Isothermal Titration Calorim. Microcalorim. (2013). doi:10.5772/53311

37. Gouin, S. & Winnik, F. M. Quantitative assays of the amount of diethylenetriaminepentaacetic acid conjugated to water-soluble polymers using isothermal titration calorimetry and colorimetry. Bioconjug. Chem. 12, 372–377 (2001).

38. Oh, E. J. et al. Control of the molecular degradation of hyaluronic acid hydrogels for tissue augmentation. J. Biomed. Mater. Res. A 86, 685–693 (2008).

39. Stejskal, E. O. & Tanner, J. E. Spin Diffusion Measurements: Spin Echoes in the Presence of a Time-Dependent Field Gradient. J. Chem. Phys. 42, 288–292 (1965).

40. Budkov, Y. A., Kolesnikov, A. L., Georgi, N. & Kiselev, M. G. A flexible polymer chain in a critical solvent: Coil or globule? EPL Europhys. Lett. 109, 36005 (2015).

41. Flory, P. J. Thermodynamics of High Polymer Solutions. J. Chem. Phys. 10, 51–61 (1942).

42. Ponsiglione, A. M., Russo, M., Netti, P. A. & Torino, E. Impact of biopolymer matrices on relaxometric properties of contrast agents. Interface Focus 6, (2016).

43. Russo, M., Bevilacqua, P., Netti, P. A. & Torino, E. A Microfluidic Platform to design crosslinked Hyaluronic Acid Nanoparticles (cHANPs) for enhanced MRI. Sci. Rep. 6, 37906 (2016).

44. Russo, M., Ponsiglione, A. M., Forte, E., Netti, P. A. & Torino, E. Hydrodenticity to enhance relaxivity of gadolinium-DTPA within crosslinked hyaluronic acid nanoparticles. Nanomed. 12, 2199–2210 (2017).

45. Strain, S. M., Fesik, S. W. & Armitage, I. M. Structure and metal-binding properties of lipopolysaccharides from heptoseless mutants of Escherichia coli studied by 13C and 31P nuclear magnetic resonance. J. Biol. Chem. 258, 13466–13477 (1983).

46. Prudêncio, M. et al. A caged lanthanide complex as a paramagnetic shift agent for protein NMR. Chem. Weinh. Bergstr. Ger. 10, 3252–3260 (2004).

47. Yoshida, H., Hatakeyama, T. & Hatakeyama, H. Characterization of water in polysaccharide hydrogels by DSC. J. Therm. Anal. 40, 483–489 (1993).

48. Yoshida, H., Hatakeyama, T. & Hatakeyama, H. Effect of Water on the Main Chain Motion of Polysaccharide Hydrogels. in Viscoelasticity of Biomaterials 489, 217–230 (American Chemical Society, 1992).

49. Panagopoulou, A. et al. Glass Transition and Water Dynamics in Hyaluronic Acid Hydrogels. Food Biophys. 8, 192–202 (2013).

50. Caravan, P., Farrar, C. T., Frullano, L. & Uppal, R. Influence of molecular parameters and increasing magnetic field strength on relaxivity of gadolinium- and manganese-based T1 contrast agents. Contrast Media Mol. Imaging 4, 89–100 (2009).

51. Debroye, E. & Parac-Vogt, T. N. Towards polymetallic lanthanide complexes as dual contrast agents for magnetic resonance and optical imaging. Chem. Soc. Rev. 43, 8178–8192 (2014).

52. Port, M. et al. Impact of rigidification on relaxometric properties of a tricyclic tetraazatriacetic gadolinium chelate. Contrast Media Mol. Imaging 1, 121–127 (2006).

53. Hermann, P., Kotek, J., Kubícek, V. & Lukes, I. Gadolinium(III) complexes as MRI contrast agents: ligand design and properties of the complexes. Dalton Trans. Camb. Engl. 2003 3027–3047 (2008). doi:10.1039/b719704g

54. Diao, Y. et al. Gel-induced selective crystallization of polymorphs. J. Am. Chem. Soc. 134, 673–684 (2012).

55. Shogbon, C. B., Brousseau, J.-L., Zhang, H., Benicewicz, B. C. & Akpalu, Y. A. Determination of the Molecular Parameters and Studies of the Chain Conformation of Polybenzimidazole in DMAc/LiCl. Macromolecules 39, 9409–9418 (2006).

56. Tao, Z. Molecular Dynamics Simulation Study of PEO-based Polymer Electrolytes in Aqueous Solution. 132

57. Teraoka, I. Polymer solutions: An introduction to physical properties. (2002).

58. Shetye, S. P., Godbole, D. A., Shilpa, D. & Gajare, P. Hydrogels: Introduction, Preparation, Characterization and Applications. 1, 25

59. Tondera, C. et al. In Vivo Examination of an Injectable Hydrogel System Crosslinked by Peptide–Oligosaccharide Interaction in Immunocompetent Nude Mice. Adv. Funct. Mater. 27, 1605189 (2017).

60. Pasqui, D. et al. Polysaccharide-Based Hydrogels: The Key Role of Water in Affecting Mechanical Properties. Polymers 4, 1517–1534 (2012).

61. Mikhailov, O. V. Molecular nanotechnologies of gelatin-immobilization using macrocyclic metal chelates. Nano Rev. 5, (2014).

62. Riess, G. Micellization of block copolymers. Prog. Polym. Sci. 28, 1107–1170 (2003).

63. Pomogailo, P. A. D. Polvmer-Immobilised Clusters of (he Platinum Group Metals. 11

64. Sethi, R. et al. Enhanced relaxivity of Gd3+-based contrast agents geometrically confined within porous nanoconstructs. Contrast Media Mol. Imaging 7, (2012).

65. Aime, S., Frullano, L. & Crich, S. G. Compartmentalization of a Gadolinium Complex in the Apoferritin Cavity: A Route To Obtain High Relaxivity Contrast Agents for Magnetic Resonance Imaging. Angew. Chem. 114, 1059–1061 (2002).

66. Vogler, E. A. Role of Water in Biomaterials.

67. Průšová, A., Šmejkalová, D., Chytil, M., Velebný, V. & Kučerík, J. An alternative DSC approach to study hydration of hyaluronan. Carbohydr. Polym. 82, 498–503 (2010).

68. Ivanov, D. & Neamtu, A. MOLECULAR DYNAMICS EVALUATION OF HYALURONAN INTERACTIONS WITH DIMETHYLSILANEDIOL IN AQUEOUS SOLUTION. 10

69. Guillaumie, F. et al. Comparative studies of various hyaluronic acids produced by microbial fermentation for potential topical ophthalmic applications. J. Biomed. Mater. Res. A 92, 1421–1430 (2010).

70. Velasco, D., Tumarkin, E. & Kumacheva, E. Microfluidic encapsulation of cells in polymer microgels. Small Weinh. Bergstr. Ger. 8, 1633–1642 (2012).

71. Peppas, N. A., Huang, Y., Torres-Lugo, M., Ward, J. H. & Zhang, J. Physicochemical foundations and structural design of hydrogels in medicine and biology. Annu. Rev. Biomed. Eng. 2, 9–29 (2000).

72. Johnson, D. L. Elastodynamics of gels. J. Chem. Phys. 77, 1531–1539 (1982).

73. Ström, A., Larsson, A. & Okay, O. Preparation and physical properties of hyaluronic acid-based cryogels. J. Appl. Polym. Sci. 132, art. no. 42194 (2015).

74. Utech, S. & Boccaccini, A. R. A review of hydrogel-based composites for biomedical applications: enhancement of hydrogel properties by addition of rigid inorganic fillers. J. Mater. Sci. 51, 271–310 (2016).

75. Phinikaridou, A. et al. Noninvasive magnetic resonance imaging evaluation of endothelial permeability in murine atherosclerosis using an albumin-binding contrast agent. Circulation 126, 707–719 (2012).

Chapter 4.

APPLICATION OF THE HYDRODENTICITY TO THE DESIGN OF NANOSTRUCTURES FOR ENHANCED MRI

4.1. SUMMARY OF THE CHAPTER

Recently, rational design of a new class of contrast agents (CAs), based on biopolymers (hydrogels), have received considerable attention in Magnetic Resonance Imaging (MRI) diagnostic field. Several strategies have been adopted to improve relaxivity without chemical modification of the commercial CAs, however, understanding the MRI enhancement mechanism remains a challenge.

Here, the effect of the hydration of the hydrogel structure on the relaxometric properties, called *Hydrodenticity*, is used to develop Gadolinium-based polymer nanovectors with improved MRI relaxation time.

The ability to tune the hydrogel structure is first proved through a high pressure homogenization technique. Then, a Microfluidic Flow-Focusing approach able to produce crosslinked Hyaluronic Acid Nanoparticles (cHANPs),analyzed regarding the crosslink density and mesh size, and connected to the characteristic correlation times of the Gd-DTPA.

Hydrodenticity explains the boosting (up to 12 times) of the Gd-DTPA relaxivity by tuning hydrogel structural parameters, potentially enabling the reduction of the administration dosage as approved for clinical use.

The experimental results indicate that the entrapment of metal chelates in hydrogel nanostructures offers a versatile platform for developing different high performing CAs for diagnosis of diseases.

4.2. INTRODUCTION

We have recently published some works in this field explaining the impact of biopolymer matrices on relaxometric properties of CAs and showing a microfluidic approach to produce hydrogel nanoparticles loading clinical relevant Gd-based CAs, improving relaxometric properties of CAs without their chemical modification [93]. Other authors also proposed some strategies to fabricate nanostructures based on the effect of rigidification and confinement of metal-chelates to boost relaxometric properties [27,51,80,151].

Despite the valuable role of the CAs for MRI, this case history confirms the importance of developing systems able to enhance relaxivity of clinical relevant Gd-based CAs and also to protect the chelate from transmetallation phenomena and control accumulation and clearance in a specific organ [152,153].

In this scenario, we have proved that, by changing structural parameters of an hydrogel matrix containing a CA through a Microfluidic Flow-Focusing approach, it is possible to affect the dipolar coupling between the electronic magnetic moment of the metal ion and the nuclear magnetic moment of the water protons (relaxation rate). This effect results from the complex equilibrium established by the elastic stretches of polymer chains, water osmotic pressure and hydration degree of GdCAs, that we have called *Hydrodenticity.*

Hydrodenticity, hence, refers to the status of the hydrated Gd-DTPA with the coordination water subjected to osmotic pressure deriving from elastodynamics equilibrium of swollen gels [148,149,154]. We hypothesize that the attainment of this equilibrium is reached when the normal energetic stability of the meshes is compromised by the presence of the Gd-DTPA and evolves to a new spontaneous

equilibrium involving the formation of nanocompartments, called “Gado-Meshes”, in which water is in an abnormal aggregate state that influences the relaxivity. The capability to control the organization of these nanocompartments within the nanoparticles can be applied to define a new class of medical products useful to improve the properties of CAs for MRI.

The tunability of the hydrogel properties is here achieved by two approaches: (1) high pressure homogenization; (2) microfluidic flow focusing approach.

Within the nanostructures, the properties of *Hydrodenticity* can be modulated to obtain desired crosslink density, mesh size, hydrophilicity and loading capability, playing on the biodegradable behavior and relaxometric properties of the Gd-loaded nanostructures.

4.3. HIGH PRESSURE HOMOGENIZATION TO PRODUCE POLYMER NANOPARTICLES BASED ON HYDRODENTICITY

Recent recommendations from Food and Drug Administration (FDA) and European Medicine Agency (EMA) about the Gd deposition in the brain and other tissues have highlighted the importance to design polymer biocompatible NPs with enhanced relaxivity without chemical modification of the clinical relevant CAs [38,155]. Thus, crosslinked NPs formed by HA, a biodegradable, biocompatible, non-toxic, non-immunogenic and non-inflammatory linear polysaccharide [156], could represent a successful candidate among nanovectors for MRI applications [157]. Indeed, in the last decades, it is undisputed the growing research interest toward the therapeutic action of HA and in developing new diagnostic tools based on this polymer [157]. In this work, starting from the above-presented results, we aim to apply the *Hydrodencity* in the design of biocompatible hydrogel nanostructures to obtain improved relaxometric properties. We propose a concrete example of the concept of *Hydrodenticity* applied to the production of crosslinked HA NPs for MRI, loaded with Gd-DTPA. An emulsion-based method is used to obtain stable W/O nanoemulsions as templates.

4.3.1. STUDY OF EMULSION STABILITY

Stable W/O emulsions are prepared by stirring appropriate amounts of oil phase (Mineral oil) and aqueous phase containing different concentrations of Span-80 (S80) or S80 with Tween-85 (S80/T85). The pH, ranging from 12 to 14 is adjusted by adding appropriate amounts of NaOH from a stock solution (0.2 M). Further details are reported in the Materials and Method Section. As expected, in the absence of any surfactant, W/O emulsions prepared in the same conditions split very rapidly in two phases due to their unfavourable thermo-dynamic state. Visual comparison, turbidimetry and backscattering are successfully used to study emulsion stability (see also Supporting Information) [158]. Comparing emulsions obtained at different W/O ratio, 10:90 and 20:80, but at same concentration of surfactant, the stability is more extended for emulsions with lower water content. In particular, a formulation 10/90 W/O volume ratio containing S80 (1% w/v) and T85 (0.5 % w/v) resulted the more stable. However, even though the stability of the emulsion is crucial to reduce polydispersity, an alkaline environment (addition of NaOH) is necessary for the crosslinking reaction to take place. Indeed, Balazs and Leshchiner [159] showed that the crosslinking reaction starts shortly after addition of DVS (5 - 10 min) and, that, 1 hour is sufficient for the completion of the reaction [160,161]. On the basis of these requirements, to conduct the experiments, we select the formulation with S80 (1% w/v) and NaOH (0.2 M) as the optimal trade-off to obtain an emulsion stable for at least 3 hours (see also Supporting Information), enough for the DVS to react.

4.3.2. Preparation of DVS-crosslinked nanoparticles with and without CA

The exploitation of the best process conditions to design biocompatible nanostructures based on *Hydrodenticity* and control their relaxation parameters for MRI application is reported. In particular, the effect of the homogenization, HA concentration and the role of the crosslinking reaction is analysed. Different experimental parameters and conditions are tested and details are reported in the Materials and Methods section. A preliminary mixing is performed at 5000 or 7000 rpm for 10 min, by keeping constant the temperature at 25 °C. A 5000 rpm speed is preferred to avoid and uncontrolled increasing of the temperature.

After the homogenization, a crosslinking reaction is performed at high pH values (12 - 14) and creates sulfonyl bis-ethyl linkages between the hydroxyl groups of HA [162]. This crosslinking method has the advantage of occurring at room temperature, which limits the degradation of HA in alkaline solutions. Even though the starting material DVS is highly reactive and toxic, the biocompatibility of the HA-DVS hydrogels are confirmed by histological analysis [123].

In our protocol, a study of the modalities of injection of the crosslinking agent at different steps of the homogenization process has shown that only when DVS is added after the homogenization step spherical NPs are obtained. On the contrary, when the addition of the crosslinker is performed at any time point during the homogenization phase, a shear stress behaviour of the polymer phase, interfering with the formation of that particles, is observed (see Supporting Information).

The best experimental condition for production of crosslinked NPs is reached at 0.045% v/v DVS (see Supporting Information).

Based on these results and using the same process conditions, loaded NPs are obtained by adding the CA in the water phase of the emulsion. Among several FDA approved CAs, we have chosen to encapsulate a Gd chelated, Gd-DTPA (9.13 mM).

4.3.3. Purification and characterization of HA-NPs

Ultracentrifugation (UC) and dialysis are performed to purify HA NPs. Dynamic Light Scattering (DLS) measurements are made on aqueous dilute NP suspension (1:10). The smaller NPs' size without CA (217.57 ± 34.65 nm) is obtained at 0.25% w/v of HA solution. At higher polymer concentration (0.5% w/v) particle size is higher (401.67± 77,65 nm), while the formulation with 0.1% w/v HA shows a reverse phenomenon with larger particles (760.15 ± 86 nm), probably due to less stability of the nuclei that tend to coalesce. When Gd-DTPA is added to the process, the particle size at HA 0.25% w/v is slightly increased (258.77 ± 15.65 nm) for the same process conditions. After purification, NPs are investigated by electron microscopy techniques (SEM and TEM). The morphology of the NPs observed revealed that the particles are spherical in shape and monodisperse (see Supporting Information).

Loading Capability (LC) and Encapsulation Efficiency (EE) is determined through ICP-MS by comparing the theoretical amount initially used to prepare the particles and the Gd encapsulated in the system after ultracentrifugation. The higher encapsulation results for 0.25 % w/v HA (1:2 w/w HA/Gd-DTPA ratio). Results show that probably ionic nature of Gd-DTPA impacts on its encapsulation. The zeta potential value of the 0.25% HA-NPs, with and without CA, indicate that they had a negatively charged surface (-37.4 ± 1.34 mV and -31.8 ± 0.88 mV, respectively), due to the carboxylic group of HA.

4.3.4. RELAXIVITY STUDIES

T1 and T2 measurements at 60 MHz (1.5 Tesla) and 120 MHz (3 Tesla): Relaxivity and relaxation times are measured for both unloaded and loaded NPs and compared with free Gd-DTPA solution. Measurements are performed on a 120 MHz (3 Tesla) MRI system and on a 60 MHz (1.5 T) benchtop relaxometer.

Relaxivity results obtained at 120 MHz are presented on a per millimolar Gd basis in Figure 4.1 and show a maximum r1 of 33.3 $s^{-1}mM^{-1}$ (i.e. 10 times higher compared to free Gd-DTPA). Even though all the proposed formulations of Gd-DTPA-loaded HA nanostructures show an increase of the r1 signal, as reported in Figure 4.1A, the highest boosting of the relaxivity is provided by the NPs obtained using the formulation at 0.25% HA and 1:2 w/w HA/Gd-DTPA (Figure 4.1A-C).

A)

Sample	r_1 [$mM^{-1}s^{-1}$]
Gd-DTPA	3.59 ± 0.27
Gd-loaded 0.1% HA-NPs	15.4 ± 1.081
Gd-loaded 0.25% HA-NPs	33.3 ± 3.908
Gd-loaded 0.5% HA-NPs	23.9 ± 1.296

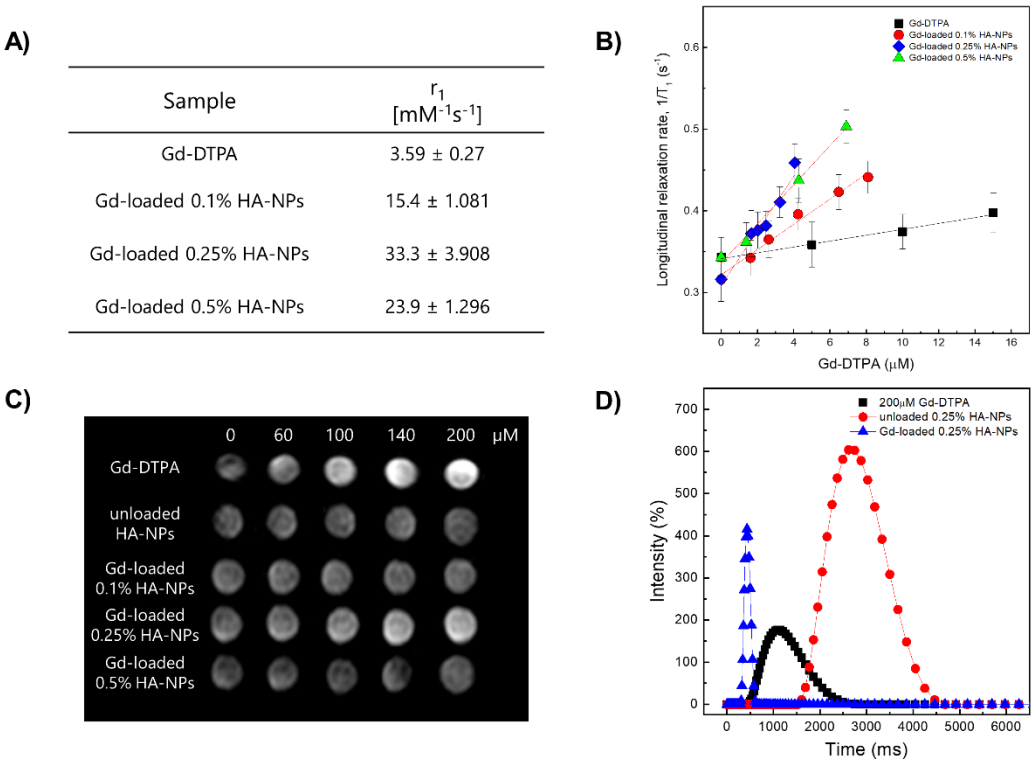

Figure 4.1 (A) Relaxivity values r1 determined at magnetic field strengths of 3T for different set of HA-NPs with respect to free Gd-DTPA in water. (B) Longitudinal relaxation rate (1/T1) versus Gd-DTPA concentration for free Gd-DTPA in water and for HA-NPs at different polymer concentrations loaded with Gd-DTPA. (C) T1-weighted images of Gd-DTPA, unloaded (used as control) and HA-NPs at different polymer concentrations loaded with Gd-DTPA. All samples are imaged at 3T, 25°C, using standard spin echo (SE) sequence. (D) Distribution of longitudinal relaxation times of (T1) of 200 μM Gd-DTPA in water (squares), unloaded 0.25% HA-NPs (circles) and 0.25% HA-NPs loaded with 200 μM Gd-DTPA (triangles).

T1 relaxation time distributions at 37°C and 60 MHz are investigated for loaded and unloaded NPs (HA at 0.25% w/v) as well as for free Gd-DTPA solution (Figure 4.1D). Compared to the 200 μM free Gd-DTPA solution, which shows a broad distribution around 1000 ms, NPs loaded with 200 μM Gd-DTPA exhibit an excellent T1 distribution with a sharp peak centered below 500 ms. Gd concentration within loaded NPs was determined through Inductively Coupled Plasma Mass Spectrometry (ICP-MS).

Loaded NPs perform far better even compared to the unloaded ones, whose distribution appears to be broad and centered around 2800 ms.

It is worth mentioning that, compared to T1 distribution for bulk water (3600 ms), unloaded NPs' distribution shows that a slight contribution to the longitudinal relaxivity is ascribable to the crosslinked polymer nanostructure, which is able by itself to tune the water mobility for a non-nanostructured material. The contribution, therefore, to the overall relaxivity is further enhanced in the ternary system, thanks to the water-mediated interaction between the polymer and metal chelate.

4.3.5. MODELLING OF NMR DISPERSION: NMRD PROFILE

The NMRD profiles as function of the static magnetic field of the aqueous solutions of Gd-DTPA and loaded and unloaded NPs (Figure 4.2) are set up in order to establish the effects caused by *Hydrodenticity* functionalities on the parameters that determine the observed relaxivities.

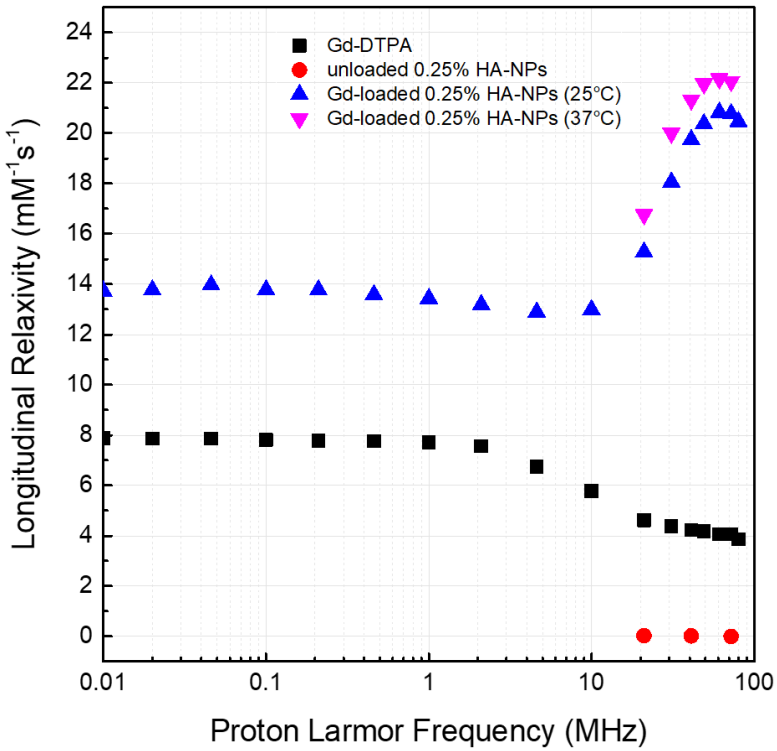

Figure 4.2 NMRD profiles showing relaxivity of Gd-DTPA in water (squares), unloaded 0.25% HA-NPs (circles), Gd-loaded 0.25% HA-NPs at 25°C (triangles) and 37°C (flipped triangles).

The longitudinal relaxation rates are recorded at 37°C as a function of resonance frequency and according to NP Gd-loading obtained by ICP-MS. The NMRD experimental curve for free Gd-DTPA shows a plateau in longitudinal relaxivity at low fields and significantly decreases as the applied magnetic field increases starting from 1 MHz. Conversely, longitudinal relaxivity (r_1) for loaded NPs (HA at 0.25% w/v) is characterized by the presence of a low-field plateau and a gradual increase starting from 10 MHz, reaching a “dispersion peak” between 60 and 70 MHz. The same peak and trend in the high field region (20 – 70 MHz) is observed for both at 25°C and 37°C. As a control, unloaded NPs do not exhibit increase in relaxivity in this field region, confirming that the nanohydrogel structure containing Gd-DTPA contributes to slowing the chelator's tumbling motion and allows water exchange

thanks to its hydrophilic properties, as hypothesized in the concept of *Hydrodenticity*.

4.3.6. DISCUSSION

The properties of *Hydrodenticity* and its application to the nanomedicine field is reported. The explanation of this concept take place through several key aspects underlying biopolymer-CA's interactions mediated by the water. A multidisciplinary approach is used: changes in polymer conformation and thermodynamic interactions of CAs and polymers in aqueous solutions are detected by isothermal calorimetric (ITC) measurements and later, these interactions are investigated at molecular level using NMR to better understand the involved the phenomena. Water molecular dynamics of these systems is also studied by means of Differential Scanning Calorimetry (DSC). In order to observe relaxometric properties variations, we have monitored the MRI enhancement of the examined structures over all the experiments.

The study of polymer-CA solutions reveals that thermodynamic interactions between biopolymers and CAs could be used to improve MRI Gd-based CA efficiency. For this reason, the optimal conditions to combine a CA with a hydrophilic biopolymer are identified and applied to the nanoscale in order to produce nanostructures of biomedical interest with high relaxivity. In particular, stable crosslinked HA NPs encapsulating Gd-DTPA are successfully prepared using a method that exploits the use of W/O nanoemulsions as templates. The aqueous emulsion droplets are shown to provide a good environment for the formation of the NPs and seemed to limit efficiently their size. NPs collected from the emulsion droplets using a purification procedure showed a size of about 200 nm and spherical shape.

The conditions of the herein presented protocol to produce these biocompatible NPs offer advantages for the encapsulation of a broad-spectrum of biomolecules and provide a potential synthetic route to design a wide range of highly efficient nanostructured MRI CAs, letting the surface available for possible functionalization.

In conclusion, this work proves that a new generation of more efficient CAs can be developed by exploiting the affinity between CAs and biopolymers. It can be done using biocompatible and clinical relevant CAs without their chemical modification as approved in the clinical practice. Furthermore, the size of the resulting NPs is in a range that makes them suitable for delivery to cells and certain tissues and further increase in relaxivity can be potentially achieved by tuning the system to the most efficient structure by choosing the correct biopolymer-CA combination and optimizing concentration and crosslinking degree of the structure. From a biomedical point of view, the possibility to tune relaxometric properties of CAs by controlling hydrogel structural parameters can pave the way to new advancements in the design of nanovectors for diagnosis and therapy. Despite the promising achievements, further studies are needed to carry out a deeper investigation and a full validation our intriguing hypothesis.

4.4. MICROFLUIDIC FLOW FOCUSING APPROACH TO PRODUCE POLYMER NANOPARTICLES BASED ON HYDRODENTICITY

4.4.1. PREPARATION OF CROSSLINKED HYALURONIC ACID NANOPARTICLES (CHANPS)

Microfluidic Flow-Focusing (MFF) systems have already been explored for the production of polymer micelles and nanoparticles [163,164]. However, an investigation of the opportunity that this approach could bring to the MRI field, given the impact of the hydrogel behaviour on the relaxometric properties, is still missing. We have recently demonstrated that, through the microfluidics, it is possible to produce stable and hydrogel nanoparticles with improved relaxometric properties [93]. Briefly, by changing the relative flow rates and the concentration of the species in the streams, we can control nanoprecipitation phenomena [164–166] and achieve the formation of small nanoparticles (see Supporting Information). In our system, starting from an HA 0.05% w/v solution, monodisperse and nanoparticles smaller than 40 nm are obtained (see Supporting Information). Subsequently, a crosslinking reaction is performed together with the formation of nanoparticles using DVS [161,167–170] as crosslinking agent at standard flow conditions. In the same work[35], we have also reported two effective crosslinking scenarios to explore and control the nature of the

interference (see Supporting Information) between the Gd-DTPA and the flow focused nanoprecipitation: **(1)** premixing of DVS into the middle channel at controlled temperature and surfactant concentration; **(2)** addition of DVS to the side channels by strictly controlling pH conditions. Both strategies, exploited through the Microfluidic Platform, have been already reported and further details in terms of crosslinking reaction and loading capability are reported in the Supporting Information. Results showing cHANPs with different concentration of NaOH and NaCl and different types of surfactants are already reported in our previous publication. Briefly, Spherical and stable nanoparticles are obtained for both strategy but the addition of DVS to the middle channel and the use of surfactants produce a smaller size down to 35 nm.

4.4.2. SWELLING BEHAVIOUR AND HYDROGEL STRUCTURAL PARAMETERS OF CHANPS

Here, starting from results in terms of the swelling ratio, crosslink density and mesh size of the cHANPs containing Gd-DTPA are discussed, aiming to evaluate the modulation of the hydrogel structure in the presence of Gd-DTPA.

As far as the swelling behaviour of the nanoparticles, results at different DVS amounts are reported in Figure 4.3a and presented in terms of swelling ratio, as defined in the Method Section.

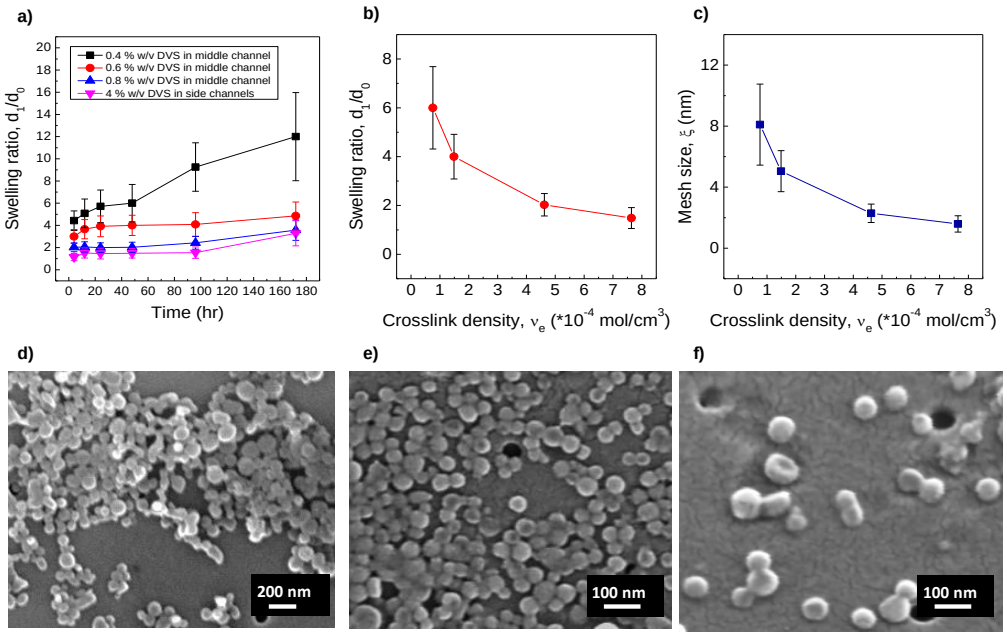

Figure 4.3 Swelling behaviour and hydrogel parameters of cHANPs. (a) Swelling ratio of of Gd-DTPA loaded cHANPs versus time at different DVS concentrations obtained according to the first (DVS in middle channel) or the second crosslinking scenario (DVS in side channels). (b) and (c) Swelling ratio (-●-) and mesh size (-■-) of Gd-DTPA loaded cHANPs versus crosslink density after 48 hours in water. d) and e) FE-SEM images of Gd-DTPA loaded cHANPs in water at 0.8% DVS (middle channel) and 4% DVS (side channels), respectively. (f) 15° C tilted FE-SEM image of Gd-DTPA loaded cHANPs at 4%.

Results clearly show that, nanoparticles are stable and do not exhibit a significant swelling behaviour until 48 h at all explored DVS conditions (see also Supporting Information). In particular, smallest nanoparticles of about 70 nm and 50 nm measured in water are only produced at DVS of 0.8% v/v and 4% v/v, respectively. For these two conditions, an increase in size up to 125 nm for 0.8% DVS and 115 nm for 4% DVS is detected only after 1 week (see Supporting Information).

Then, according to Flory-Rehner calculations, we have determined the crosslink density (ν_e) and mesh size (ξ) of cHANPs in water after 48 h (see Supporting Information). It has been already reported that lower molecular weight films gave rise to decreased molecular weights between crosslinks as well as increased effective crosslink densities and decreased mesh size, thereby indicating a more stable

structure. Even our results show that a general increase of the crosslink density of the cHANPs corresponds to an increase in the nanostructure stability, i.e. lower swelling ratio (Figure 4.3b). Furthermore, as expected, by increasing the crosslink density, a reduction in mesh size is also obtained until to a certain extent (Figure 4.3c).

Field Emission Scanning Electron Microscopy (FE-SEM) images of cHANPs at 0.8% DVS (middle channel) and 4% DVS (side channels) after 48 h in water are reported in Figure 4.3d, e and f. Higher DVS concentrations cause formation of large aggregates, as shown in the Supporting Information. It is important to highlight that cHANPs are potentially safe and biocompatible; indeed, even if DVS is highly reactive and toxic, HA-DVS biocompatibility has been confirmed by histological analysis, as previously reported by Oh et al. [123]

4.4.3. IN VITRO RELAXOMETRIC PROPERTIES

The relationship between the measured structural parameters of the hydrogel and changes in CA's relaxivity is also examined (Figure 4.4).

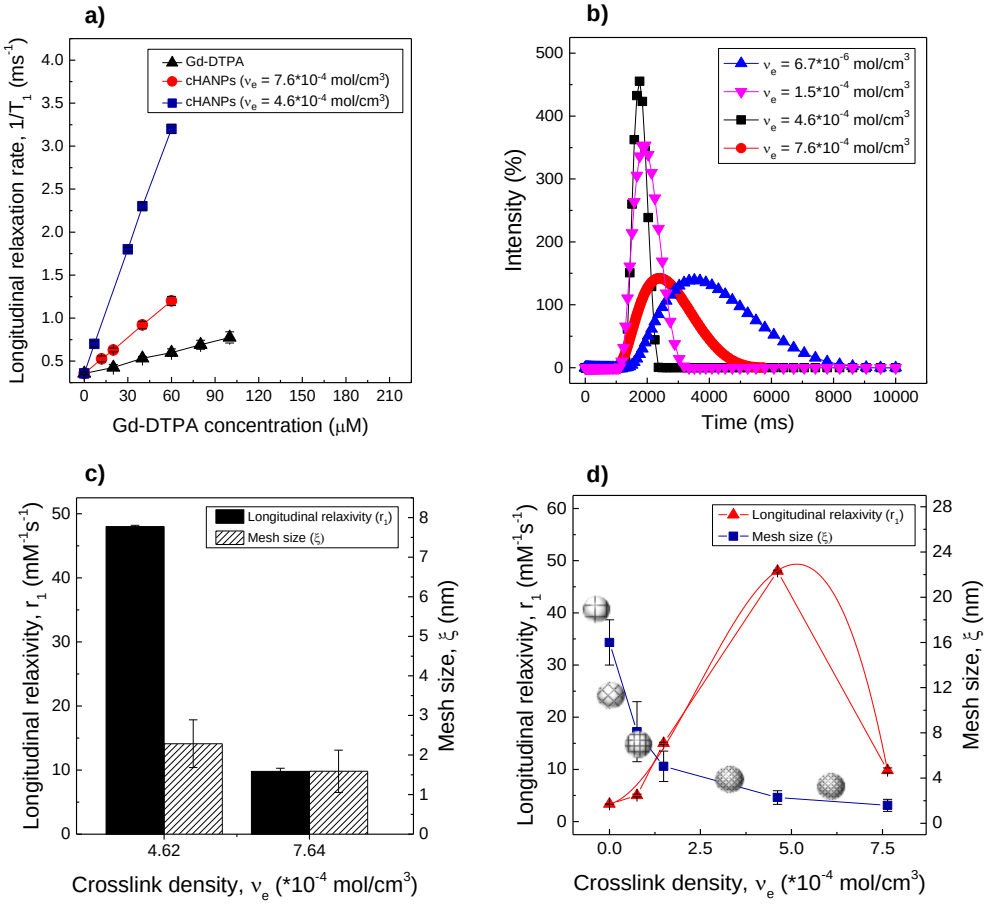

Figure 4.4 In vitro MRI and effect of the Hydrodenticity. (a) Longitudinal relaxation rate ($1/T_1$) versus Gd-DTPA concentration for (-▲-) free Gd-DTPA in water and for Gd-DTPA loaded cHANPs at different crosslink densities (-●- 7.6*10^{-4} and -■- 4.6*10^{-4} mol/cm^3), showing a relaxivity of 3.9 mM^{-1}s^{-1}, 14.09 mM^{-1}s^{-1} and 48.97 mM^{-1}s^{-1} respectively. (b) Longitudinal relaxation time distribution for cHANPs at different crosslink densities. (c) Bar chart of longitudinal relaxivity (gray columns) and mesh size (blue columns) values for cHANPs at different crosslink densities. (d) Mesh size versus crosslink density (-■-) and corresponding relaxivity values (-▲-) along with a graphical representation of cHANPs' polymer network at different mesh size values.

Given the versatility of the produced cHANPs, it is of particular interest to investigate how different reaction's strategies and formulations could result in advanced and tailorable CAs-loading functionalities. In vitro relaxivity is studied for

loaded and unloaded cHANPs and the results are presented for Gd-DTPA in water at different concentrations. For all MR experiments, T_1 values measured on loaded cHANPs show a higher relaxation rate compared to the relative "free" CA, confirming that active compounds are not only dispersed or encapsulated but even wrapped within the hydrogel polymer matrix of cHANPs. Besides, it is observed that the hydrogel structural parameters, i.e. crosslink density and mesh size, can affect not only the stability and degradation behaviour but also the MR functionality of the produced nanoparticles. Indeed, loaded cHANPs with different crosslink densities show a relaxivity (r_1) of about 48.97 $mM^{-1}s^{-1}$ and 14.09 $mM^{-1}s^{-1}$ respectively (Figure 4.4a, squares and circles). Both values are considerably higher than the value of 3.9 $mM^{-1}s^{-1}$ reported for commercial Magnevist (Figure 4.4a, triangles).

Additionally, a change in the crosslink densities of cHANPs causes differences in longitudinal relaxation time distributions (Figure 4.4b). A narrow distribution is obtained at a crosslink density of about $4.62*10^{-4}$ mol/cm^3, reflecting optimal equilibrium conditions able to boost the MRI signal. Contrary to expectations, further increase in the crosslink density does not allow a sharper relaxation time distribution, even at smaller mesh sizes. As shown in Figure 4.4c, in fact, even if the mesh sizes computed at two different crosslink densities are quite similar (1.5 nm and 2 nm for crosslink densities of $7.64*10^{-4}$ mol/cm^3 and $4.62*10^{-4}$ mol/cm^3, respectively), the highest relaxivity is not observed at the maximum crosslink density. This observation strengthens the hypothesis that an optimal equilibrium among the species should be achieved in order to boost the relaxometric properties and that the hydrogel structure plays a critical role in the relaxation enhancement (see Figure 4.4d).

For completeness, we have also evaluated the relaxivity of unloaded cHANPs and cHANPs entrapping Gd-DTPA by sorption and compared with free Gd-DTPA in water (see Supporting Information).

The comparison of MRI relaxivity values acquired for cHANPs and free Gd-DTPA supports our initial hypothesis made on *Hydrodenticity*, revealing the opportunity to select specifically the optimal range of conditions that promotes relaxation enhancement (Figure 4.4d). Hence, the high relaxivity is attributed to the equilibrium simultaneously achieved between the water content within the hydrogel structures,

expelled or retained during nanoprecipitation and crosslinking reaction, and the amount of Gd-DTPA entrapped in the formed matrix.

4.4.4. DISCUSSION

By the above-reported experiments, we have proved that a systematic and accurate tunability can be achieved by varying the crosslinking degree of the hydrogel nanoparticles in the presence of Gd-DTPA. A narrow or a broad distribution of relaxation rates on the crosslink density is shown with regards to changes in the water dynamics, hydrogel conformation and slow motion of the CAs. High control of these parameters is mainly reached through a MFF approach [93].

Starting from the observation of a peculiar swelling behaviour (Figure 4.3a) and in vitro relaxometric properties of the cHANPs (Figure 4.4), we propose an explanation, through a modified Flory Rehner theory, of how the hydrogel structural parameters can be used to improve the relaxometric properties of CAs [161].

Results show that *Hydrodenticity* can be proposed as a new concept to summarize the complex equilibrium formed by elastic stretches of polymer chains, water osmotic pressure and hydration degree of GdCAs able to boost the relaxivity.

Indeed, at the achieved minimum mesh size, crosslink density is responsible for the elastodynamic of the hydrogel and is representative of the water amount within the polymer meshes, which in turn is related to the osmotic pressure. Our results also show that the reduction in the elasticity of the matrix by increasing the crosslink density does not correspond to a maximum enhancement of the relaxivity (see Figure 4.4d). It is probably due to the expelled water from the hydrogel network that causes a reduction in the osmotic pressure within the water compartments of the meshes and a decrease of the hydrated status of Gd-DTPA, thus limiting the enhancement of the relaxometric properties in the nanostructures. These conditions promote the formation of water compartments containing Gd-DTPA called “Gado-Meshes”.

It is also well-known that the crosslink density also acts on the water diffusion, which decreases when the crosslink density increases and its slowdown in diffusion is more severe at the polymer-water interface [117,171]. Even in the Gd-loaded cHANPs, the water diffusion at various crosslink densities is correlated with the water

hydrogen bonding dynamics, and the variation of diffusion coefficient with crosslink density is related to the variation of water content in different crosslink densities. Therefore, by changing further the properties of the "Gado-Meshes" through the crosslinking reaction, relaxivity increases to an even greater extent due to the *Hydrodenticity* because of the tuning of the crosslink density and, consequently, of the aggregated water state and slow moving of the CAs.

As the *Hydrodenticity* of CAs within the Gado-Mesh does not involve the chemical modification of the CAs, the observed enhancement in relaxivity is induced by the synergistic interaction of the aggregated water with the hydrogel matrix and Gd-DTPA. Indeed, according to the Solomon- Bloembergen-Morgan theory, this effect promotes both (§) a further reduction of the water mobility and diffusion, inducing an increase of the residence lifetime (τ_M) and characteristic diffusion time (τ_D) of both IS and OS; and (§§) changes in hydrogel structures leading to the formation of nanocompartments enwrapping Gd-based CAs, causing a slow motion of the CAs and, therefore, an increase of the rotational correlation time (τ_R) of the chelate. Furthermore, it is reasonable that the conditions reached in the Gado-Mesh can control the water exchange and, therefore, the relaxivity. Indeed, relaxivity can be limited if the water exchange is too slow because the relaxation effect is poorly transmitted to the bulk. However, relaxivity can also be reduced if the water exchange is too fast because the water is not coordinated to the GdCAs long enough to be relaxed [172].

In the proposed system, at some degree of *Hydrodenticity*, the hydrated status of Gd complexes, the elastodynamic response of HA and the osmotic pressure result probably in a much slower rotation. At this point, the importance of water exchange becomes significant, but the improved relaxivity of Gd-loaded cHANPs confirms that water diffusion is high enough, and the process for relaxing the water protons of aggregated water is in any case very efficient. Finally, the relaxation time measurements clearly demonstrate how cHANPs themselves do not contribute to the relaxivity of the system (see Supporting Information). Thus, the increase in the relaxivity of the loaded cHANPs can be attributed solely to the formation of the Gado-Mesh and to the *Hydrodenticity* achieved in their organization that influences the relaxivity through the characteristic correlation times above mentioned.

Modulation of the *Hydrodenticity* through the: (i) elastic stretching of the polymer meshes (ii) osmotic pressure and (iii) hydrated state of Gd-DTPA contributes to the changes of the Inner and Outer-Sphere mechanisms of the CAs. Therefore, through the hydrogel structural parameters, we can produce a library of functional nanostructures on the needs of a particular pathology, field and material properties. Results could lead to the identification of a personalized diagnostic window (Figure 4.5) that can define the range of optimal properties between the hydrogel matrix and the CAs, being more efficient in treating a particular disease, avoiding toxic effects and increasing the performance of the MRI acquisitions.

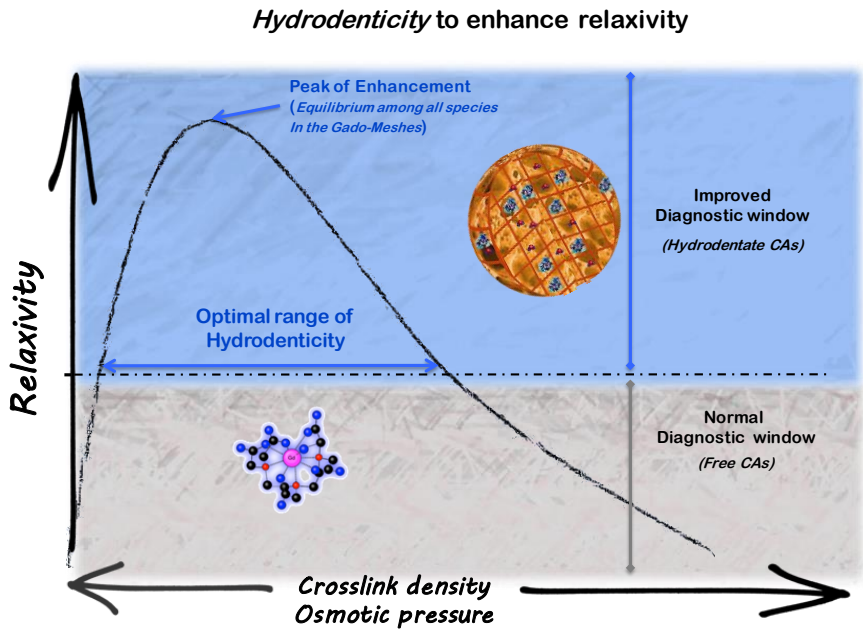

Figure 4.5 ***Hydrodenticity*** **to enhance relaxivity.** Schematic illustration of an improved diagnostic window in which it is possible to obtain a medical device for clinical use in the MRI field able to overcome the limitations related to the use of commercial CAs such as low relaxivity, limited acquisition time and reduced tissue specificity.

The introduction of the *Hydrodenticity* creates significant opportunities in controlling the behaviour of metal chelates without their chemical modifications. It

enables the increase of the relaxometric properties of the CA preserving the chemical structures as approved for the use in the clinical practice. The possibility to increase the sensitivity of the CAs represents an opportunity to reduce the administration dosage currently in use.

Furthermore, Gd-loaded cHANPs based on the concept of *Hydrodenticity* are candidate to become an important nanomedicine tool to be tested in this direction, exhibiting a relaxivity value of ~ 48.9 $mM^{-1}s^{-1}$ and ~ 14.02 $mM^{-1}s^{-1}$. Additionally, cHANPs have an average diameter of about 35 nm, do not swell and degrade for at least 48 h under shaking. Further benefits can be found in the possibility to be decorated chemically, becoming suitable for a specific target, the direct clinical application, due to the utilization and improvement of biocompatible and FDA approved products without their chemical modifications, the ease of the synthesis, the nature of the materials, and the scalability of the proposed process. In the future, the concept of *Hydrodenticity* could inspire other applications and be extended to different molecules and field of knowledge.

4.5. MICROFLUIDIC FLOW FOCUSING APPROACH TO PRODUCE COACERVATED CHITOSAN-HYALURONIC ACID NANOPARTICLES BASED ON HYDRODENTICITY

Nanostructured materials, such as polymer nanoparticles (PNPs), have attracted considerable interest over the last years due to their multifunctional properties that can be modulated depending on the particular application[173]. Indeed, PNPs are widely used for the improvement of imaging techniques and treatments. Their peculiar features can potentially reduce limitations related to the fast clearance of drugs and diagnostic agents from the bloodstream and to the low detection and therapeutic efficacy. Advantages of PNPs as nanovectors also include controlled release, protection of active molecules, specific targeting and the ability to carry one or more therapeutic and/or imaging agents at the same time for theranostic purposes[174].

Several hydrophilic polymers, such as Hyaluronic Acid (HA), Chitosan (CS) and Dextran are widely used to manufacture PNPs for biomedical applications. Among

them, HA and its derivatives have been investigated for the development of several carrier systems for cancer diagnosis, staging and therapy[157]. HA has also been used in combination with CS and the usefulness of this combination is well documented for different bio-applications, like drug delivery and diagnostics[157].

For example, Chen and co-workers[175] report a very interesting example of nanotheranostic system in which diagnosis and therapy are combined. This nanocarrier has a yolk-shell structure with a radioluminescent yolk based on Gd_2O_3: Eu nanospheres, an up conversion luminescent in a silica shell, and a coating constituted by HA/CS combination for pH-triggered drug release.

Particularly remarkable results have been achieved by Courant et al.[80], who develop a new and straightforward synthesis of high-relaxivity Gadolinium-PNPs for Magnetic Resonance Imaging (MRI) applications. For biocompatibility reasons, CS and HA are chosen as polymer matrix, which also enables a boost in the relaxivity of their Gadolinium-PNPs.

Furthermore, recently, Russo et al.[93] have produced core-shell polymer nanoparticles for multimodal imaging applications through a complex coacervation process driven by temperature. Nanovectors, made of a CS-core and a HA shell, are designed to entrap a contrast agents for MRI, boosting its performances, together with an additional optical tracer.

As outlined so far, different protocols to combine CS and HA can be implemented to prepare hybrid nanovectors. Each method needs to take into account critical factors like the nature of the encapsulated drug/agent, the drug release mechanism, the administration route and the target site. The most used techiniques include: ionotropic gelation, complex coacervation, self-assembly and nano- and micro-emulsion techniques.

Among these, the ionotropic gelation proved to be the easiest and cleaner way to synthesize chitosan-based nanoparticles (NPs). It is based on the ability of polyelectrolytes to crosslink in the presence of oppositely charge to form hydrogels. Anions forms meshwork structure through their combination with the polyvalent cations and induce gelation by binding to the anion blocks. TPP bonds to the charged amino groups of chitosan and relies only on electrostatic interaction avoiding toxicity of reagents. Temperature, pH of crosslinking solution, mixing time, mass ratio of CS

to TPP, acetic acid concentration and chitosan molecular weight are factors that affect NPs size, shape and surface charge intensity[176–180].

However, a fine control over the final product's features is difficult to achieve through the traditional preparation techniques. In these terms, microfluidic technology offers several advantages over batch processes in order to optimize quality process and produce material of required characteristics. Reactions in microfluidic devices are carried out with small amount of fluids within small channels. It enables fine control and manipulation of fluids and their interfaces, rapid and uniform heat and mass transfer thanks to the established laminar flow.

In particular, microfluidics proved to be a promising and effective tool for the rational design of PNPs as imaging probes and drug delivery systems. As showed in recent studies conducted by Russo et al.[90–94], microfluidics allows tuning nanohydrogels' structural characteristics by changing process parameters, consequently improving contrast agent encapsulation and efficacy as a result of the *Hydrodenticity* concept, defined as the equilibrium between water osmotic pressure, elastodynamics of polymer chains and hydration degree of the contrast agent responsible for the enhancement in the relaxivity of MRI contrast agents.

The aim of this work consists in the implementation of the ionotropic gelation in a microfluidic platform to produce CS-HA NPs, with the purpose to overcome some drawbacks of the traditional procedures, such as polydispersity and expensive and time-consuming purification/recovery steps.

4.5.1. NANOPARTICLES' PRODUCTION THROUGH HYDRODYNAMIC FLOW FOCUSING

Production process used to generate NPs is a *hydrodynamic flow focusing* where fluids with different velocities flow side by side into microfluidic channels. More accurately, a central stream is squeezed between two adjacent streams at higher flow rate. The ratio between the flow rate of the middle channel (μL/min) and the flow rate used for both side channels (μL/min) has been called Flow Rate Ratio (FR^2) and calculated as follows:

$$FR^2 = \frac{Flow\ Rate|_{middle\ channel}}{Flow\ Rate|_{side\ channel}}$$

A higher FR^2 leads to a narrow central stream and vice versa representing a direct way to control NPs characteristic. Hydrodynamic flow focusing and mixing process are strictly linked phenomena[181–183]. A schematic representation of the process to produce the nanoparticles is shown in Figure 4.6:

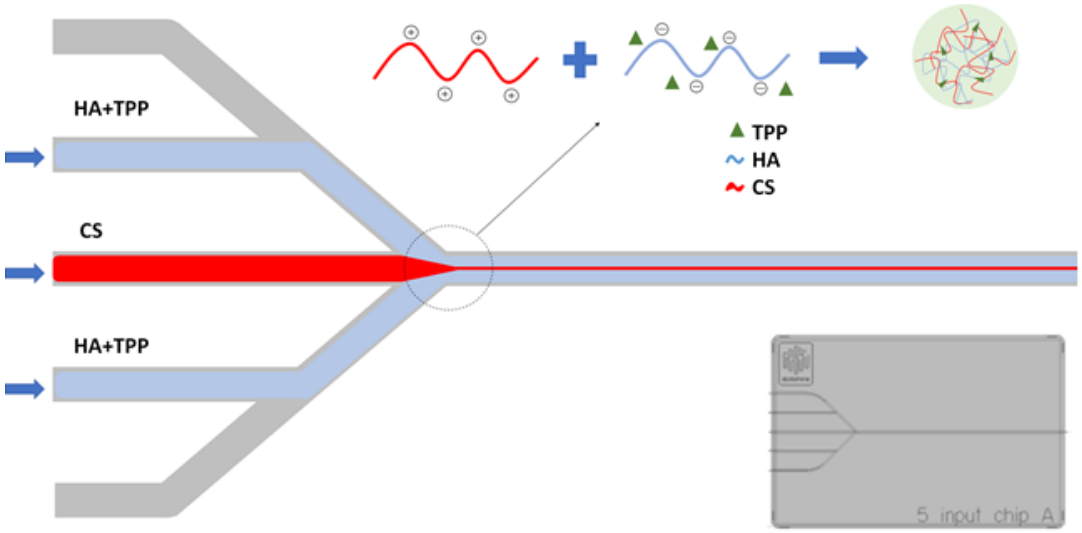

Figure 4.6 Representation of hydrodynamic flow focusing within microfluidic chip. Middle and side streams include two different polymers that leads to NPs formation through an ionotropic gelation via CS-TPP crosslinking followed by HA-CS complex coacervation.

4.5.2. Comparison between batch and microfluidic system: effect of chitosan concentration

It has been decided to start from CS:HA weight ratio used in traditional batch system, as described by Callewaert et al.[87], but using lower compounds concentrations (CS 2.5 mg/mL; HA 0.8 mg/mL; TPP 1.2 mg/mL) suitable for the microfluidic platform. SEM images reveals that, changing CS concentration at the same flow rate and CS:HA ratio, obtained coacervates show a considerable size and polydispersity reduction when CS concentration grows (Figure 4.7).

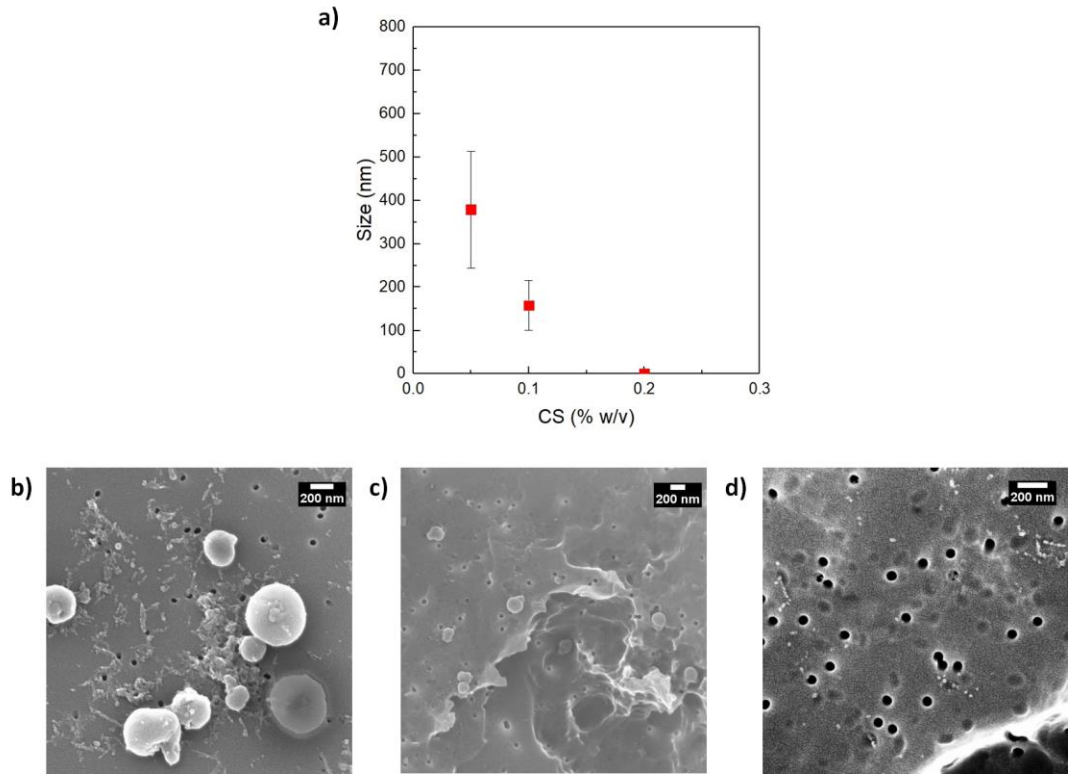

Figure 4.7 a) Tests carried out from Callawaert studies in batch with a 6 to 1 CS: HA ratio and flow rate ratio equal to 0.5 using compounds concentrations 1/400 compared to Callawaert ones (CS 2.5 mg/mL; HA 0.8 mg/mL; TPP 1.2 mg/mL). **b)** CS= 0.05 mg/mL. **c)** CS = 0.1 mg/mL. **d)** CS=0.2 mg/mL. SEM images reveal that, changing CS concentration but using the same flow rate and CS: HA ratio, obtained coacervate shows a considerable size and polydispersity reduction when CS concentration grows.

4.5.3. CONCENTRATION EFFECT AT $FR^2 = 0.5$

Experiments at fixed $FR^2 = 0.5$ have been carried out in two different conditions: (1) high flow rates, i.e. middle channel flow rate > 1 μL/min; (2) low flow rates, i.e. middle channel flow rates < 1 μL/min. In both conditions, two values of CS:HA ratio were tested.

Results show that, regardless the condition (high or low flow rates), size grows when CS: HA increases, although starting nuclei are different, and there is a double NPs population when CS: HA value is 3.125 (Figure 4.8).

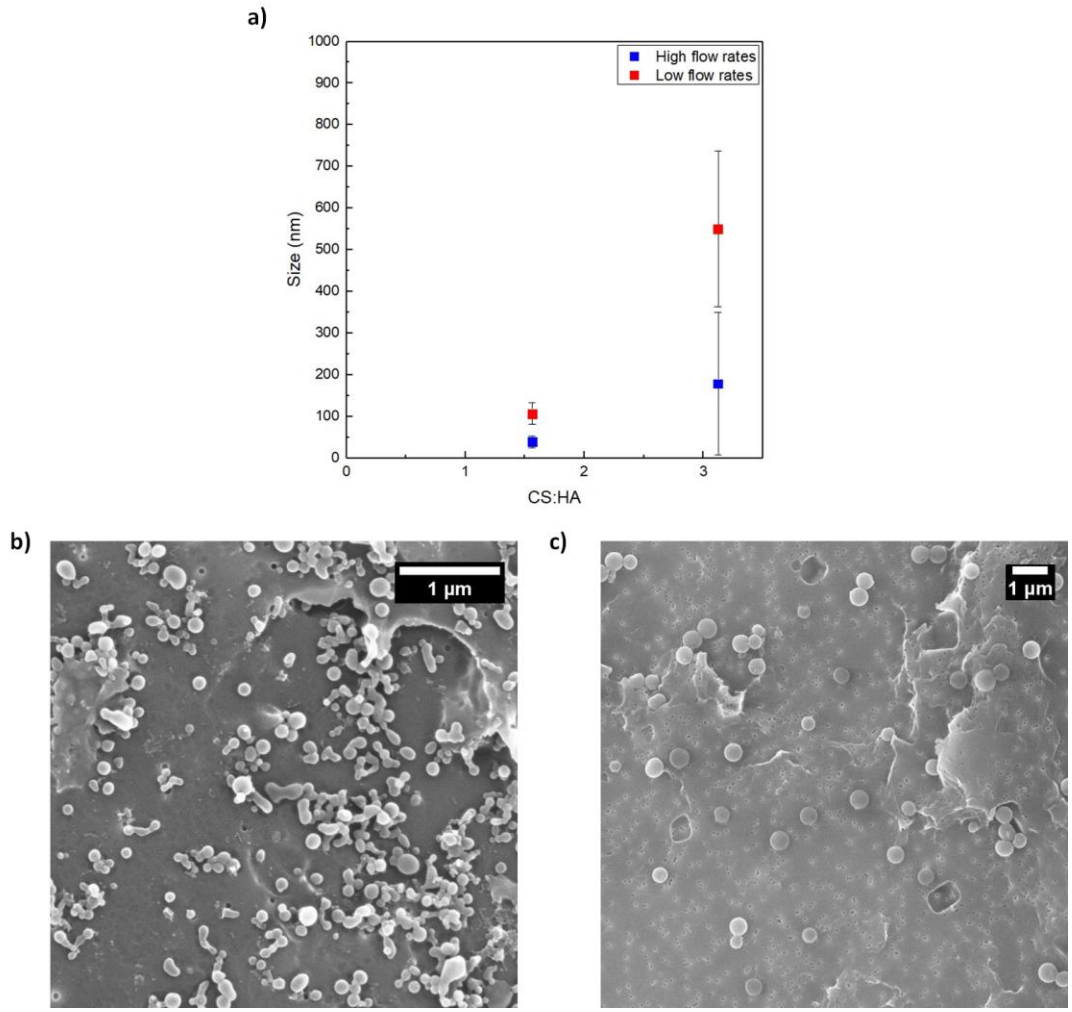

Figure 4.8 a) graphic trend of NPs size for different CS: HA ratio shows a higher standard deviation at 3.125 due to double NPs population development. Independently of high or low flow rates, size grows when CS: HA increase although starting nuclei are different. **b)** SEM images CS: HA = 1.56 **c)** SEM images CS: HA =3.125.

4.5.4. FLOW RATE EFFECT AT TPP = 0.003% AND TPP = 0.012%

In this case, once HA and CS concentrations have been set (HA 0,002 %w/v and CS 0,00625 %w/v), two different crosslinker concentrations are tested using different flow rates. Therefore, varying CS:HA ratio through various tested flow rate ratios, working ranges more suitable to NPs heavy co-precipitation are identified. As in the previous case, a NPs size control through the change of process parameter is observed.

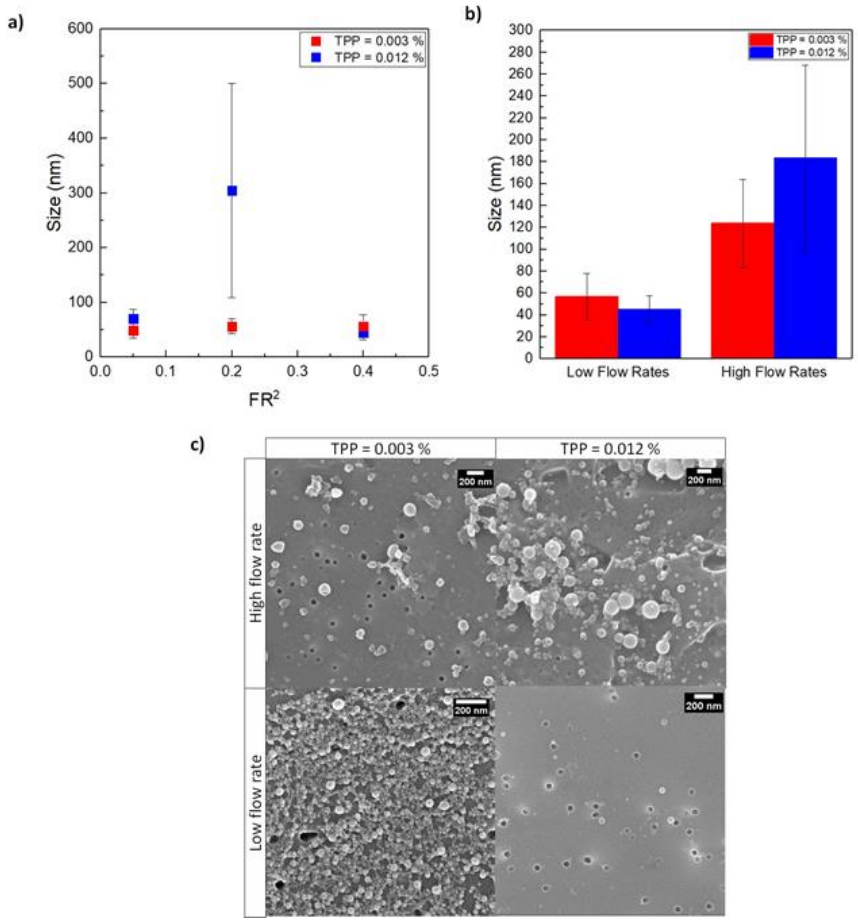

Figure 4.9 a) NPs size trend evaluated at three different FR^2 (0.05, 0.2 and 0.4) depending on TPP concentration (0.012 or 0.003%). **b)** Histogram that compare NPs size at both high and low flow rates at different TPP concentration with a flow rate ratio equal to 0.4. **c)** SEM images at different TPP concentration and flow rate.

Size trend (Figure 4.9a) shows that TPP concentration interferes in coprecipitation process. When TPP = 0.003% size and polydispersity are very similar independently

of flow rate ratios. Instead, at TPP = 0.012% and FR^2 = 0.2, NPs are more polydisperse, while, at FR^2 = 0.4 and 0.05, they lead to coprecipitates with size and polydispersity comparable to the one obtained at TPP = 0.003%. Moreover, histograms in Figure 4.9b and SEM images in Figure 4c reveal that size and polydispersity are influenced by the flow rates. In fact, represented parameters grow proportionally with them.

4.5.5. MORPHOLOGICAL TREND OF NPS

Plots in Figure 5 show NPs morphology obtained by varying FR^2 and CS:HA ratio into two flow rates regimes.

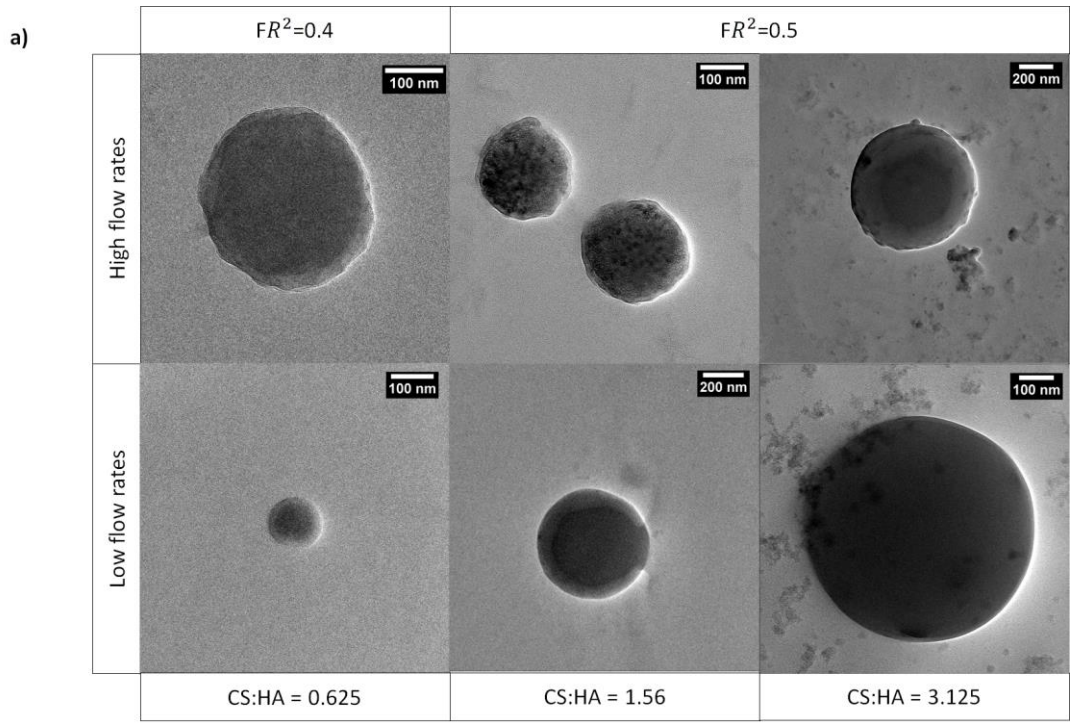

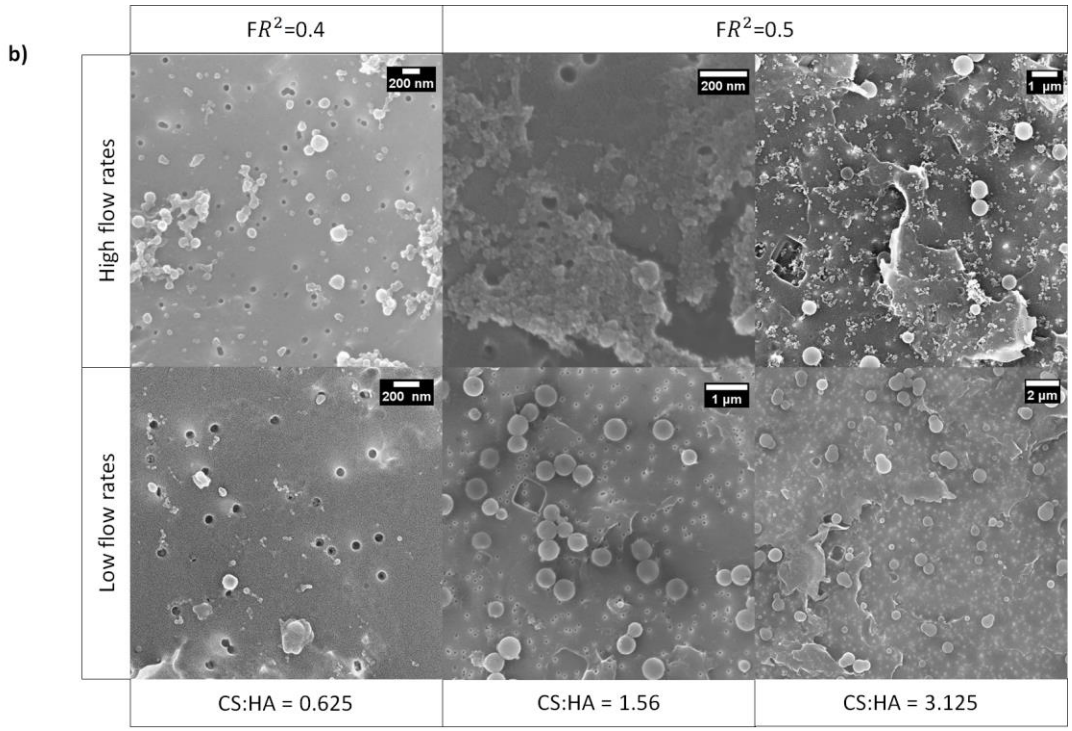

Figure 4.10 NPs morphological characterization at **a)** TEM and **b)** SEM for different CS: HA ratio, flow rate ratio and flow rate conditions. Low flow rates allow to modulate morphology and obtain different structure as full core, co-precipitates or core-shell. On the other hand, higher flow rates use leads to NPs with a mainly core-shell morphological structure.

Low flow rate conditions promote different morphology like full core, co-precipitates or core-shell NPs thanks to parameters modulation while higher flow rates use leads to NPs with a mainly core-shell morphological structure (Figure 4.10a). Consequently, it is obvious that microfluidics can control morphology development thanks to flow rates management.

4.5.6. Gd-DTPA encapsulation

The best process condition for NPs formation, selected in the previous tests (FR^2= 0,5), are used and Gadolinium is added in polycationic solutions with concentration equal to those of CS.

After dialysis in water or ethanol, 300 μL of the sample are collected in specific tube and brought at 22 °C to analyze relaxation time at MINISPEC at 1.5 T by use three different sequences to detect T_1 and T_2. The relaxation time distribution is obtained by CONTIN Algorithm. In Figure 4.11, two different cases are represented.

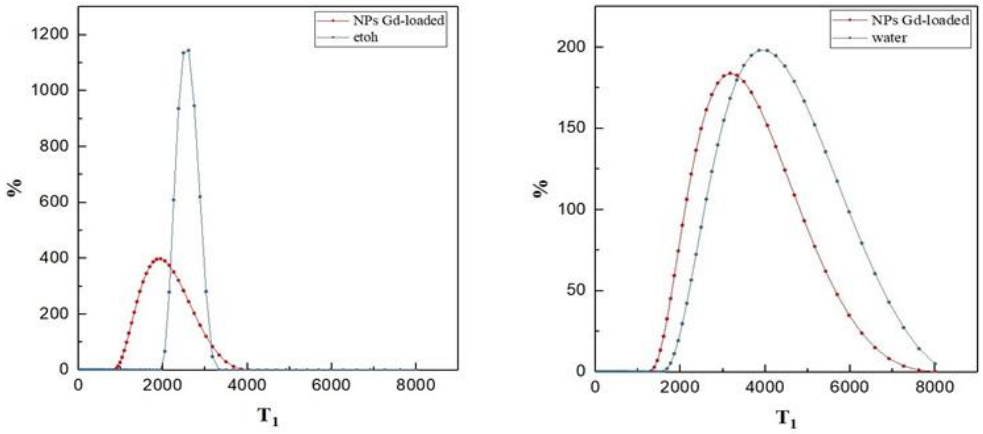

Figure 4.11 Longitudinal relaxation time distribution. Comparison between water and Gd-loaded NPs.

In both situations a reduction of the relaxation time can be observed compared to the solvent and so Gadolinium is encapsulated inside NPs allows to enhance relaxivity.

4.5.1. FLUOROPHORE ENCAPSULATION

Finally, in the last two tests, ATTO488 fluorophore has been introduced in the polyanionic solution (35 μg/mL) in order to demonstrate that NPs are able to encapsulate, at the same time, two diagnostic agents and so, theoretically, even a drug. ATTO488 amount has been evaluated through spectrofluorometric measurements and it shows an estimated concentration from fluorescence signal of 7 pmol.

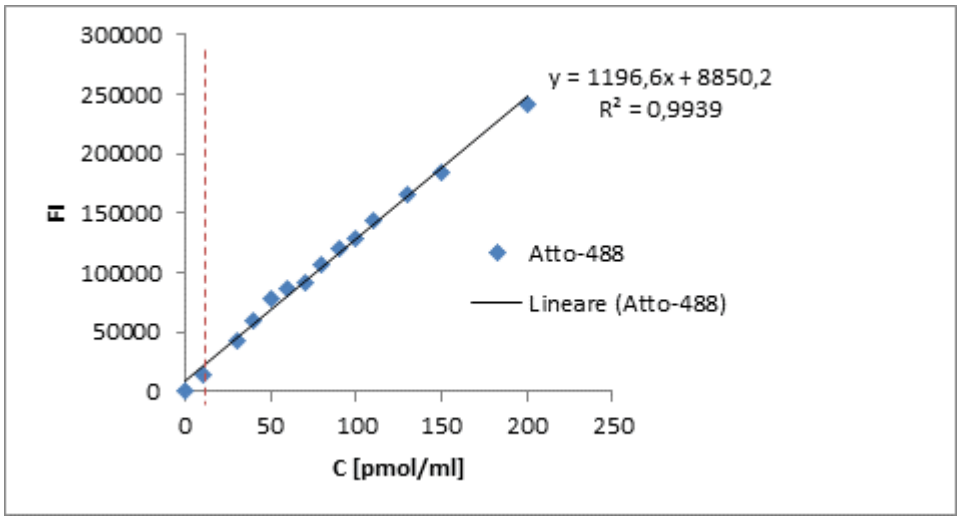

Figure 4.12 Calibration straight line for NPs in the range 0-200 pmol/mL

4.5.2. DISCUSSION

Microfluidic flow focusing is well-established and high-throughput technique to produce NPs. In this paper, we adopt the flow focusing approach to form NPs by ionotropic gelation between HA and CS and using TPP as crosslinker.

We demonstrate that, by varying process parameters (flow rates, polymer concentration and crosslink density), it is possible modulate NPs' size, morphology and structures. During the experiment design, a wide range of these parameters has been explored to investigate their influence on the ionotropic gelation reaction and on the final output of the process.

The experiments we carried out show that the implemented microfluidic process does not need great compound concentrations as in the batch. Indeed, high polymer concentrations could be a limiting factor in the formation of hybrid NPs along microchannels, because the accumulation of materials at the chip junction results in a reduction of the process controllability and in the consequent increase in polydispersity or even in the formation of big aggregates rather than NPs, as shown in Figure 4.7.

The CS:HA ratio also affects the result of the process as shown in Figure 4.8. In fact, fixed the flow rate ratio and HA concentration, an increment of the CS concentration and so in the ratio with the polyanionic polymer cause a growth of the NPs standard deviation in size independently of flow rates condition as previously explained.

The crosslink density, combined with variations in flow rates, proved to be another controllable parameter to modulate NPs' size and morphology, as shown in Figure 4.9. This is due to their influence on the binding process between anionic and cationic blocks. High TPP concentration, i.e. higher availability of crosslinker, does not always lead to the formation of more stable and smaller NPs if it is not balanced by appropriate flow rates. Indeed, an increase in the TPP should correspond to a change in the flow rates regime in order to allow proper mixing and avoid random aggregation. For this reason, flow rates lower than 10 μL/min, both side and middle streams, are optimal to make available TPP in a right amount to lead to NPs formation avoiding polymer macroaggregates. These low flow rates allow to have a mixing time at the chip junction that ensure uniform reaction condition and more homogeneous production.

As result of these considerations, NPs morphological structure is the outcome of the modulation of different factors involved in the microfluidic ionotropic gelation process, as shown in Figure 4.10.

Microfluidic flow focusing approach is able to lead to nanoparticles formation and, through the control of process parameters and using different components concentration, it is possible obtain different NPs size and morphological structures. However, the most important advantage consists in the opportunity to change structural parameter of hydrogel matrix to obtain a relaxivity boost using *Hydrodenticity* concept. This equilibrium between water osmotic pressure, polymer chains and hydration degree of the contrast agent can be obtained thanks to the hydrophilic behaviour of hyaluronic acid and chitosan together with sodium tripolyphosphate used as crosslinker. In this way, we are able to modulate crosslink density, mesh size, hydrophilicity and loading capability and therefore increase GdCAs relaxivity. Crosslink density is directly responsible of the water amount in the polymer meshes and, consequently, of the osmotic pressure. In fact, water content

increases when crosslink density decreases and this is related to a variation of diffusion coefficient and of the water hydrogen bonding. Therefore, the tunability of the crosslink density leads to an increment of the interaction of water with polymer chains of the hydrogel and Gd ions. *Hydrodenticity* is thus able to influence the characteristic correlation times of the Solomon-Bloembergen-Morgan theory and, consequently, it allows a relaxivity increment of GdCAs. The great amount of water, that can be contained in the polymeric matrix, allows to enhance each single contribution given by the three coordination spheres surrounding the metal complex. Therefore, *Hydrodenticity* not only influence directly the relaxation time but, through the organization of the Gd-DTPA surrounding area, is able to change spheres mechanism. The formation of nanomeshes entrapping GdCAs increases the rotational correlation time of the metal chelate and changes both the diffusion correlation time of the bulk water and the residence lifetime of the inner sphere water molecules. Obviously, water exchange must not be neither too slow since it is important to transmit the relaxation effect nor too fast because it means that water is not coordinated enough with Gd. A higher number of hydrogen nuclei around Gd chelates in the inner sphere, where they have direct coordination, leads to an increase of the residence lifetime but, at the same time, a reduction of the relaxation time in this sphere and so an enhancement of the inner sphere relaxivity contribution.

We obtained NPs made up of chitosan and hyaluronic acid with different morphological structures through ionotropic gelation followed by complex coacervation. They can be loaded with Gd-DTPA to improve relaxometric properties of the CAs without chemical modifications of the metal chelate but using a microfluidic approach as tools to obtain desired crosslink density, mesh size, hydrophilicity and loading capability of the NPs structure. Therefore, thanks to the *Hydrodenticity*, it is possible to obtain different structural characteristics of hydrogel nanoparticles that indirectly influence GdCAs relaxation. Through the definition of this new concept, we are able to overcome biological limits of current clinical CAs improving potentially the tissue specificity, stability of the chelates, imaging diagnostic window, reducing the administration dosage and, at the same time, increase the performance of the GdCAs for the MRI image acquisition. Finally, we demonstrated that our NPs are able to encapsulate another compound that could be

a drug or a diagnostic agent and so reduce the time taken up over treatments or clinic exams.

4.6. MICROFLUIDIC FLOW FOCUSING APPROACH TO PRODUCE CHITOSAN-LOADED LIPOSOME NANOSTRUCTURES BASED ON HYDRODENTICITY

Today, medical diagnostic methodologies have an enormous impact on the diagnosis and in the clinical management of the diseases. In this scenario, the integration of different imaging modalities enables to acquire information on specific biological processes. Among different diagnostic techniques, Magnetic Resonance Imaging (MRI) is a highly flexible, reproducible and non-invasive imaging modality. In contrast to the other medical imaging methods, which expose patients to ionizing radiation, MRI uses strong non-ionizing electromagnetic fields in the radio frequency range, offers excellent spatial resolution, is operator independent and provides 3D data [16,17]. Compared to other imaging techniques (i.e., nuclear medicine techniques), it shows low sensitivity and long acquisition time. Furthermore, the use of contrast agents (CAs) is often required in MRI scans in order to improve the enhancement of MRI signals [27]. The majority of these agents are paramagnetic ion complexes, which contain lanthanide elements such as Gadolinium (Gd), or superparamagnetic iron oxide (SPIO) conjugates [20]. These compounds shorten the T1 (or longitudinal) and T2 (or transverse) relaxation time, thereby increasing signal intensity on T1-weighted images or reducing signal intensity on T2-weighted images. Their effectiveness remains limited owing to nephrotoxic effects, lack of tissue specificity, low relaxivity and short circulation half-lives. Moreover, McDonald et al. [38,184,185] have recently reported results about progressive Gd deposition in the brain after repeated intravenous administration of CAs. As a result, the Food and Drug Administration (FDA) has alarmed the medical community and has recommended healthcare professionals to limit the use of Gd-based CAs unless necessary and to report any possible related side effects. Despite the valuable role of the CAs for MRI, these latest results confirm the need to have a biocompatible system able to boost a clinical relevant Gd-chelate without its chemical modification.

According to these parameters and by exploiting the versatile properties of nano- and bio-materials several nanostructured CAs with enhanced relaxivity have been investigated. This chapter aims to describe and evaluate clinical aspects related to the use of biomaterials such as polymer nanoparticles and liposomes for MRI applications[186].

Liposomes are structures composed of hydrophobic head groups and hydrophilic tail groups. They can be prepared by adding lipids in organic solution, which is slowly evaporated to produce a thin film. The film is then hydrated with a desired aqueous buffer and sonicated. Liposomes are generally nano-scaled structures and can be further size refined by passage through physical membrane pores of known size (extrusion). Liposomes are typically characterised by their size, shape and lamellarity. They may be composed of a single bilayer (unilamellar), a few bilayers (oligolamellar), or multiple bilayers (multilamellar). Due to their aqueous cavity and "tunable" bilayer, liposomes have traditionally been used as drug delivery vehicles, encapsulating water-soluble drugs within the aqueous cavity in order to improve drug pharmacokinetics [187].

4.6.1. LIPOSOMES AND MRI

As far as the ability of liposomes to boost the MRI contrast, in order to make liposomes effective paramagnetic CAs for MRI, two main approach have been adopted: (a) encapsulation of Gd-chelates in the hydrophilic domain or (b) immobilization of the chelates on the bilayer membrane surface. On one hand, the former strategy permits to achieve higher Gd payload (theoretically, up to tens to hundreds of thousand Gd can be encapsulated within a single ~100 nm liposome[1]) and to leave the outer surface of the liposome unobstructed and available for the attachment of targeting ligands. Whereas, on the other hand, the latter strategy enables a better water accessibility than the encapsulated Gd since bulk water can easily reach Gd-chelates bound to the exterior surface of the liposome.

The increase in the relaxivity, indeed, strongly depends on the access of water molecules to the metal-chelate coordination domain and on the fast exchange rates between bulk water and coordinated water. For this reason, some concerns have emerged since the permeability barrier imposed by the vesicle membrane decreases

the exchange between bulk water and the water complexed to encapsulated metal-chelates, thereby preventing the relaxivity enhancement. As a result, the relaxivity of liposomes encapsulating CAs is generally lower than that of the corresponding small molecular CAs.

To overcome the limitations of both immobilization and encapsulation strategies, dual-mode liposomal CAs have been developed, which contain both core-encapsulated and surface-conjugated Gd-chelates and are able to combine large loading capability (Gd concentration per unit of liposomal particle) with high image contrast (see following figure) [33].

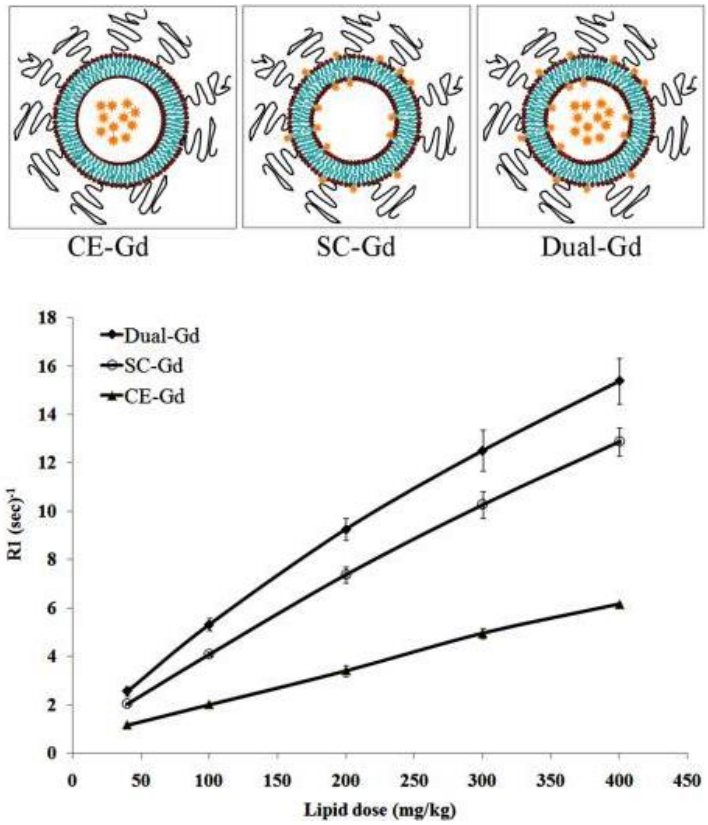

Figure 4.13 Schemes of core-encapsulated gadolinium chelate (CE-Gd) liposomes, surface-conjugated gadolinium chelate (SC-Gd) liposomes and liposomes containing both encapsulated and conjugated gadolinium chelates (Dual-Gd) and T1 relaxation rates (R1) of liposomal-Gd formulations for different lipid concentrations. [Adapted from [33]: *Zhou Z, Lu ZR. Gadolinium-based contrast agents for magnetic resonance cancer imaging. Wiley Interdisciplinary Reviews:*

Nanomedicine and Nanobiotechnology. 2013;5(1):1-18.]

The improved structural stability of the polymersome bilayer architecture has made them an attractive alternative to liposome, which are often limited in clinical applications by their low stability in circulation [188].

As far as the MRI CAs, the use of polymersomes has primarily focused on the loading of superparamagnetic iron oxide nanoparticles (SPIONs), showing a T2 contrast equal or higher than commercially available CAs (e.g. Sinerem and Endorem) and providing a powerful tool that allies imaging to drug release. However, porous polymersomes have been also developed to encapsulate paramagnetic metal complexes [189]. Indeed, the porosity of the polymersome membrane improves the water exchange rate so that the overall developed structure exhibits a relaxivity augmentation in comparison with normal Gd-chelates. This strategy has allowed to overcome one of the main limitation of liposomes, which are known to generally reduce the relaxivity of the encapsulated Gd-based CAs [189].

4.6.2. LITERATURE REVIEW: LIPOSOMES AND POLYMERSOMES FOR ENHANCED MRI CONTRAST

The interest in developing functionalized liposome and polymersome nanostructures has increased over the years.

Just since the end of the 1980's, Unger et al. [190] found that liposomal Gd-DTPA resulted in significant contrast enhancement between the liver and tumor in T1-weighted MR images. They studied size effect with liposomes in a size range of 70 to 400 nm and discovered that liposomal Gd-DTPA with a size of 70 nm created greater contrast enhancement thanks to the larger surface-area-to-volume ratio. By comparison, free Gd-DTPA without liposomes caused a statistically significant reduction in contrast between tumor and liver and reduced lesion detection. Liposomal Gd-DTPA also resulted in sustained vascular enhancement for 1 hour after administration. Their results suggest that paramagnetic liposomes may become a useful MRI CA permitting significant improvement in metastasis detection, which was assessed by five blinded radiologists.

This interest towards liposome applications to MRI and cancer detection remained alive even decades later. In 2008, indeed, Karathanasis et al. [191] evaluated 100 nm liposomes loaded with Gd(DTPA-BMA) for brain tumor MRI in a rat glioma model. The r1 and r2 relaxivities of the developed liposomal CAs were 0.65 and 20.7 $mM^{-1}s^{-1}$ per Gd-chelate (measured at 25 °C and 9.4 T), respectively. Different from usual T1-shortening Gd-CAs, this liposomal encapsulated agent was used as a T2 agent due to its high r2 relaxivity and produced negative signal enhancement. The tumor enhancement of the liposomal CA was visible for a period of three days. Using a 9.4 T MRI system, authors were able to track the intratumoral distribution of the Gd-loaded nanocarrier in a rat glioma model for a period of three days due to improved magnetic properties of the CA being packaged in a nanocarrier. Such a nanocarrier provides a tool for non-invasively assessing the suitability of tumors for nanocarrier mediated therapy and then optimizing the treatment protocol for each individual tumor. Additionally, the ability to image the tumor in high resolution can potentially constitutes a surgical planning tool for tumor resection.

In the following year, Cheng et al. [188] synthesized a composite MR contrast platform, consisting of dendrimer conjugates encapsulated in porous polymersomes. The porous polymersomes, ~130 nm in diameter, were produced through the aqueous assembly of the polymers, polyethylene oxide-b-polybutadiene (PBdEO), and polyethylene oxide-bpolycaprolactone (PEOCL). Subsequent hydrolysis of the caprolactone (CL) block resulted in a highly permeable outer membrane. To prevent the leakage of small Gd-chelate through the pores, Gd was conjugated to PAMAM dendrimer via diethylenetriaminepentaacetic acid dianhydride (DTPA dianhydride) prior to encapsulation. The obtained nanoparticles exhibit improved permeability to water flux and a large capacity to store Gd-chelates within the aqueous lumen, resulting in enhanced longitudinal relaxivity. As a result of the slower rotational correlation time of Gd-labeled dendrimers, the porous outer membrane of the nanovesicle, and the high Gd payload, these functional nanoparticles were found to exhibit a relaxivity (R1) of 292, 109 $mM^{-1}s^{-1}$ per particle. The polymersomes were also found to exhibit unique pharmacokinetics with a circulation half-life of >3.5 hrs and predominantly renal clearance. When injected into living subjects, the gradual destabilization of the polymersomes allow the Gd-labeled dendrimers to be predominantly cleared by the kidneys, while still maintaining a relatively long

circulation time of >3.5 hrs. This could provide an important advantage over other long circulating MRI CAs, which generally require metabolism of the CA in the liver and exhibit prolonged retention in the body. In addition, with their work the authors showed also a way to prevent the leakage of encapsulated Gd through the membrane pores of the nanoconstruct.

Zou et al. [192], for example, report an amphiphilic MRI-traceable liposome NPs encapsulating Gd-DOTA for *in vivo* inner ear visualization through MRI. They design these multifunctional NPs through the film hydration method that allows the encapsulation of Gd-DOTA inside the hydrophilic core of the NPs. They observe acceptable relaxivity values allowing visible signal characteristics for MRI. *In vivo* studies demonstrate that these systems are efficiently taken up by the inner ear after both transtympanic and intracochlear injection. The latter shows better NPs distribution throughout the inner ear, including the cochlea and vestibule, and induced stronger MRI signals on T1-weighted images.

Bui et al. [193] produce lipid NPs containing phospholipids that express Gd-chelate or DTPA by incorporating DTPA-PE into the lipid core of the NPs and then adding Gd^{3+} to preformed NPs (for binding to Gd^{3+} as Gd-DTPA-PE chelate). They also add 10-mole percentage of lipid conjugated to mPEG-PE to lipid nanoparticles in order to increase the bound water on the lipid nanoparticle surface, thereby increasing the MRI contrast. In this case, the following nanoparticle system shows an higher longitudinal relaxivity (33-fold) than the current FDA approved Gd-chelated CAs. In addition, intravenous administration of these Gd-LNP at only 3% of the recommended clinical Gd dose produce MRI signal-to-noise ratios of greater than 300 times in all vasculatures.

Kielar et al. (2010) [194] aimed to synthesize of a DOTA-like Gd complex functionalized with two hydrophobic chains on adjacent donor groups, endowing it with the ability to self-assemble into micelles and be incorporated into liposomes. The liposomes were prepared using a thin-layer deposition/extrusion technique, and their analysis using DLS showed that their diameters were in the range 45-60 nm. The r1 values of the two types of complexes embedded in liposomes were 17.0 and 40.0 $mM^{-1}s^{-1}$ (measured at 298 K and 0.47 T), respectively. The remarkable relaxivity gain observed (135% at 0.47 T; 99% at 1.41 T) for GdDOTA(GAC12)2 relative to the monosubstituted derivative results from the strong reduction in the

flexibility of the system associated with the hindered local rotation about the two aliphatic chains. These data were compared with related values for GdDMPE-DTPA, a neutral DTPA monoamide derivative carrying a fatty acid chain that exhibits slow water exchange (r1=12 at $mM^{-1}s^{-1}$ both 0.47 and 1.41 T). Next, authors noted that increasing the rate of water exchange resulted in an enhancement of r1 by 42%, whereas simultaneous optimization of water exchange and local rotation increased the relaxivity by ∼233%. Liposomes incorporating this paramagnetic building unit showed an unprecedented relaxivity enhancement relative to the derivative bearing only a single glutamic acid arm due to a favorable water exchange rate and optimized rotational rigidity. In addition, the used GdDOTA derivatives proved to be more stable and much more kinetically inert than other Gd chelates typically used in micelles and liposomes.

Kamaly and collegues [187] synthesize a bimodal imaging liposome for cell labeling and tumour imaging. The lipid molecules are able to bear both fluorophore and CA on the same structure, thereby representing a useful probe for both MRI and fluorescence microscopy utility. Very briefly, they conjugate a rhodamine moiety onto a DOTA-bearing C-18 dialkyl lipid and complex Gd into the molecule to obtain the bimodal lipid Gd DOTA Rhoda DSA 1. The lipid is used to label IGROV-1 human ovarian carcinoma cells and to image xenograft tumours in mice. The new paramagnetic and fluorescent lipid proved to be a valuable probe to obtain anatomical information, through MRI, and liposome biodistribution, through ex vivo fluorescence microscopy.

Kono et al. [195] synthesize multi-functional pegylated liposomes having both highly thermosensitive polymers and newly synthesized Gd-chelate-attached dendron lipid (G3-DL-DOTA-Gd) with a compact conformation. The multifunctional liposomes show temperature-responsive drug release and MR imaging functions. In particular, authors load liposomes with Dox and tested the stability of the nanostructures, showing that liposomes are able to retain Dox below physiological temperature but release it immediately above 40°C. As far as the MRI properties, the developed liposomes exhibit the ability to shorten the longitudinal relaxation time with a relaxivity (5.5 $mM^{-1}s^{-1}$) higher than that of free Gd-DOTA (4.6 $mM^{-1}s^{-1}$).

In addition, Na and co-worker [196] report dual functional liposomes co-encapsulating Dox and Gd as therapeutic and diagnostic carriers. They measure MR relaxivity and

cellular uptake showing that the liposomes can entrap 3.6 mM of Dox and 1.9 mM of Gd. Although the low relaxivity (5.5 $mM^{-1}s^{-1}$) compared to that of MRbester® due to limited water diffusion across the liposome membrane, the surface charge induced good cellular uptake, allowing a higher accumulation of Gd into cells than MRbester®. Additionally, Dox is more easily internalized to the nucleus compared to Doxil®.

Li et al. [197], instead, prepare fluorescent and paramagnetic liposomes for early tumor diagnosis by incorporating a RGD-coupled-lipopeptide, synthesized using a cyclic RGD peptide headgroup coupled to palmitic acid anchors via a KGG tripeptide spacer, into lipid bilayers. As far as the paramagnetic liposomes, they adopted the thin film hydration method and hydrated the lipid film with commercial Gd-DTPA as MRI contrast agent. *In vivo* MRI scanning demonstrate that the signal enhancement in tumor after injection of RGD-targeted liposomes is significantly higher than non-targeted liposomes and pure Gd-DTPA. In addition, biodistribution study also show specific tumor targeting of RGD-targeted paramagnetic liposomes *in vivo*, proving them an effective means for noninvasive diagnosis of early tumor.

Liao et al. [198] design a core-shell NPs system composed of a PLGA core and a paramagnetic liposome shell for simultaneous MRI and targeted therapeutics. They encapsulate Dox within biocompatible and FDA-approved PLGA NPs, and DTPA-Gd is conjugated to the amphiphilic octadecyl-quaternized lysine-modified chitosan (OQLCS). The paramagnetic liposome shell is based on Gd-DTPA-conjugated OQLCS (Gd-DTPA-OQLCS), folate-conjugated OQLCS (FA-OQLCS), and PEGylated OQLCS (PEG-OQLCS). Briefly, the carboxyl groups of DTPA used as a chelating agent are combined with the amino groups of OQLCS. Then Gd is incorporated into the complex. As a result, the NPs show paramagnetic properties with an approximately 3-fold enhancement in the longitudinal relaxivity (r1 = 14.381 mM−1s−1) compared to the commercial Gd-DTPA complex and exceptional antitumor effects without systemic toxicity.

Another remarkable example as reported by Gianolio et al. [199]. They prepare pH-responsive Gd-DO3Asa-loaded liposomes which maintain the pH responsiveness of the unbound paramagnetic complex, and their relaxivities are markedly affected by the magnetic field strength, exhibiting a steep change in the relaxivity in the pH range 5-7.5. Moreover, they provide a ratiometric method for measurement of the pH based

on a comparison of the relaxation effects at different magnetic fields, offering an alternative tool for accessing measurement of the pH without prior knowledge of the concentration of the paramagnetic agent.

More recently, several liposomes and polymersomes have been developed to increase CAs' relaxivity, improve cancer detection and for molecular imaging applications.

Smith et al. (2013) [200] developed a simple process to load Gd exclusively on a liposome surface using a polymeric fastener. The fastener, so named for its ability to physically link two functional components together, consisted of chitosan substituted with diethylenetriaminepentaacetic acid (DTPA) to chelate gadolinium, as well as octadecyl chains to stabilize the modified chitosan on the liposome surface. The assembly strategy, mimicking the mechanisms by which viruses and proteins naturally anchor to a cell, provided greater T1 relaxivity than liposomes loaded with gadolinium in both the interior and outer leaflet. Liposomes were prepared by a film hydration method followed by sonication. The lipid film, formed as described above, was then hydrated with the aqueous mixture of gadolinium and DTPA-chitosan-g-C18. The proposed process decouples particle assembly and functionalization and has considerable potential to enhance imaging quality while alleviating many of the difficulties associated with multifunctional particle fabrication. The average diameters of liposomes before and after one-hour incubation in serum-supplemented PBS were 4.3 ± 2 and 3.7 ± 2 μm respectively. Gadolinium loaded on the liposome modified by DTPA-chitosan-g-C18 significantly enhanced MR signal, compared to the liposome modified with DTPA-chitosan. At a given liposome concentration, R1 of the suspension was increased with DTPA-chitosan-g-C18. However, the molar relaxivity of immobilized gadolinium was nearly the same across samples. Therefore, authors interpreted that the enhancement of R1 attained with DTPAchitosan-g-C18 is due solely to the higher loading of gadolinium on the liposome surface, noting that 30% of the DTPA-chitosan was desorbed upon exposure to $GdCl^3$. Furthermore, the relaxivity was enhanced beyond that of the clinically used unconjugated DTPA-Gd complex with a molar relaxivity of 4.85 $mM^{-1}s^{-1}$. Authors also evaluated Gadolinium-coated liposomes in vivo using murine ischemia models to highlight the diagnostic capability of the system.

Cittadino et al. (2013) [201] investigated the in vitro (relaxometry) and in vivo (melanoma tumour model on mice) MRI performance of liposomes incorporating either LIPO-GdDOTA-(GAC12)2 (LIPO=liposome, GA=glutaric acid) or an amphiphilic monoamide Gd agent conjugated with C18 chains LIPOGdDOTAMA(C18)2 as a reference. The liposomes were prepared using a thin-layer deposition/extrusion technique. The mean hydrodynamic size of the liposomes was found to be around 140 nm with a polydispersity index value lower than 0.2. Through the NMRD profiles, authors showed a marked relaxivity difference over the entire frequency range investigated, and their shape is rather similar and typical of macromolecular systems characterised by a reduced rotational tumbling rate. They distinguished: 1) a region of constant relaxivity at low fields (0.01–0.5 MHz); 2) a dispersion around 1–3 MHz; 3) a peak centred about 20–30 MHz; and 4) a steep decrease of r1 at higher fields. However, although for LIPO-GdDOTAMA(C18)2 the r1 peak (r1=11.4 $mM^{-1}s^{-1}$) is broad and centred at 30 MHz, for LIPO-GdDOTA(GAC12)2 it is narrower and with a maximum at 20 MHz (r1=40.0 $mM^{-1}s^{-1}$). As far as the in vivo studies, after about 7 h post-injection the contrast enhancement observed for the more efficient liposomes decreases rapidly and becomes lower than for LIPO-GdDOTAMA(C18)2. The relaxometric data and the quantification of the Gd complexes in the organs indicated that: 1) the differences in the contrast enhancement can be attributed to the different rate of water exchange and rotational dynamics of the Gd complexes; 2) the rapid contrast decrease is caused by a faster clearance of GdDOTA(GAC12)2 from the organs. The overall results highlighted clearly the superior relaxometric performance of the liposomes loaded with GdDOTA(GAC12)2 relative to the liposome formulation based on the GdDOTAMA(C18)2 complex. Therefore, GdDOTA(GAC12)2 complex may represent a good candidate for the development of improved MRI protocols based on paramagnetically labelled lipidic nanoparticles.

Subsequently, Hossann et al. [202] investigate formulations of 6 clinically approved CAs encapsulated into thermosensitive liposomes (TLs):

(1) Gd-DTPA (Magnograf®) from Marotrast GmbH, Jena, Germany;

(2) Gd-BOPTA (Multihance®) from Bracco Imaging Deutschland GmbH (Konstanz, Germany);

(3) Gd-DOTA (Dotarem®) from Guerbet GmbH (Sulzbach/Taunus, Germany);

(4) Gd-BT-DO3A (Gadovist™) from Bayer Vital GmbH (Leverkusen, Germany);

(5) Gd-DTPA-BMA (Omniscan™) from GE Healthcare Buchler GmbH & Co. KG (Braunschweig, Germany);

(6) Gd-HP-DO3A (Prohance®) from Bracco Imaging Deutschland GmbH (Konstanz, Germany).

They observe that Omniscan™ and Prohance® are the most promising candidates to be encapsulated into DPPG2-TSL. In particular, Prohance® allows the highest loading capability (256 mM) due to the lowest osmolality and yields the highest relaxivity. Omniscan™ is the only formulation that could be stored at 4°C for weeks. The other CAs induce phospholipid hydrolysis, which results in unwanted CA leakage, and therefore reduce the shelf life of TSL. Nevertheless, Omniscan™ is associated with Nephrogenic Systemic Fibrosis (NSF) [105]. The Human Serum Albumin (HSA) and Immunglobulin G (IgG) contribute to the increase of MRI signal at 30°C by increasing Pd. A high concentration of encapsulated CA is a prerequisite to achieve a sufficiently high $\Delta r1$ during heat triggered CA release combined with a low r1 at 37°C. Hence, the optimal CA is characterized by a non-ionic structure and a low contribution to osmolality.

Cheng et al. (2014) [203] developed a highly efficient MRI CA based on stabilized porous phospholipid liposomes with encapsulated Gd-labeled dextran. Unilamellar liposomes were prepared using the film hydration method. To prevent small Gd-chelates (i.e. Gd-DOTA) from leaking through the porous bilayer membranes, Gd-DOTA was attached to large molecular weight dextran prior to encapsulation (this attachment increased proton relaxivity of GdDOTA by slowing the molecular rotation). In particular, 1 mL of Gd-DOTA-dextran (10 mg/mL) was added to the dried lipid film (2 mg of lipid) while non-entrapped Gd-DOTA-dextran was removed through repeated washing on centrifugal filter devices. The mean diameter of the liposomes was found to be about 100 nm. The highly porous membrane leads to a high relaxivity of the encapsulated Gd. Gd-DOTA-dextran encapsulated within the porous liposomes had an r1 of 9.9 $mM^{-1}s^{-1}$, which was similar to the r1 of Gd-DOTA-dextran (9.4 $mM^{-1}s^{-1}$) in bulk water. This indicates that Gd-DOTA-dextran

encapsulated within the porous liposomes experiences a fast water exchange rate with surrounding bulk water. In contrast, Gd-DOTA-dextran encapsulated within the nonporous liposomes had an r1 of only 4 $mM^{-1}s^{-1}$, which is more than a 2.4-fold lower than the r1 for Gd-DOTA-dextran encapsulated into porous liposomes. Furthermore, the r1 measured from Gd-DOTA-dextran encapsulated into liposomes is 2.6-fold higher than the r1 of clinically used Gd-DOTA (3.9 $mM^{-1}s^{-1}$). By conjugating cancer-targeting ligands to their unobstructed outer surface, these CAs have the promise for use as targeted molecular imaging agents.

Other authors report further interesting strategies for the development of new liposome-complexes. Kozlowska et al. [204], for example, synthesize liposomes loaded with Gd ions using different membrane-incorporated chelating lipids and functionalized with monoclonal anti-CD138 (syndecan-1) antibody for multiple myeloma and non-Hodgkin's lymphoma diagnosis. In this case, the use of the polychelating amphiphilic polymer increases both the Gd content and the longitudinal relaxivity of the Gd-loaded liposomes as compared to Gd-DTPA-BSA equivalents.

Then, Park and co-workers [205] develop nanohybrid liposomes coated with amphiphilic hyaluronic acid-ceramide for targeted delivery of anticancer drug and *in vivo* cancer imaging. Dox, an anticancer drug, and Magnevist, a Gd-based CA for MRI, are loaded into this nanohybrid liposomal formulation. They find that *in vitro* release and *in vivo* clearance of Dox as well as cellular uptake from the nanohybrid liposome is enhanced than that from conventional liposome, thanks to the prolonged circulation of the nanohybrid liposome in the blood stream and to the HA–CD44 receptor interactions.

Silva et al. (2015) [206] sinthesized complexes of Gd with N-octanoyl-N-methylglucamine (L8) and N-decanoyl-N-methylglucamine (L10). These complexes were incorporated in liposomes as an attempt to further enhance the relaxivity. Liposomes were prepared by the thin-film method. Both the free and liposome-incorporated gadolinium complexes showed high relaxation effectiveness, compared to commercial CA gadopentetate dimeglumine (Magnevist). The high relaxivity of these complexes was attributed to the molecular rotation that occurs more slowly, because of the elevated molecular weight and incorporation in liposomes. The results established that these paramagnetic complexes are highly potent CAs, making them

excellent candidates for various applications in molecular MR imaging. The fact that relaxivity of GdL8 complex was unaffected by incorporation into liposomes may be due to the reduced vesicle diameter (141 nm), resulting in elevated relaxation times, or to little restriction of the rotational flexibility of the complex. In addition to the greater diameter of the vesicle (169 nm) of Lipo-GdL10 sample, other factors may contribute to the significant increase of GdL10 relaxivity upon liposome incorporation. It is known that the incorporation of metal compound into nanoparticles can increase r1 due to the restriction of rotational flexibility of the compounds. Furthermore, the exposition of the metal at the external aqueous surface of the particle may facilitate the interaction of water molecules with the paramagnetic center. Incorporation into liposomes did not increase the relaxivity of Lipo-GdL8 complex (r1 ~ 11.92 $mM^{-1}s^{-1}$). However, an increase in relaxivity was observed for Lipo-GdL10 incorporated in liposomes. r1 and r2 relaxivities of the compound increase from approximately 12.3 to 15.5 and from 13.6 to 16.7 $mM^{-1}s^{-1}$. Moreover, the relaxivity values observed with complexes liposome incorporation are about three times higher than those of the commercial CAs used clinically (r1 ~ 3.0–5.0 $mM^{-1}s^{-1}$).

Gu et al. (2015) [207] developed a novel gadolinium-loaded liposomes guided by GBI-10 aptamer to enhance magnetic resonance imaging (MRI) diagnosis of tumor. Nontargeted gadolinium-loaded liposomes were achieved by incorporating amphipathic material, Gd-(N,N-bis-stearylamidomethyl-N′-amidomethyl)-diethylenetriamine tetraacetic acid, into the liposome membrane using lipid film hydration method. GBI-10, as the targeting ligand, was then conjugated onto the liposome surface to get GBI-10-targeted gadolinium-loaded liposomes (GTLs). Both nontargeted (NTLs) gadolinium-loaded liposomes and GTLs displayed good dispersion stability, optimal size, and zeta potential for tumor targeting, as well as favorable imaging properties with enhanced relaxivity compared with a commercial MRI CA, gadopentetate dimeglumine. Both NTLs and GTLs had average diameters at ~120 nm with a narrow particle size distribution index (0.30), implying their good dispersion stability, which may be an optimal size for tumor targeting. For NTLs and GTLs, the r1 values were 4.7±0.3 $mM^{-1}s^{-1}$ and 4.5±0.2 $mM^{-1}s^{-1}$, respectively, both significantly higher than that of Gd-DTPA solution. The increased r1 values suggest that Gd-loaded liposomal systems of NTLs and GTLs could act as an ideal T1 CA.

Increased cellular binding of GTLs to C6 cells was also confirmed by confocal microscopy, flow cytometry, and MRI, demonstrating the promise of this novel delivery system as a carrier of MRI CA for the diagnosis of tumor. These studies provide a new strategy furthering the development of nanomedicine for both diagnosis and therapy of tumor.

Huang et al. (2015) [208] developed a dual-imaging diagnostic polymersome system featured with highly hydrated multilamellar wall structure capable of simultaneously embedding a hydrophobic near-infrared fluorophore, Cy5.5, and a paramagnetic probe, Gd cations. The polymersomes were obtained from the self-assembly of lipid-containing copolymer, poly(acrylic acid-co-distearin acrylate), in aqueous solution. The Cy5.5 and Gd species were loaded into polymersomes via hydrophobic association (loading efficiency of Cy5.5 ca 74%) and electrostatic complexation (Gd ca 83%), respectively. Owing to the highly hydrated structure of vesicular membrane, the superior contrast enhancement of Gd-loaded liposomes in MRI was obtained as a result of prolonged rotational correlation time of Gd cations and fast water exchange from Gd to bulk solution. The system exhibits a 15-fold higher longitudinal relaxivity value (ca 60 $mM^{-1}s^{-1}$) than that (4 $mM^{-1}s^{-1}$) of the commercial CA, Magnevist, in phosphate buffered saline. The in vivo characterization demonstrates that liposomes exhibit a signal-to-noise ratio in T1-weighted MR image contrast similar to that of Magnevist, yet with a Gd dose 5-fold lower. Along with their non-toxicity at the dose used, these results demonstrate the great potential of the CGLPs as an advanced diagnostic nanodevice. An excellent contrast in NIR imaging at tumor site was attained following the intravenous injection of liposomes into Tramp-C1 tumor-bearing mice (C57BL/6).

Xiao et al. [209] report liposomes loaded with Sorafenib (SF) and commercial Gd-based CA (Gd-DTPA) for theranostic applications. Thin film hydration method is used to prepare liposomes exhibiting spherical shapes or ellipsoidal shapes, uniform particle size distribution (around 180 nm), negative zeta potential, high encapsulation efficiency and drug loading. As far as the longitudinal relaxivity, they achieve a value of 3.2 $mM^{-1}s^{-1}$, slightly lower than the commercial CA (4.5 $mM^{-1}s^{-1}$) and the MRI test show longer imaging time and higher signal enhancement at the tumor tissue. Furthermore, they demonstrate *in vivo* antitumor efficacy of the developed SF/Gd-liposomes on hepatocellular carcinoma (HCC) in mice. To sum up, the authors show

that SF/Gd liposomes could be promising nano-carriers for MRI-guided *in vivo* visualization of the delivery and HCC treatment.

Lorenzato et al. (2016) [210] showed that co-loading of a paramagnetic and a superparamagnetic MRI CA, affecting R1 and R2 respectively, in thermosensitive liposomes, allows for both monitoring liposomal biodistribution, as well as liposomal release. They developed three different thermosensitive liposomes (TSL) using the thin-film hydration technique, loaded either with a chelated gadolinium complex, citrated iron oxide nanoparticles or both. The first liposome formulation was hydrated with 250 mM of ProHance, the second formulation was hydrated with citrated-USPIO solution (50 mM iron content), the third formulation was hydrated with both 250 mM ProHance and citrated-USPIO solution (50 mM iron content), respectively. The authors measured and compared the MR properties before and after heating of these dual MRI CA formulations. They also investigated the utility of these formulations in an ex vivo renal vasculature system, showing that, when intact, the transverse relaxivity of the liposomes is high allowing detection of carriers in tissue. After heating the longitudinal relaxivity steeply increases indicating release of the small molecular contents. By choosing the appropriate MR sequences, availability and release have been evaluated without interference of one CA with the other. Regardless of the molecular cargo, these preparations showed a similar hydrodynamic radius (≈100 nm). Normalized to the phosphorus concentration, before release, Gd-loaded liposomes relaxivities r1, r2, and r2 * were found to be 0.1 $mM^{-1}s^{-1}$, 1.6 $mM^{-1}s^{-1}$ and 3.8 $mM^{-1}s^{-1}$, respectively. For the two citrated-USPIO loaded liposomes, Gd-TSM and TSM, similarly low r1 values (r1 TSM = 0.1 $mM^{-1}s^{-1}$ and r1 Gd-TSM = 0.3 $mM^{-1}s^{-1}$) were measured, whereas high r2 (r2 TSM = 8.8 $mM^{-1}s^{-1}$, r2 Gd-TSM = 13.2 $mM^{-1}s^{-1}$) and r2* (r2* TSM = 11.9 $mM^{-1}s^{-1}$, r2* Gd-TSM = 19.4 $mM^{-1}s^{-1}$) relaxivities were observed. After heating to 43 °C during 15 min, no significant variations were measured for free Citrated-USPIOs or TSM whereas r1, r2, and r2* of Gd-TSM were found to increase by a factor 14.0, 1.1 and 1.2. For Gd-TSL, finally, r1, r2, and r2* changed by a factor 27, 20 and 2.65, respectively. This concept allowed for MR monitoring of the drug delivery process, from the biodistribution of the carriers to the localized release of the contents.

Liu et al. (2016) [211] encapsulated Magnevist (Gd-DTPA) into liposomes conjugated with IL-13 and characterized them by particle size distribution, cytotoxicity, and

MRI relaxivity. The average size of IL-13-liposome-Gd-DTPA was 137±43 nm with relaxivity of 4.0±0.4 $mM^{-1}s^{-1}$ at 7 Tesla. No significant cytotoxicity was observed with MTS assay and serum chemistry in mice. The MRI signal intensity was enhanced up to 15% post injection of IL-13-liposome-Gd-DTPA in normal brain tissue following a similar time course as that for the pituitary gland outside of the Blood-Brain-Barrier (BBB). IL-13-liposome-Gd-DTPA is able to pass through the uncompromised BBB and detect an early stage glioma that cannot be seen with conventional contrast-enhanced MRI.

In the end, Tian et al. [212] synthesize Gd-DTPA-loaded mannosylated liposomes (M-Gd-NL) and test their ability to target macrophages in Acute Pancreatitis (AP) and discriminate between mild and severe AP. Lipid film-based method is used to synthesize DSPE-PEG2000-Man liposomes encapsulating DPPE-DTPA-Gd, with size around 100 nm. *In vitro* tests show efficient bind and readily release of Gd-DTPA into macrophages, resulting in enhanced MRI ability. Indeed, M-Gd-NL show a longitudinal relaxivity 1.8-1.9 higher than Gd-DTPA, as a consequence of the embedding of DPPE-DTPA-Gd into the bilayer of liposomes, which slowed down the tumbling motion of Gd complexes. As far as the safety profile, M-Gd-NL do not show any severe organ toxicity in rats, thus proving to be promising nanocarriers for clinical use and for the early detection of AP.

Table 4.1 Literature review about liposomes for MRI

Architecture	Size	Relaxivity (r1) $mM^{-1}s^{-1}$	Tracer	Application	Year	Ref
Liposomes	70 – 400 nm	-	Gd-DTPA	MRI Metastasis detection	1989	[190]
Liposomes	100 nm	0.65 – 20.7	Gd(DTPA-BMA)	MRI Glioma detection	2008	[191]
Polymersomes	130 nm	292 – 109 per particle	Gd-PAMAM-(DTPA dianhydrid)	MRI Relaxivity enhancement Leakage prevention	2009	[188]
Liposomes	130 nm	0.033 – 2.2	GdDOTA	MRI inner ear visualization	2010	[192]

Liposomes	88 nm	13.6	GdDTPA	MRI Relaxivity enhancement Vascular Contrast	2010	[193]
Liposomes	45 – 60 nm	17.0 – 40.0	GdDOTAGAC12 GdDOTA(GAC12)2	MRI Relaxivity enhancement Improve stability	2010	[194]
Liposomes	48 – 110 nm	4.6 – 6.2	GdDOTA	Temperature-triggered release	2011	[195]
Liposomes	95 – 120 nm	6.4	$GdCl_3$	Theranostic Doxorubicin delivery	2011	[196]
Liposomes	100 nm	-	GdDTPA	Tumour targeting	2011	[197]
Polymersomes	430 nm	14.4	GdDTPA	MRI and Targeted Therapeutics	2011	[198]
Liposomes	120– 140 nm	11.2 – 17.7	Gd-DO3Asa	MRI enhancement	2012	[199]
Liposomes	4.3 – 3.7 µm	6.9	DTPA-chitosan-g-C18	MRI Ischemia detection	2013	[200]
Liposomes	140 nm	11.0 – 40.0	GdDOTAMA(C18)2 GdDOTA(GAC12)2	MRI Relaxivity enhancement Excretion efficiency	2013	[201]
Liposomes	150	0.1 – 6.0	Gd-DTPA, Gd-BOPTA, Gd-DOTA, Gd-BT-DO3A, Gd-DTPA-BMA, and Gd-HP-DO3A	Relaxivity enhancement Encapsulation efficiency	2013	[202]
Liposomes	100 nm	9.9	Gd-DOTA-dextran	MRI Molecular imaging	2014	[203]
Polymeromes	170 nm	36	Gd–DTPA	Detection of myeloma and non Hodgkin's lymphoma	2014	[204]
Polymeromes	130 nm	6	Gd–DTPA	Cancer diagnosis and therapy	2014	[205]
Liposomes	141 – 196 nm	11.9 – 15.5	Gd-(N-octanoyl-N-methylglucamine) Gd-(N-decanoyl-N-methylglucamine)	MRI Molecular imaging	2015	[206]

Liposomes	120 nm	4.5 – 4.7	Gd-(N,N-bis-stearylamidomethyl-N′-amidomethyl)-DTPA	MRI Metastasis detection	2015	[207]
Polymersomes	-	60.0	Gd^{3+}	Mltimodal imaging (MRI + optical)	2015	[208]
Liposomes	180 nm	3.2	Gd-DTPA	Drug delivery and hepatocellular carcinoma treatment	2016	[209]
Liposomes	100 nm	0.2 – 4.9	ProHance citrated-USPIO	MRI	2016	[210]
Liposomes	137 nm	4.0	Magnevist	MRI Glioma detection BBB crosing	2016	[211]
Liposomes	100 nm	8.3 – 8.9	Gd-DTPA	improved MRI in acute pancreatitis	2017	[212]

4.6.3. CHITOSAN-LOADED LIPOSOME NANOSTRUCTURES

4.6.3.1. Effect of EtOH concentration

In figure 4.14, the effect of two different EtOH volumetric fraction used in the solvent mixture to solubilize lipids (0.072 mg/ml) is shown.

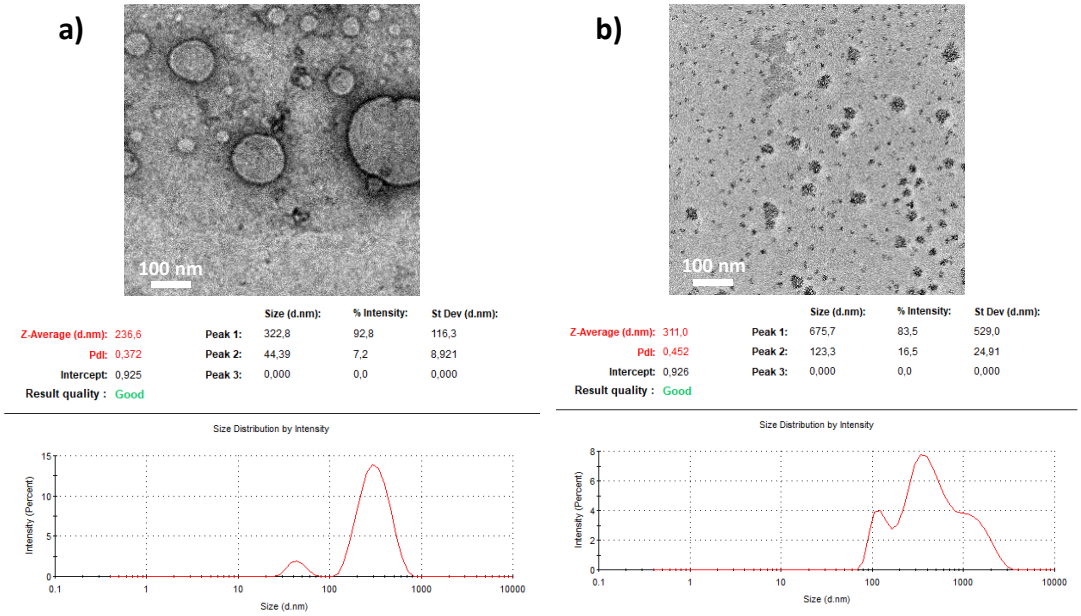

Figure 4.14 a) TEM image and size distribution of chitosan-liposomes obtained at 65% EtOH + 35% water in the side channels; **b)** TEM image and size distribution of chitosan-liposomes obtained at 80% + 20% water EtOH in the side channels.

The optimal condition to make the self-assembly process effective can be observed in terms of liposomes production, morphology and size distribution. In particular, by solubilizing liposomes in a solvent mixture made of 65% EtOH and 35% MilliQ water, lower size and polydispersity can be achieved after the processing through the microfluidic platform.

4.6.4. EFFECT OF CHITOSAN CONCENTRATION

Figure 4.15 shows the effect of chitosan concentration on the liposomes formation and production.

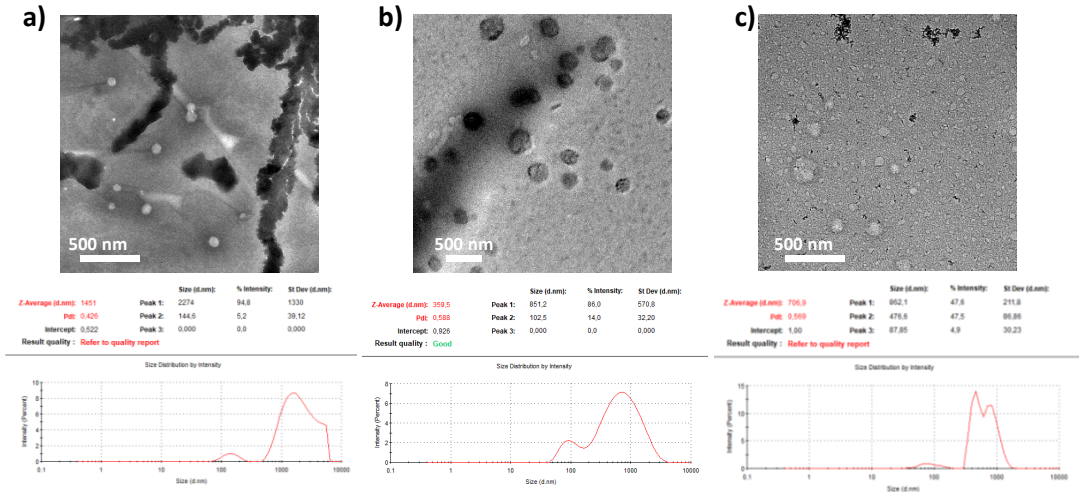

Figure 4.15 TEM image and size distribution of chitosan-liposomes obtained at 0 mg/ml (**a**), 0.1 mg/ml (**b**) and 0.375 mg/ml (**c**) chitosan concentration.

The best condition can be found at a chitosan concentration of 0.1 mg/ml. In fact, not only the size distribution is better, in terms of both size and polydispersity, than the trials with only acetic acid (Figure 4.15a) and the trial with 0.375 mg/ml (Figure 4.15c), but also the structure of the liposomes seems to be able to encapsulate the polymer within the liposome core (darker liposome core in the TEM image).

4.6.5. EFFECT OF ACETIC ACID CONCENTRATION

Figure 4.16 shows the effect of increased acetic acid concentration on the liposome formation.

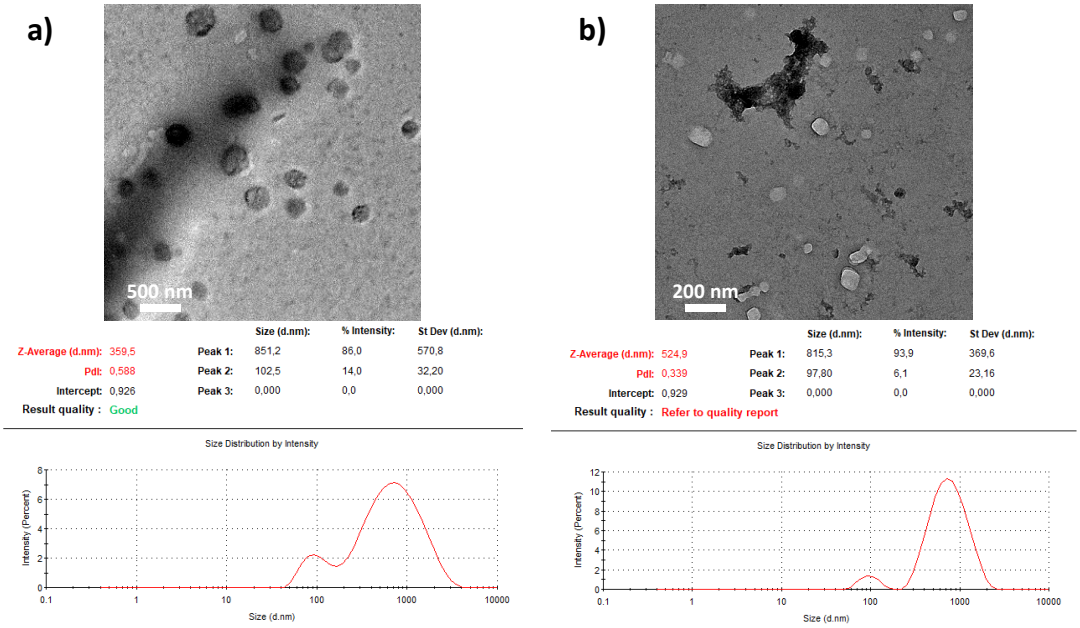

Figure 4.16 a) TEM image and size distribution of chitosan-liposomes obtained at 1% acetic acid; **b)** TEM image and size distribution of chitosan-liposomes obtained at 10% acetic acid.

In the case of 10% v/v acetic acid, the chitosan is no more entrapped into the liposome's core.

4.6.6. FLOW RATES OPTIMIZATION

In figure 4.17, a comparison between two different flow rates used for the middle channel of the microfluidic platform is shown.

In particular, Figure 7.5a shows chitosan-liposomes at 1 µL/min while Figure 7.5b shows the same liposomes obtained at 3 µL/min.

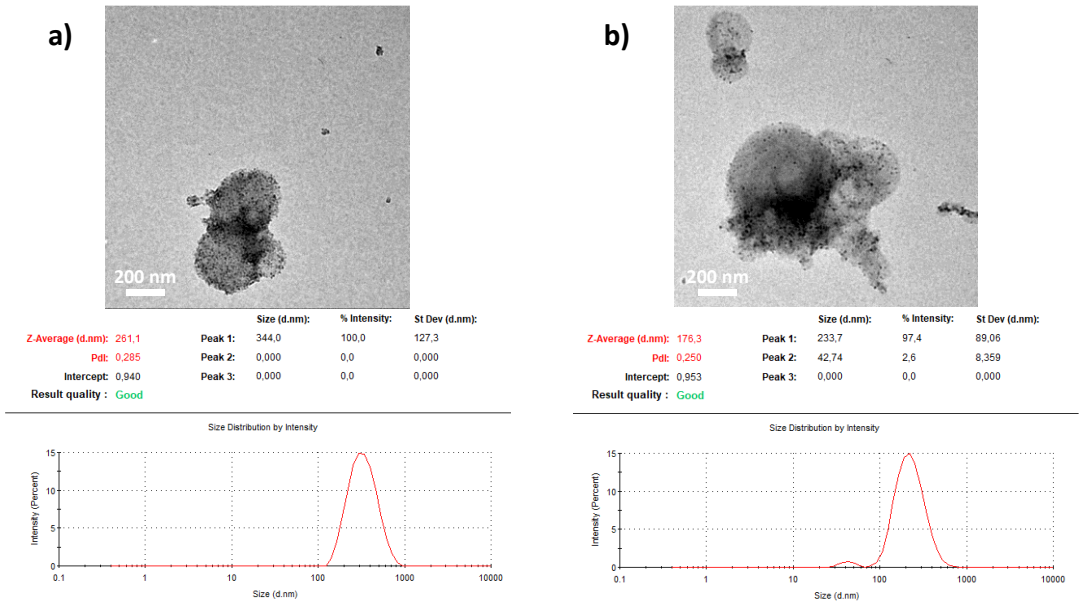

Figure 4.17 a) TEM image and size distribution of chitosan-liposomes obtained with a flow rate in the middle channel equal to 1 µL/min; **b)** TEM image and size distribution of chitosan-liposomes obtained with a flow rate in the middle channel equal to 3 µL/min;

The slightly higher flow rate in the middle channel represents not only an advantage in terms of higher throughput but also in terms of lower size and polydispersity.

4.6.7. Gd-DTPA encapsulation

Figures 4.18 and 4.19 compare unloaded and Gd-loaded chitosan-liposomes at two different flow rate conditions (1 µL/min and 3 µL/min). As already highlighted in the previous paragraph, the value of 3 µL/min is the best flow rate condition even in the case of Gd-loaded liposomes. Smaller and less polydisperse chitosan-liposomes encapsulating Gd-DTPA can be obtained with a middle channel flow rate set at 3 µL/min.

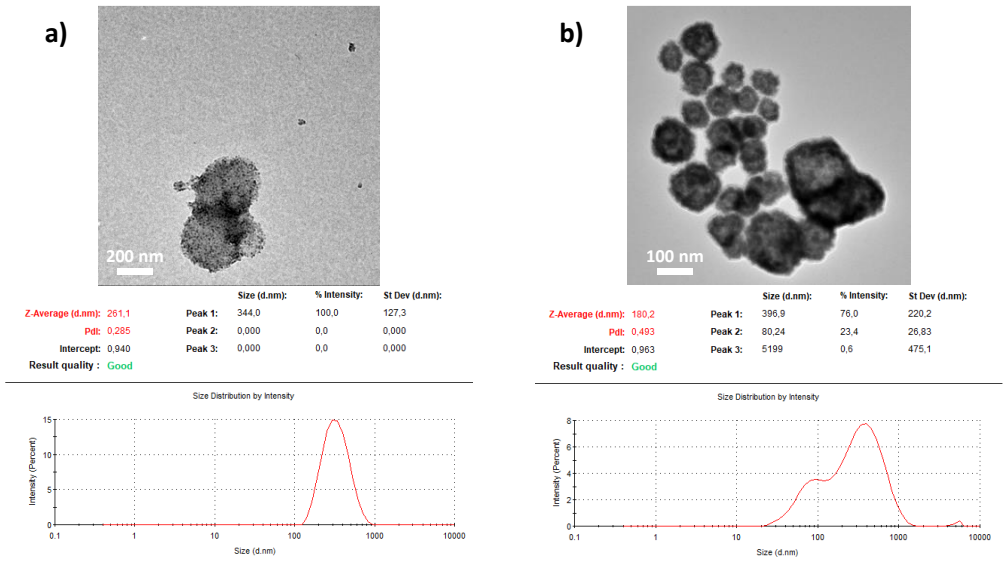

Figure 4.18 a) TEM image and size distribution of chitosan-liposomes obtained with a flow rate in the middle channel equal to 1 µL/min; **b)** TEM image and size distribution of Gd-loaded chitosan-liposomes obtained with a flow rate in the middle channel equal to 1 µL/min.

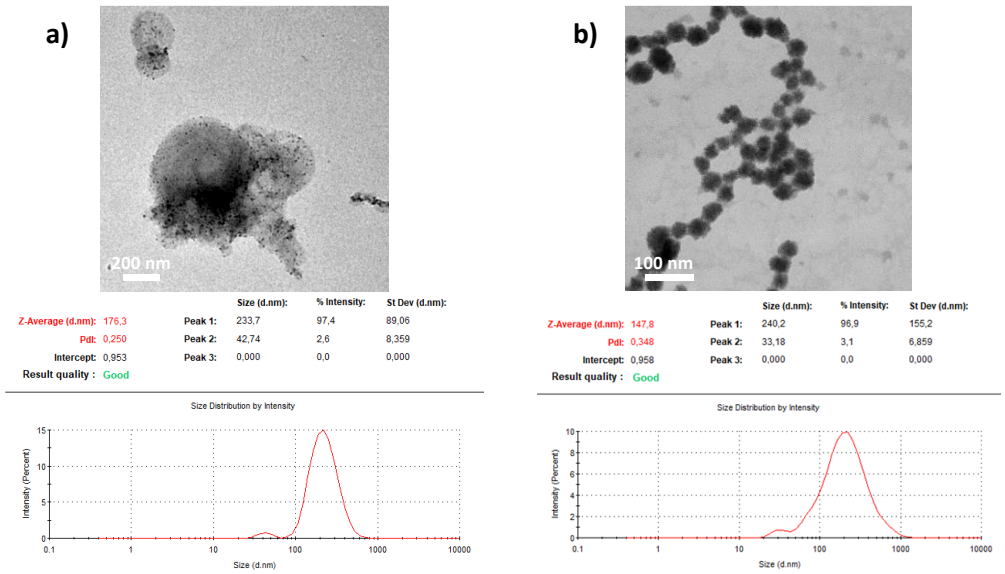

Figure 4.19 a) TEM image and size distribution of chitosan-liposomes obtained with a flow rate in the middle channel equal to 3 µL/min; **b)** TEM image and size distribution of Gd-loaded chitosan-

liposomes obtained with a flow rate in the middle channel equal to 3 μL/min.

Moreover, in terms of longitudinal relaxation time (T_1), the best process condition is obtained at 3 μL/min flow rate in the middle channel. As showed in Table 4.2 and 4.3, the T_1 of Gd-loaded chitosan-liposomes, is far lower than that of the unloaded chitosan-liposomes. Furthermore, after a dialysis to remove the excess of Gd-DTPA, the signal for the Gd-loaded chitosan-liposomes is still significant, meaning that the Gd-DTPA is encapsulated into the liposomes core.

Table 4.2 Longitudinal relaxation time (T_1).

Flow rate middle channel (μL/min)	Gd-DTPA	T_1 (ms)
1	unloaded	2350 ± 20
1	loaded	1410 ± 20
3	unloaded	2200 ± 20
3	loaded	810 ± 10

Table 4.3 Longitudinal relaxation time (T_1) after dialysis.

Flow rate middle channel (μL/min)	Gd-DTPA	T_1 (ms)
3	unloaded	3360 ± 30
3	loaded	1753 ± 8

4.6.8. DISCUSSION

Chitosan-loaded liposomes encapsulating a Gd-based CA are synthetized through an hydrodynamic flow focusing approach. On one hand, the chitosan gel structure entrapped within the core of the liposomes together enhances the relaxometric properties of the encapsulated CA; on the other, the lipid bilayer of the liposome prevents from leaking of the contrast agents, potentially favouring the biocompatibility of the nanostructure and its interactions with the surrounding bio-environment.

4.7. CHAPTER 4 REFERENCES

1. Russo, M., Bevilacqua, P., Netti, P. A. & Torino, E. A Microfluidic Platform to design crosslinked Hyaluronic Acid Nanoparticles (cHANPs) for enhanced MRI. Sci. Rep. 6, 37906 (2016).
2. Port, M. et al. Impact of rigidification on relaxometric properties of a tricyclic tetraazatriacetic gadolinium chelate. Contrast Media Mol. Imaging 1, 121–127 (2006).
3. Sethi, R. et al. Enhanced relaxivity of Gd3+-based contrast agents geometrically confined within porous nanoconstructs. Contrast Media Mol. Imaging 7, (2012).
4. Courant, T. et al. Hydrogels Incorporating GdDOTA: Towards Highly Efficient Dual T1/T2 MRI Contrast Agents. Angew. Chem. Int. Ed. 51, 9119–9122 (2012).
5. Bryson, J. M., Reineke, J. W. & Reineke, T. M. Macromolecular Imaging Agents Containing Lanthanides: Can Conceptual Promise Lead to Clinical Potential? Macromolecules 45, 8939–8952 (2012).
6. Kircher, M. F. et al. A Brain Tumor Molecular Imaging Strategy Using A New Triple-Modality MRI-Photoacoustic-Raman Nanoparticle. Nat. Med. 18, 829–834 (2012).
7. Cole, A. J., David, A. E., Wang, J., Galbán, C. J. & Yang, V. C. Magnetic brain tumor targeting and biodistribution of long-circulating PEG-modified, cross-linked starch-coated iron oxide nanoparticles. Biomaterials 32, 6291–6301 (2011).
8. Ström, A., Larsson, A. & Okay, O. Preparation and physical properties of hyaluronic acid-based cryogels. J. Appl. Polym. Sci. 132, art. no. 42194 (2015).
9. Utech, S. & Boccaccini, A. R. A review of hydrogel-based composites for biomedical applications: enhancement of hydrogel properties by addition of rigid inorganic fillers. J. Mater. Sci. 51, 271–310 (2016).
10. Khabaz, F., Mani, S. & Khare, R. Molecular Origins of Dynamic Coupling between Water and Hydrated Polyacrylate Gels. Macromolecules 49, 7551–7562 (2016).
11. McDonald, R. J. et al. Intracranial Gadolinium Deposition after Contrast-enhanced MR Imaging. Radiology 275, 772–782 (2015).
12. Boyken, J., Frenzel, T., Lohrke, J., Jost, G. & Pietsch, H. Gadolinium Accumulation in the Deep Cerebellar Nuclei and Globus Pallidus After Exposure to Linear but Not Macrocyclic Gadolinium-Based Contrast Agents in a Retrospective Pig Study With High Similarity to Clinical Conditions. Invest. Radiol. 53, 278–285 (2018).
13. Jin, Y.-J., Ubonvan, T. & Kim, D.-D. Hyaluronic Acid in Drug Delivery Systems. J. Pharm. Investig. 40, 33–43 (2010).
14. Tripodo, G. et al. Hyaluronic acid and its derivatives in drug delivery and imaging: Recent advances and challenges. Eur. J. Pharm. Biopharm. Off. J. Arbeitsgemeinschaft Pharm. Verfahrenstechnik EV 97, 400–416 (2015).

15. Mengual, O., Meunier, G., Cayré, I., Puech, K. & Snabre, P. TURBISCAN MA 2000: multiple light scattering measurement for concentrated emulsion and suspension instability analysis. Talanta 50, 445–456 (1999).

16. Balazs, E. A. & Leshchiner, A. Cross-linked gels of hyaluronic acid and products containing such gels. (1986).

17. Sahiner, N. & Jia, X. One-Step Synthesis of Hyaluronic Acid-Based (Sub)micron Hydrogel Particles: Process Optimization and Preliminary Characterization. Turk. J. Chem. 32, 397–410 (2008).

18. Collins, M. N. & Birkinshaw, C. Investigation of the swelling behavior of crosslinked hyaluronic acid films and hydrogels produced using homogeneous reactions. J. Appl. Polym. Sci. 109, 923–931 (2008).

19. Quignard, F., Di Renzo, F. & Guibal, E. From natural polysaccharides to materials for catalysis, adsorption, and remediation. Top. Curr. Chem. 294, 165–197 (2010).

20. Oh, E. J. et al. Control of the molecular degradation of hyaluronic acid hydrogels for tissue augmentation. J. Biomed. Mater. Res. A 86, 685–693 (2008).

21. Bicudo, R. C. S. & Santana, M. H. A. Production of hyaluronic acid (HA) nanoparticles by a continuous process inside microchannels: Effects of non-solvents, organic phase flow rate, and HA concentration. Chem. Eng. Sci. 84, 134–141 (2012).

22. Capretto, L. et al. Mechanism of co-nanoprecipitation of organic actives and block copolymers in a microfluidic environment. Nanotechnology 23, 375602 (2012).

23. Anton, N. et al. A new microfluidic setup for precise control of the polymer nanoprecipitation process and lipophilic drug encapsulation. Soft Matter 8, 10628–10635 (2012).

24. Sah, E. & Sah, H. Recent Trends in Preparation of Poly(lactide-co-glycolide) Nanoparticles by Mixing Polymeric Organic Solution with Antisolvent. Journal of Nanomaterials (2015). doi:10.1155/2015/794601

25. Collins, M. N. & Birkinshaw, C. Comparison of the effectiveness of four different crosslinking agents with hyaluronic acid hydrogel films for tissue-culture applications. J. Appl. Polym. Sci. 104, 3183–3191 (2007).

26. Shimojo, A. A. M., Pires, A. M. B., Lichy, R., Rodrigues, A. A. & Santana, M. H. A. The crosslinking degree controls the mechanical, rheological, and swelling properties of hyaluronic acid microparticles. J. Biomed. Mater. Res. A 103, 730–737 (2015).

27. Shimojo, A. A. M. et al. The Performance of Crosslinking with Divinyl Sulfone as Controlled by the Interplay Between the Chemical Modification and Conformation of Hyaluronic Acid. J. Braz. Chem. Soc. 26, 506–512 (2015).

28. Baier Leach, J., Bivens, K. A., Patrick, C. W. & Schmidt, C. E. Photocrosslinked hyaluronic acid hydrogels: natural, biodegradable tissue engineering scaffolds. Biotechnol. Bioeng. 82, 578–589 (2003).

29. Wu, Y., Joseph, S. & Aluru, N. R. Effect of cross-linking on the diffusion of water, ions, and small molecules in hydrogels. J. Phys. Chem. B 113, 3512–3520 (2009).

30. Ori, G., Massobrio, C., Pradel, A., Ribes, M. & Coasne, B. Structure and Dynamics of Ionic Liquids Confined in Amorphous Porous Chalcogenides. Langmuir 31, 6742–6751 (2015).

31. deMello, J. & deMello, A. Microscale reactors: nanoscale products. Lab. Chip 4, 11N-15N (2004).

32. Patel, T., Zhou, J., Piepmeier, J. M. & Saltzman, W. M. Polymeric Nanoparticles for Drug Delivery to the Central Nervous System. Adv. Drug Deliv. Rev. 64, 701–705 (2012).

33. Zhong, Y., Meng, F., Deng, C. & Zhong, Z. Ligand-directed active tumor-targeting polymeric nanoparticles for cancer chemotherapy. Biomacromolecules 15, 1955–1969 (2014).

34. Chen, H. et al. Multifunctional yolk-in-shell nanoparticles for pH-triggered drug release and imaging. Small Weinh. Bergstr. Ger. 10, 3364–3370 (2014).

35. Koukaras, E. N., Papadimitriou, S. A., Bikiaris, D. N. & Froudakis, G. E. Insight on the formation of chitosan nanoparticles through ionotropic gelation with tripolyphosphate. Mol. Pharm. 9, 2856–2862 (2012).

36. Patil, J. S., Kamalapur, M. V., Marapur, S. C. & KADAM, D. V. Ionotropic Gelation and Polyelectrolyte Complexation : the Novel Techniques to Design Hydrogel Particulate Sustained , Modulated Drug Delivery System : a Review. in (2010).

37. Patil, P., Chavanke, D. & Wagh, M. A REVIEW ON IONOTROPIC GELATION METHOD: NOVEL APPROACH FOR CONTROLLED GASTRORETENTIVE GELISPHERES. 4, 6

38. Fan, W., Yan, W., Xu, Z. & Ni, H. Formation mechanism of monodisperse, low molecular weight chitosan nanoparticles by ionic gelation technique. Colloids Surf. B Biointerfaces 90, 21–27 (2012).

39. Kashyap, P. L., Xiang, X. & Heiden, P. Chitosan nanoparticle based delivery systems for sustainable agriculture. Int. J. Biol. Macromol. 77, 36–51 (2015).

40. Ponsiglione, A. M., Russo, M., Netti, P. A. & Torino, E. Impact of biopolymer matrices on relaxometric properties of contrast agents. Interface Focus 6, (2016).

41. Russo, M., Bevilacqua, P., Netti, P. A. & Torino, E. Commentary on "A Microfluidic Platform to Design Crosslinked Hyaluronic Acid Nanoparticles (cHANPs) for Enhanced MRI". Mol. Imaging 16, (2017).

42. Russo, M., Ponsiglione, A. M., Forte, E., Netti, P. A. & Torino, E. Hydrodenticity to enhance relaxivity of gadolinium-DTPA within crosslinked hyaluronic acid nanoparticles. Nanomed. 12, 2199–2210 (2017).

43. Russo, M. et al. PEGylated crosslinked hyaluronic acid nanoparticles designed through a microfluidic platform for nanomedicine. Nanomed. 12, 2211–2222 (2017).

44. Capretto, L., Carugo, D., Mazzitelli, S., Nastruzzi, C. & Zhang, X. Microfluidic and lab-on-a-chip preparation routes for organic nanoparticles and vesicular systems for nanomedicine applications. Adv. Drug Deliv. Rev. 65, 1496–1532 (2013).

45. Karnik, R. et al. Microfluidic platform for controlled synthesis of polymeric nanoparticles. Nano Lett. 8, 2906–2912 (2008).

46. Dou, Y. et al. A review on self-assembly in microfluidic devices. J. Micromechanics Microengineering 27, 113002 (2017).

47. Callewaert, M. et al. Tuning the composition of biocompatible Gd nanohydrogels to achieve hypersensitive dual T1/T2 MRI contrast agents. J. Mater. Chem. B 2, 6397–6405 (2014).

48. Mansfield, P. Snapshot magnetic resonance imaging (Nobel lecture). Angew. Chem. Int. Ed Engl. 43, 5456–5464 (2004).

49. Caravan, P., Ellison, J. J., McMurry, T. J. & Lauffer, R. B. Gadolinium(III) Chelates as MRI Contrast Agents: Structure, Dynamics, and Applications. Chem. Rev. 99, 2293–2352 (1999).

50. Xue, S., Qiao, J., Pu, F., Cameron, M. & Yang, J. J. Design of a novel class of protein-based magnetic resonance imaging contrast agents for the molecular imaging of cancer biomarkers. Wiley Interdiscip. Rev. Nanomed. Nanobiotechnol. 5, 163–179 (2013).

51. Kanda, T., Matsuda, M., Oba, H., Toyoda, K. & Furui, S. Gadolinium Deposition after Contrast-enhanced MR Imaging. Radiology 277, 924–925 (2015).

52. Muldoon, L. L. & Neuwelt, E. A. Dose-Dependent Neurotoxicity (Seizures) Due to Deposition of Gadolinium-based Contrast Agents in the Central Nervous System. Radiology 277, 925–926 (2015).

53. Biffi, S. et al. Applications of nanoparticles in cancer medicine and beyond: optical and multimodal in vivo imaging, tissue targeting and drug delivery. Expert Opin. Drug Deliv. 12, 1837–1849 (2015).

54. Kamaly, N. & Miller, A. D. Paramagnetic Liposome Nanoparticles for Cellular and Tumour Imaging. Int. J. Mol. Sci. 11, 1759–1776 (2010).

55. Zhou, Z. & Lu, Z.-R. Gadolinium-based contrast agents for magnetic resonance cancer imaging. Wiley Interdiscip. Rev. Nanomed. Nanobiotechnol. 5, 1–18 (2013).

56. Cheng, Z., Thorek, D. L. J. & Tsourkas, A. Porous Polymersomes with Encapsulated Gd-labeled Dendrimers as Highly Efficient MRI Contrast Agents. Adv. Funct. Mater. 19, 3753–3759 (2009).

57. De Oliveira, H., Thevenot, J. & Lecommandoux, S. Smart polymersomes for therapy and diagnosis: fast progress toward multifunctional biomimetic nanomedicines. Wiley Interdiscip. Rev. Nanomed. Nanobiotechnol. 4, 525–546 (2012).

58. Unger, E. C. et al. Hepatic metastases: liposomal Gd-DTPA-enhanced MR imaging. Radiology 171, 81–85 (1989).

59. Karathanasis, E. et al. MRI mediated, non-invasive tracking of intratumoral distribution of nanocarriers in rat glioma. Nanotechnology 19, 315101 (2008).

60. Zou, J. et al. Manufacturing and in vivo inner ear visualization of MRI traceable liposome nanoparticles encapsulating gadolinium. J. Nanobiotechnology 8, 32 (2010).

61. Bui, T. et al. Novel Gd Nanoparticles Enhance Vascular Contrast for High-Resolution Magnetic Resonance Imaging. PLoS ONE 5, (2010).

62. Kielar, F., Tei, L., Terreno, E. & Botta, M. Large relaxivity enhancement of paramagnetic lipid nanoparticles by restricting the local motions of the Gd(III) chelates. J. Am. Chem. Soc. 132, 7836–7837 (2010).

63. Kono, K. et al. Multi-functional liposomes having temperature-triggered release and magnetic resonance imaging for tumor-specific chemotherapy. Biomaterials 32, 1387–1395 (2011).

64. Na, K., Lee, S. A., Jung, S. H. & Shin, B. C. Gadolinium-based cancer therapeutic liposomes for chemotherapeutics and diagnostics. Colloids Surf. B Biointerfaces 84, 82–87 (2011).

65. Li, W. et al. RGD-targeted paramagnetic liposomes for early detection of tumor: in vitro and in vivo studies. Eur. J. Radiol. 80, 598–606 (2011).

66. Liao, Z. et al. Multifunctional Nanoparticles Composed of A Poly(dl-lactide-coglycolide) Core and A Paramagnetic Liposome Shell for Simultaneous Magnetic Resonance Imaging and Targeted Therapeutics. Adv. Funct. Mater. 21, 1179–1186 (2011).

67. Gianolio, E. et al. Relaxometric investigations and MRI evaluation of a liposome-loaded pH-responsive gadolinium(III) complex. Inorg. Chem. 51, 7210–7217 (2012).

68. Smith, C. E. et al. A polymeric fastener can easily functionalize liposome surfaces with gadolinium for enhanced magnetic resonance imaging. ACS Nano 7, 9599–9610 (2013).

69. Cittadino, E. et al. In Vivo Magnetic Resonance Imaging Detection of Paramagnetic Liposomes Loaded with Amphiphilic Gadolinium(III) Complexes: Impact of Molecular Structure on Relaxivity and Excretion Efficiency. in (2013).

70. Hossann, M. et al. Non-ionic Gd-based MRI contrast agents are optimal for encapsulation into phosphatidyldiglycerol-based thermosensitive liposomes. J. Control. Release Off. J. Control. Release Soc. 166, 22–29 (2013).

71. Thomsen, H. S. et al. Nephrogenic systemic fibrosis and gadolinium-based contrast media: updated ESUR Contrast Medium Safety Committee guidelines. Eur. Radiol. 23, 307–318 (2013).

72. Cheng, Z. et al. Stabilized porous liposomes with encapsulated Gd-labeled dextran as a highly efficient MRI contrast agent. Chem. Commun. Camb. Engl. 50, 2502–2504 (2014).

73. Kozlowska, D. et al. Gadolinium-loaded polychelating amphiphilic polymer as an enhanced MRI contrast agent for human multiple myeloma and non Hodgkin's lymphoma (human Burkitt's lymphoma). RSC Adv. 4, 18007–18016 (2014).

74. Park, J.-H. et al. Hyaluronic acid derivative-coated nanohybrid liposomes for cancer imaging and drug delivery. J. Control. Release Off. J. Control. Release Soc. 174, 98–108 (2014).

75. Silva, S. R. et al. Gadolinium(III) Complexes with N-Alkyl-N-methylglucamine Surfactants Incorporated into Liposomes as Potential MRI Contrast Agents. Bioinorg. Chem. Appl. 2015, 942147 (2015).

76. Gu, M.-J. et al. In vitro study of novel gadolinium-loaded liposomes guided by GBI-10 aptamer for promising tumor targeting and tumor diagnosis by magnetic resonance imaging. Int. J. Nanomedicine 10, 5187–5204 (2015).

77. Huang, W.-C., Chen, Y.-C., Hsu, Y.-H., Hsieh, W.-Y. & Chiu, H.-C. Development of a diagnostic polymersome system for potential imaging delivery. Colloids Surf. B Biointerfaces 128, 67–76 (2015).

78. Xiao, Y. et al. Sorafenib and gadolinium co-loaded liposomes for drug delivery and MRI-guided HCC treatment. Colloids Surf. B Biointerfaces 141, 83–92 (2016).

79. Lorenzato, C. et al. MRI monitoring of nanocarrier accumulation and release using Gadolinium-SPIO co-labelled thermosensitive liposomes. Contrast Media Mol. Imaging 11, 184–194 (2016).

80. Liu, X. et al. MRI contrast agent for targeting glioma: interleukin-13 labeled liposome encapsulating gadolinium-DTPA. Neuro-Oncol. 18, 691–699 (2016).

81. Tian, B. et al. Mannose-coated gadolinium liposomes for improved magnetic resonance imaging in acute pancreatitis. Int. J. Nanomedicine 12, 1127–1141 (2017).

Chapter 5.

CONCLUSION AND FUTURE OUTLOOK

5.1. CONTRIBUTION TO THE FUNDAMENTAL UNDERSTANDING AND APPLICATIONS

Macromolecular Gadolinium Contrast Agents (GdCAs) offer high relaxivities and are thus promising GdCAs for Magnetic Resonance Imaging (MRI). In the last decades, indeed, several strategies have been developed to improve the relaxivity of GdCAs by using polymers and nanostructured materials and, more recently, the crucial role of polymer matrices in enhancing the relaxometric properties of GdCAs has been widely recognised.

Unfortunately, despite these promising properties of macromolecular GdCAs, a comprehensive knowledge of the complex phenomena, which rule the interaction between polymers and GdCAs and are responsible for the relaxation enhancement, is still lacking. The fundamental understanding of those energetic and thermodynamic contributions, capable to boost the efficacy of commercial GdCAs by exploiting the properties of FDA approved biopolymers, is of crucial importance also because the relaxivity of clinically-used GdCAs is far below its theoretical limit and could be largely increased. The in-depth knowledge and the proper control of the behaviour of a *library* of different biopolymers combined with GdCAs could significantly contribute to the development of new advanced nanostructures for MRI.

We have observed that, in the presence of a crosslinked matrix, it is possible to modulate the water content of the system and, therefore, the hydration of the CA, by adjusting the crosslinking degree of the hydrogel structure.

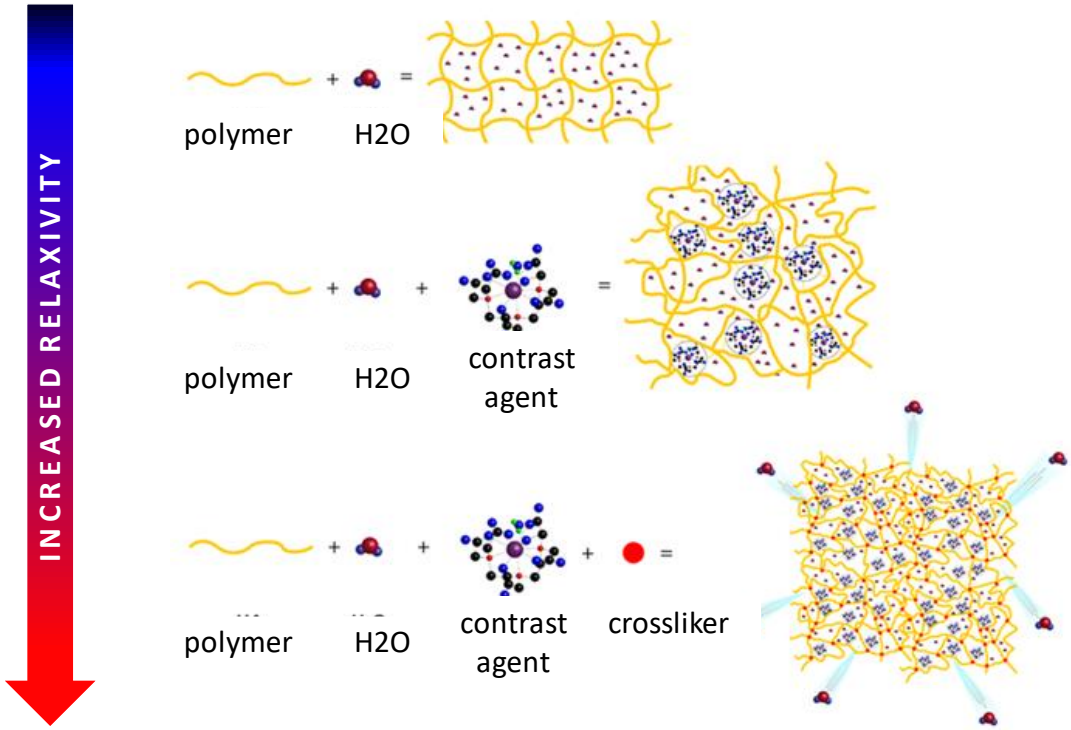

Figure 5.1 Graphical representation of the increased relaxivity obtained by tuning the hydrogel composition.

This is due to the highly relaxing nano-scaled sinks forming around the GdCA, that we called Gado-Meshes. These nanocompartments create a favourable environment for the enhancement of the relaxivity due to the modulation of the characteristic correlation times (diffusion correlation time, residence lifetime, rotational correlation time) obtained through the polymer chain wrapping the GdCA as shown in Figure 5.2.

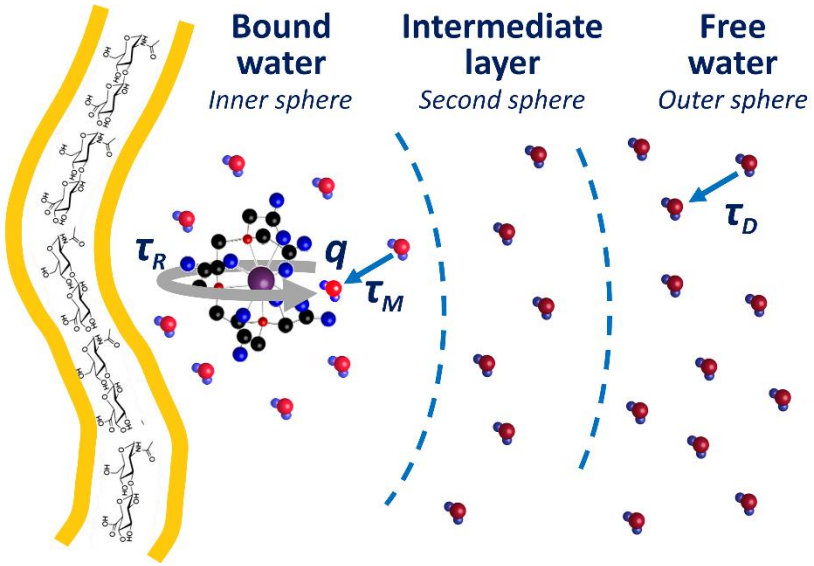

Figure 5.2 Schematic representation of the Gado-Mesh.

In these conditions, a more stable polymer network can be obtained, promoting more efficient water-polymer and water-CA interactions that boost the relaxivity to higher values. The crosslinking degree is proposed as an advanced tool to modulate the hydrogel network and its properties, enabling the tuning of the relaxometric properties. We defined as *Hydrodenticity* the complex equilibrium between the water osmotic pressure, the elastodynamic forces of the polymer chains and the hydration degree of the CA which is able to increase the relaxivity of the CA itself.

On the basis of the concept of *Hydrodenticity*, we produced different nanostructures for enhanced MRI, as summarized in the figure below (Figure 5.3):

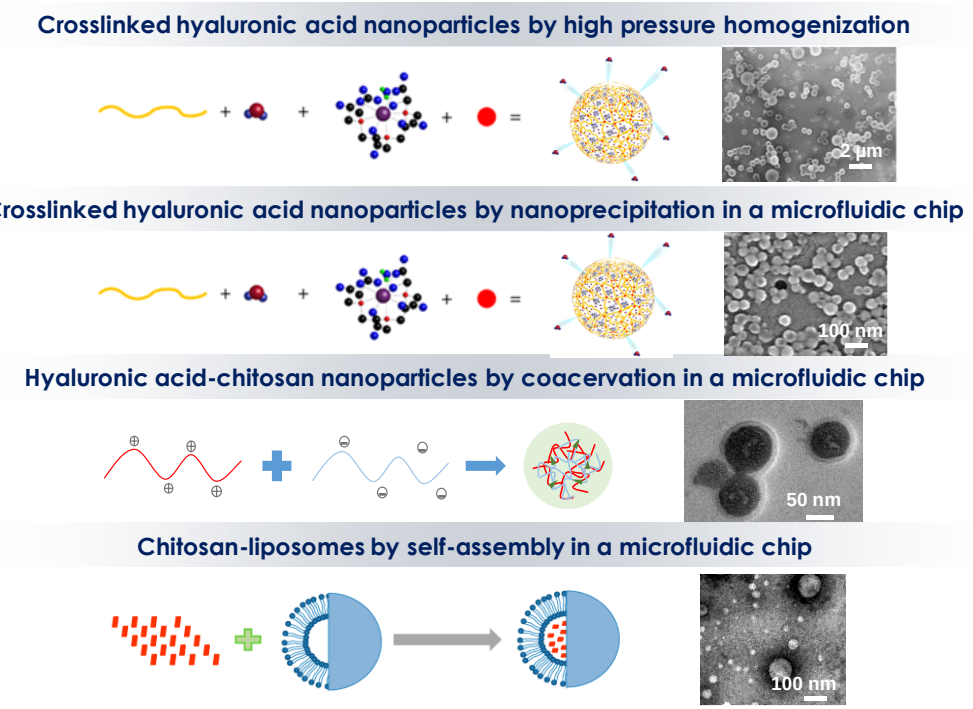

Figure 5.3 Nanostructures for enhanced MRI developed starting from the concept of *Hydrodenticity*.

Capitalizing on recent advances in nanotechnology together with a more fundamental insight in the behavior of these biopolymer systems could pave the way to the engineering of better and safer MRI CAs. Our findings about the interaction between biopolymer matrices and CAs could provide a flexible platform affording ample control over the physical attributes of the CAs and allow developing novel polymer-based CAs with increased relaxivity without inducing any chemical modification to the CA's structure and biocompatibility.

In addition, a better knowledge of the dynamics and properties of these systems could be scaled to nano-scale dimensions, inspiring the development of new nanostructured MRI CAs with tuneable relaxometric properties as well as the production of metallopolymer complexes or magnetic and conductive polymer-based materials with applications in areas such as sensors, memory devices, nanolithography and controlled release.

5.2. DRAFT OF A PRELIMINARY MODEL FOR THE STUDY OF POLYMER CONTRAST AGENTS

The well-known Solomon-Bloembergen-Morgan (SBM) model has been theorized to describe the relaxation mechanisms and calculate the contrast agents' relaxivity. As widely discussed in this thesis, the SBM model calculates the relaxivity as a function of multiple parameters characterizing the behaviour of the contrast agents and of the surrounding water molecules.

We implemented this model using MatLab and we are now working to make it specific for the description of the relaxation enhancement in polymer-based contrast agents. The following figure is only an example of how the model simulates the behaviour of contrast agents with different rotational correlation times (τ_R).

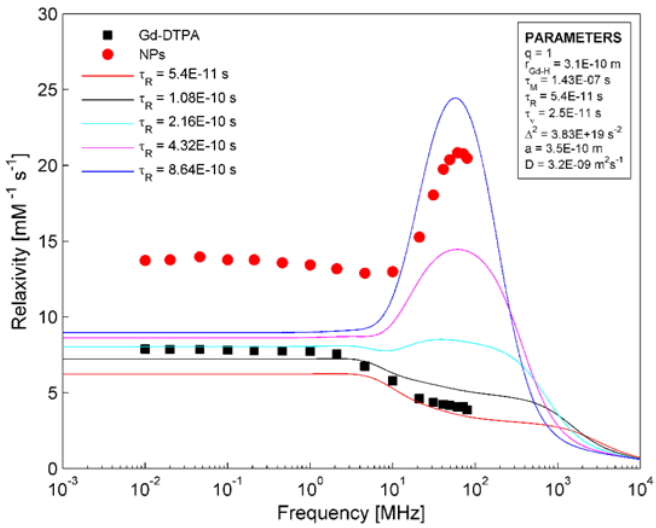

Figure 5.4 MatLab simulations of NMRD profiles for different types of contrast agents.

Different Nuclear Magnetic Resonance Dispersion (NMRD) profiles are shown changing the value of τ_R and real relaxivity data from free Gd-DTPA and Gd-loaded polymer nanoparticles are also plotted.

Further and in-depth studies are needed to complete and validate the drafted model.

5.3. FUTURE ACTIVITIES

Future studies will be dedicated to:

1. Test in vivo the efficacy of the obtained nanostructures;
2. Decorate and functionalize the nanostructures with peptides and ligands to make them specific for certain biological targets;
3. Develop and implement predictive models to describe the polymer-CA interactions and design new structures polymer-metal complexes with increased relaxivity;
4. Design further nanostructures by using different biopolymers (e.g. PLGA, PLGA-PEG) and different MRI CAs;
5. Build a library of biocompatible and clinically approved nanostructures that efficiently combines polymers and commercial MRI CAs for different diagnostic needs;
6. Design nanostructures for multimodal imaging and theranostic applications as well as for precision medicine.

APPENDIX:
SUPPORTING INFORMATION AND NANOSTRUCUTRES' SYNTHESIS

A.1. IMPACT OF BIOPOLYMERS ON RELAXOMETRIC PROPERTIES OF CONTRAST AGENTS: DEFINITION OF HYDRODENTICITY

Supporting data, figures and tables.

Table S1. Water self-diffusion coefficient measured at different Pulse Gradient Amplitudes for 0.25 and 5 % w/v HA hydrogel solution at varying crosslinking degrees (different DVS concentrations). Diffusion coefficients have been measured 8 and 24 hours after crosslinking reaction.

HA (% w/v)	**DVS (µL)**	**D after 8h (*10^{-9} m^{2}s^{-1})**	**D after 24h (*10^{-9} m^{2}s^{-1})**
0	0	3.19 ± 0.01	3.19 ± 0.01
0.25	0	3.05 ± 0.01	3.06 ± 0.02
0.25	5	3.01 ± 0.02	3.02 ± 0.01
0.25	10	2.97 ± 0.03	2.98 ± 0.02

0.25	15	2.95 ± 0.03	2.96 ± 0.02
0.25	20	2.92 ± 0.02	2.94 ± 0.02
0.25	25	2.90 ± 0.02	2.92 ± 0.03
5	10	2.88 ± 0.02	2.87 ± 0.01
5	20	2.85 ± 0.01	2.85 ± 0.02
5	30	2.83 ± 0.02	2.85 ± 0.01
5	40	2.84 ± 0.01	2.84 ± 0.02

Table S2. Range of water self-diffusion coefficient measured for Gd-DTPA solutions at different Gd-DTPA concentrations.

Gd-DTPA (µM)	**D (*10^{-9} m^2s^{-1})**
0	3.19 ± 0.01
50	3.12 ± 0.02
100	3.14 ± 0.02
150	3.09 ± 0.02
200	3.18 ± 0.01
500	3.11 ± 0.02
1000	3.13 ± 0.03

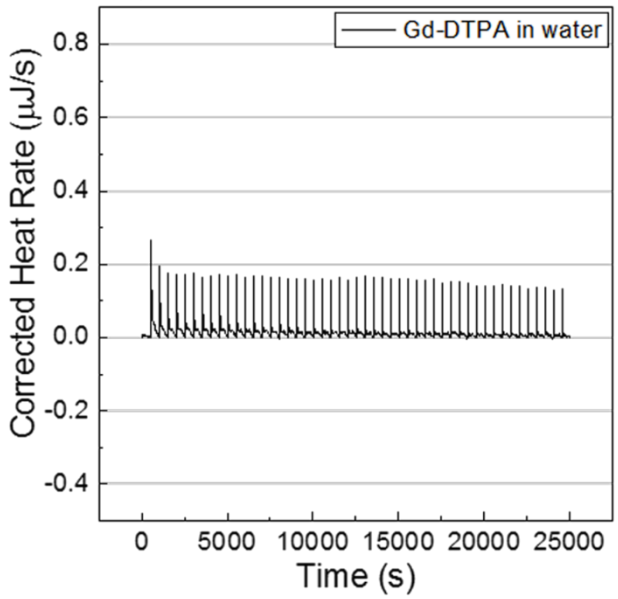

Figure S1. Titration curves of Gd-DTPA in water at 25 °C and 200 rpm.

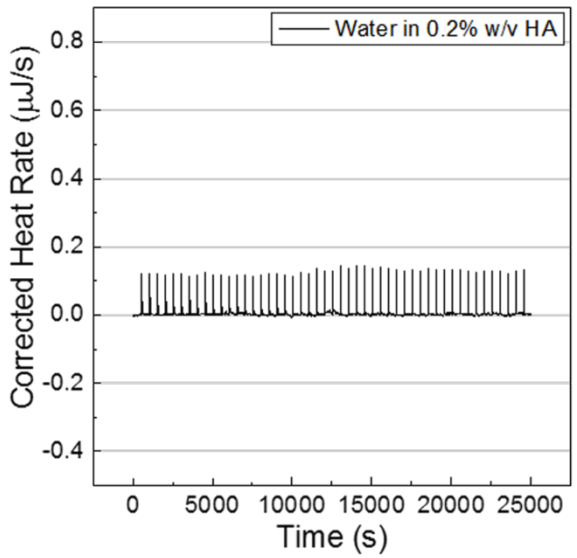

Figure S2. Titration curves of water into 0.2% w/v HA solutions at 25 °C and 200 rpm.

Table S3. Relaxation rates ($1/T_1$) and relaxivity values for: (Sample 1) Gd-DTPA in water; (Sample 2) Gd-DTPA in 0.3% w/v HA solution; (Sample 3) Gd-DTPA in 0.3% w/v HA solution crosslinked with 2.4% w/v DVS; (Sample 4) Gd-DTPA in 0.5% w/v HA solution; (Sample 5) Gd-DTPA in 0.5% w/v HA solution crosslinked with 4% w/v DVS; (Sample 6) Gd-DTPA in 0.7% w/v HA solution; (Sample 7) Gd-DTPA in 0.7% w/v HA solution crosslinked with 5.6% w/v DVS

Gd-DTPA (mM)	**Sample 1 (s^{-1})**	**Sample 2 (s^{-1})**	**Sample 3 (s^{-1})**	**Sample 4 (s^{-1})**	**Sample 5 (s^{-1})**	**Sample 6 (s^{-1})**	**Sample 7 (s^{-1})**
0.000	0.265 ± 0.003	0.264 ± 0.001	0.273 ± 0.000	0.273 ± 0.001	0.331 ± 0.001	0.265 ± 0.003	0.301 ± 0.001
0.010	0.299 ± 0.000	0.309 ± 0.000	0.342 ± 0.001	0.315 ± 0.001	0.301 ± 0.001	0.309 ± 0.001	0.313 ± 0.001
0.020	0.330 ± 0.001	0.347 ± 0.001	0.348 ± 0.001	0.339 ± 0.001	0.360 ± 0.001	0.345 ± 0.000	0.342 ± 0.001
0.025	-	-	0.351 ± 0.001	-	-	-	-
0.030	0.361 ± 0.000	0.372 ± 0.001	0.381 ± 0.001	0.384 ± 0.001	0.382 ± 0.001	0.373 ± 0.001	0.403 ± 0.007
0.035	0.379 ± 0.001	0.388 ± 0.001	-	0.392 ± 0.001	-	-	-
0.040	0.397 ± 0.002	0.398 ± 0.002	0.449 ± 0.001	0.400 ± 0.005	0.445 ± 0.001	0.398 ± 0.003	0.402 ± 0.006
0.050	0.441 ± 0.003	0.434 ± 0.025	0.436 ± 0.001	0.450 ± 0.001	0.510 ± 0.002	0.445 ± 0.001	0.468 ± 0.001
0.060	0.450 ± 0.001	0.463 ± 0.001	0.510 ± 0.001	0.493 ± 0.001	0.485 ± 0.001	0.452 ± 0.001	0.549 ± 0.003
0.070	0.485 ± 0.001	0.496 ± 0.001	0.512 ± 0.001	0.505 ± 0.001	-	-	-
0.080	0.528 ± 0.001	0.562 ± 0.003	0.599 ± 0.004	0.503 ± 0.001	0.610 ± 0.015	0.548 ± 0.002	0.547 ± 0.001
0.100	-	0.588 ± 0.069	0.702 ± 0.002	0.599 ± 0.004	0.590 ± 0.001	0.594 ± 0.002	0.595 ± 0.007
0.130	-	0.685 ± 0.000	0.722 ± 0.002	0.678 ± 0.001	0.701 ± 0.001	0.675 ± 0.002	0.699 ± 0.001

0.150	-	0.754 ± 0.001	0.805 ± 0.002	0.757 ± 0.002	0.797 ± 0.001	0.755 ± 0.001	0.786 ± 0.002
0.180	-	-	-	-	-	0.845 ± 0.002	1.043 ± 0.003
0.200	0.880 ± 0.002	0.909 ± 0.003	1.075 ± 0.002	0.904 ± 0.008	1.098 ± 0.004	0.971 ± 0.002	0.896 ± 0.004
0.250	-	-	-	-	-	1.071 ± 0.003	1.126 ± 0.004
Relaxivity ($mM^{-1}s^{-1}$)	3.067 ± 0.044	3.185 ± 0.050	3.805 ± 0.164	3.114 ± 0.061	3.655 ± 0.225	3.256 ± 0.064	3.410 ± 0.205

A.2. HIGH PRESSURE HOMOGENIZATION TO PRODUCE POLYMER NANOPARTICLES BASED ON HYDRODENTICITY

Materials: All chemicals used are of analytical reagent grade quality and are employed as received. Sorbitan monooleate (Span® 80) (S80), Polyoxyethylenesorbitan trioleate (Tween® 85) (T85), Mineral oil (light oil, 0.8 gr/cm at 25°C), Divinyl sulfone (DVS, 118.15 Da), Diethylenetriaminepentaacetic acid gadolinium(III) dihydrogen salt hydrate (Gd-DTPA, 547.57 Da), Sodium hydroxide pellets (NaOH), Acetone and Ethanol are purchased from Sigma Aldrich Chemical (Italy). Sodium Hyaluronate, with an average molecular weight of 850 kDa (purity 99%; Hyasis® 850P) and 42 kDa, is respectively supplied by Novozymes Biopharma and Bohus Biotech (Sweden) as dry powder and used without purification.

Magnevist® (Bracco Imaging, Italy), a contrast agent commercially available, is used in this study. The water is purified by distillation, deionization, and reserve osmosis (Milli-Q Plus) and systematically used for sample preparation, purification and analysis. All experiments are repeated in triplicate and conducted at room temperature, 25°C.

Isothermal Titration Calorimetry: Titration experiments are performed by using a Nano ITC Low Volume calorimeter (TA Instruments). CA and polymer are prepared in double-distilled filtered water without any additives. The sample cell (700 μL) and the syringe (50 μL) are filled with aqueous solutions of HA and Gd-DTPA respectively. Syringe Gd-DTPA concentration is fixed at 1.5 mM, while different HA concentrations in the sample cell are tested, ranging from 0.3 to 0.7% w/v. The measurements are performed at 25 °C and at fixed stirring rate of 200 rpm. Fifty Injections, each of 1 μL of Gd-DTPA, are delivered in intervals of 500 s. The concentration of polymer is expressed as the mass of the repeat unit (unit mol/L).

Data analysis and processing to provide ITC and enthalpy change (ΔH) profiles is carried out using the NanoAnalyze (TA instruments) and the OriginPro software.

NMR Spectroscopy: ^{1}H NMR spectra are recorded at 25 °C with Varian Agilent NMR spectrometer operating at 600 MHz to observe chemical interactions between polymer and chelating agent (DTPA). The NMR samples consisted of water solution of HA-DTPA at different molar ratios (HA/DTPA ranging from 0 to 0.5), with 10% v/v D_2O.

Diffusion-ordered NMR Spectroscopy (DOSY) are also performed and the z-gradient strengths (Gz) is varied in 20 steps from 500 to 32500 G/cm (maximum strength). The gradient pulse duration (δ) and the diffusion delay (Δ) are kept costant, 2 ms for δ and ranging from 7 to 1000 ms for Δ. After Fourier transformation and baseline correction, DOSY spectra are processed and analysed using Varian software VNMRJ (Varian by Agilent Technologies, Italy) in order to obtain the values of water self-diffusion coefficient.

Differential Scanning Calorimetry: For all measurements the HA/water solution (Mw = 42 kDa) is used. The aqueous solutions are prepared in a concentration range of polymer 0.3–0.7% w/v. Next, Gd-DTPA is added as CA at different molar ratio HA/Gd-DTPA (from 1:0.25 to 1:3) and stirred for 12 h. The hydrated polymer samples, with and without CA, are sealed at room temperature in a Tzero hermetic pans prior to analysis. DSC measurements are performed in a TA Instruments'

Q20™ calorimeter on samples between 5 and 10 mg. The samples are cooled down from 25°C to -50°C followed by heating scan up to 25°C. The same heating and cooling rate are 10°C/min for all runs. Samples are tested in triplicate to ensure reproducibility. For DSC and ITC measurements, we used low molecular weight HA (42 kDa) to highlight better the energetic contributions of different components without exceeding the maximum scale of the instruments.

Time-Domain Relaxometry: The spin-lattice relaxation times (T1) are measured in a Bruker Minispec (mq 60) bench-top relaxometer operating at 60 MHz for protons (magnetic field strength: 1.41 T). Measurements are taken at 37°C, and before NMR measurements, the tube is placed into the NMR probe for about 15 min for thermal equilibration. Experiments are made using water solutions of Gd-DTPA (from 0 to 0.1 mM) and HA (0.3, 0.5 and 0.7% w/v) crosslinked with DVS (DVS/HA weight percentage ratio equal to 1:8). T1 values are determined by both saturation (SR) and inversion recovery (IR) pulse sequences. The relaxation recovery curves are fitted using a multi-exponential model. Relaxivities, r_1, are calculated from the slope of the regression line of 1/T1 [s^{-1}] versus concentration with a least-squares method.

Emulsion preparation: The emulsions are prepared at different water to oil (W/O) ratio (10/90 and 20/80 v/v). Mineral oil is used as oil phase (or continuous phase, P_C) and W/O emulsions are made by varying the concentration of surfactants for the P_C and water phase (or dispersed phase, P_D) and the concentration of NaOH (from 0 to 0.2 M) for the P_D in order to obtain emulsion systems. In particular, a pair of non-ionic surfactants, Span-80 (S80) and Tween-85 (T85), are used to prepare mixtures with a range from 4.3 to 7.65 of HLB values. Depending on the initial HLB to be used, mixtures of S80 and T85 are pre-dissolved in the appropriate S80/T85 mass ratios (from 50/50 to 75/25) in P_C and P_D, respectively. P_D containing T85 and NaOH, is added dropwise to P_C and W/O emulsions are prepared using a high-shear homogenizer (Silverson L5M-A, Silverson Machines Ltd, Waterside, UK). Homogenization of the Emulsion is performed from 5000 to 7000 rpm for 10 min at room temperature (25°C).

Temporal emulsion stability determination: The stability of emulsions is evaluated, at regular time intervals, by visual observation, measuring the height of the phase separated by creaming in centrimeters as a function of the time. In addition, an optical characterization of emulsion stability made is using a Turbiscan (Turbiscan LabThermo) by static multiple light scattering (MLS), sending a light beam from an electroluminescent diode (λ=880 nm) through a cylindrical glass cell containing the sample. The emulsion sample without dilution is placed in a cylindrical glass cell and two synchronous optical sensors receive the light transmitted through the sample (180° from the incident light) and the light backscattered by the droplets in the sample (45° from the incident light). The optical reading head scans the height of the sample in the cell (about 40 mm), by acquiring transmission and backscattering data every 40 μm. Transmitted and backscattered light are monitored as a function of time and cell height for a period of 24 hours at an interval of 30 min at 25°C.

Preparation of DVS-crosslinked nanoparticles: Based on these preliminary results, P_D/P_C ratio in all samples is set at 10/90 v/v. In particular, for the preparation of cross-linked NPs, HA powder (Mw = 850 kDa) is dissolved at different concentrations (from 0.1 to 0.5% w/v) under alkalyn condition (NaOH ranging from 0 to 0.2 M) by vigorous stirring at room temperature for 4 hours until a homogenous solution is obtained. Mineral oil and S80 (from 0.5 to 2% w/v) are separately mixed by stirring. P_D is added drop-wise in the P_C without stirring and all the components are completely mixed by homogenization at various times (5-15 minutes) and speeds (5000 - 7000 rpm). Then, the cross-linking agent (DVS) is added to the final emulsion (40 ml), which is kept in agitation on a laboratory tube rotator for 24 hours in order to obtain a homogeneous DVS distribution in the P_D. To test DVS activity, various conditions of crosslinking reaction are explored: (1) at different DVS concentrations (from 0.01 to 0.5% v/v); (2) at three starting times of reaction (beginning, during and post homogenization) and (3) at different temperatures (4 and 25°C).

Loading of HA NPS with Contrast agents: After identifying the protocol to obtain NPs, Gd-DTPA is chosen as CA and mixed in the P_D before homogenization. Gd-

loaded HA NPs (HA-Gd NPs) are prepared using different HA/CA mass ratios (1:1, 1:2 and 1:5). DVS are added post homogenization to the batch at room temperature using the same procedure reported above.

Collection of the nanoparticles: Recovery of the NPs and their separation from W/O emulsion system is made using dialysis and/or ultracentrifugation. For dialysis method, the obtained emulsion is placed in a pre-washed cellulose membrane tubing (Spectra/Por® Dialysis Tubing, cut-off of 25 kDa). Organic impurities (Mineral oil and S80) are removed dialyzing first against solvents as acetone and/or ethanol, and gradually against water. Dialyzing solutions are changed at regular time intervals. In the case of ultracentrifugation, 1 ml of the emulsion is added to 5 ml of ethanol and mixed for 2 hours. Then, this mix is centrifuged with an ultracentrifuge (Beckman-Coulter OPTIMA MAX-XP) at 55000 rpm for 20 min at 15°C. The resulting pellet is washed twice and resuspended in MilliQ water. The second step of ultracentrifugation (70000 rpm, 10 min, 15°C) is applied to the pellet in order to obtain purified NPs.

Characterization of the nanoparticles: To determine size distribution of NPs, dynamic light scattering (DLS) are performed using a Zetasizer S-90 1000 HS (Malvern Instruments, UK).

All samples are diluted (1:10) with deionized water to prevent the effects of multiple scattering. The measurement temperature is set at 25°C. The morphology and size of NPs are investigated using a ULTRA PLUS field emission Scanning Electron microscope (FE-SEM Carl Zeiss, Oberkochen, Germany) and a Transmission Electron microscopy (TEM, TECNAI). In the first case, the samples are coated with gold (7 nm).

Determination of Gadolinium loading by ICP-MS: The quantitative determination of loaded Gd in HA NPs is assessed by ICP-MS (NexION 350, Perkin Elmer) without any previous digestion processes. For all examinations, purified NP

suspensions are used. The non-encapsulated Gd-complexes are separated from the NPs by high speed centrifugation (55000 rpm, 20 min, 15 °C).

MRI Testing: To explore the potential of Gd-loaded HA NPs as MRI contrast agent, MRI in vitro test is performed at two different magnetic fields, 1.5 T and 3 T MR (Philips Achieva) using Sense Head 8 coil. The T1-weighted MR images of HA NPs, unloaded and loaded with Gd-DTPA at different concentrations using an inversion recovery sequence are measured with the following parameters: TR = 2500 ms; TE = 12 ms; TI = 50, 100, 200, 400, 800, 1100, 1800 ms; FOV= 180x146 mm; slice thickness = 4 mm, acquisition matrix = 360x292.

The signal intensity of the samples is measured on the obtained T1-weighted MR images and compared to Gd-DTPA.

NMR dispersion measurements: The proton 1/T1 NMRD profiles are measured using a fast-field-cycling Stelar SmarTracer relaxometer over a continuum of magnetic field strengths from 0.00024 to 0.25 T (which correspond to 0.01 - 10 MHz proton Larmor frequencies). The uncertainty of these measurements is less than 1%. Additional data points in the range 15 - 70 MHz are obtained using a Stelar Relaxometer and a Bruker WP80 NMR electromagnet adapted to variable-field measurements (15 - 80 MHz proton Larmor frequency).

Supporting data, figures and tables.

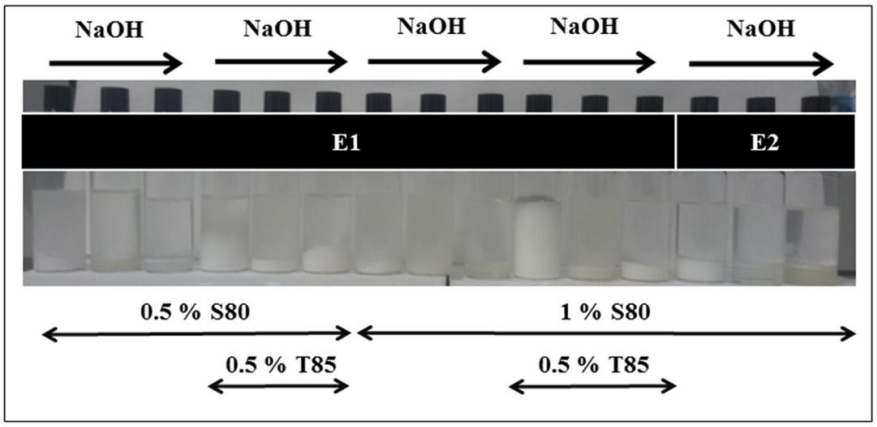

Figure S3. Photografic image of the appearance of emulsions at 25 °C by the effect of increasing concentration of surfactants and NaOH [(a) 0 M; (b) 0.1 M; (c) 0.2 M] on stability of W/O (10/90 and 20/80) emulsion after 12 h.

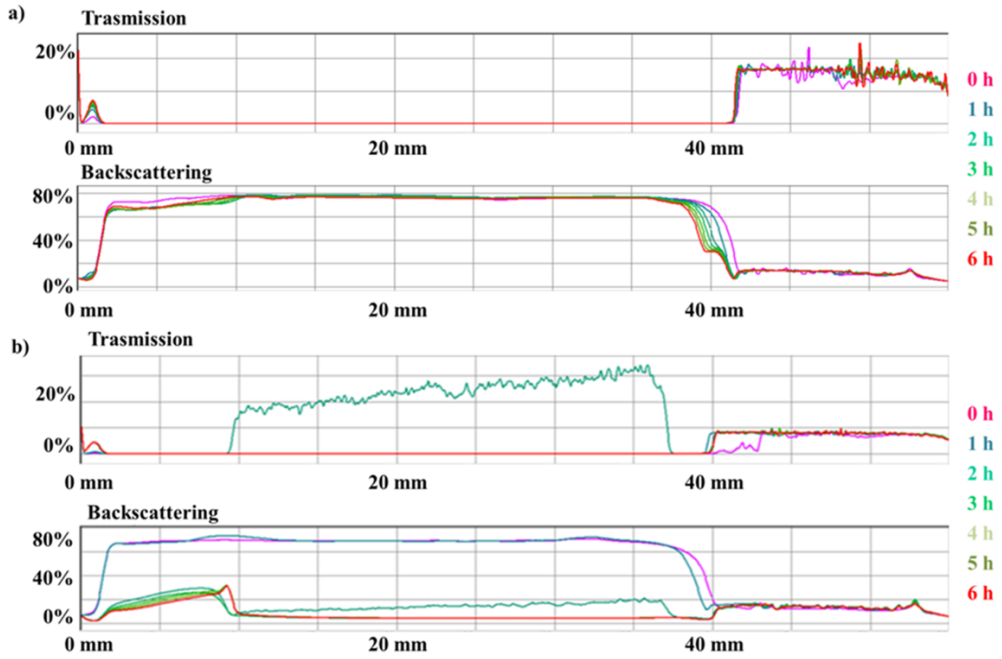

Figure S4. Trasmission and backscattering spectra of W/O (10/90) emulsion (total volume, 20 ml; 5000 rpm, 10 min) with 1% w/v of S80 without (a) and with (b) 0.2 M NaOH.

Table S4. Experimental conditions for production of HA-NPs.

Pd / Pc [a]	**HA** [b] **[% w/v]**	**NaOH [M]**	**DVS** [c] **[% v/v]**	**Span-80 [% w/v]**
10 / 90	0.1	0	0.045	1
		0.1		
		0.2		
	0.25	0		
		0.1		
		0.2		

	0
0.5	0.1
	0.2

[a)] Pd is the volume of the disperse phase, Pc is the volume of the continuous phase; [b)] Hyaluronic Acid; [c)] Divinyl Sulfone

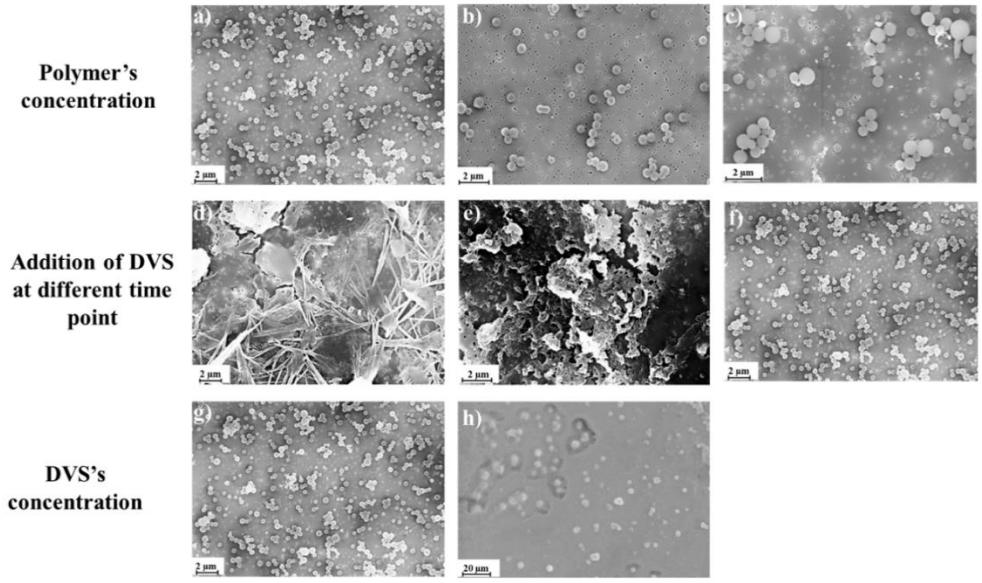

Figure S5. Optimization of HA NPs synthesis. SEM images of crosslinked nanoparticles (0.5% w/v HA; 18 µL (0.045% v/v) of DVS; 40 mL of W/O (10/90) emulsion; 5000 rpm, 10 min, RT, using high-shear homogenizer) under various conditions: **HA's concentration**, (a) 0,5% w/v; (b) 0,25% w/v and (c) 0,1% w/v. **Start of reaction**, (d) during, (e) end and (f) after homogenization. **DVS's concentration**: (g) 18 µL and (h) 200 µL (0.5% v/v).

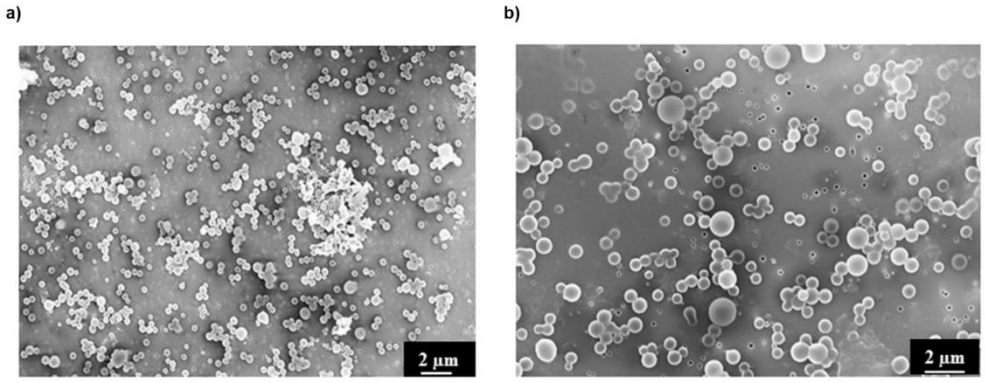

Figure S6. SEM images of crosslinked HA nanoparticles (0.5% w/v of HA; 1% w/v of S80; 0.045% v/v of DVS) without **(a)** and with (**b)** contrast agent.

A.3. MICROFLUIDIC FLOW FOCUSING APPROACH TO PRODUCE POLYMER NANOPARTICLES BASED ON HYDRODENTICITY

Materials. Sodium Hyaluronate (Mw = 42 kDa) is purchased from Bohus Biotech (Sweden). Diethylenetriaminepentaacetic acid gadolinium(III) dihydrogen salt hydrate Gd-DTPA (empirical formula: C14H2OGdN3O10xH2O; Mw = 547.57 g/mol). Non ionic surfactant Span80 (formula C24H44O6 Formula Weight: 428.62 g/mol). Divinyl Sulfone (or Vinyl Sulfone) contains < 650 ppm hydroquinone as inhibitor (purity 97%; density 1.117 g/ml at 25°C (lit.); molecular formula: C4H6O2S; Mw = 118.15 g/mol). Acetone (CHROMASOLV, for HPLC ≥ 99.8; molecular formula: CH3COCH3; Mw = 58.08 g/mol). Ethanol (ACS reagent, ≥ 99.5 (200 proof), absolute; molecular formula: CH3CH2OH; Mw = 46.07 g/mol). Sodium Hydroxide NaOH (ACS reagent, ≥ 97.0%, Mw = 40.00 g/mol). Gadolinium Chloride Solution $GdCl_3$ (Mw = 263.61 g/mol) and Sodium Chloride NaCl (ACS reagent, ≥ 99.0%, Mw = 58.44 g/mol) are purchased from Sigma-Aldrich Co. The water, used for synthesis and characterization, is purified by distillation, deionization, and reserve osmosis (Milli-Q Plus).

Microfluidic set-up for Flow-Focusing approach. Our microfluidic device "Droplet Junction Chip", (depth x width 190 µm x 390 µm) is purchased from Dolomite Centre Ltd. It is a glass microfluidic device designed for generating droplets. The internal surface of the channel is coated with the hydrophobic material. On the chip there are two separate droplet junctions, which can be used in combination. For our experiments, we used only X-junction with three inlet channels and a single outlet channel that can be used to mix and react three reagents. The device has a Flow-Focusing geometry with 90° angle between the inlets to enhance the diffusion process. It is compatible with Chip Interface H for fluidic connections. Three-way isolation Ethylene tetrafluoroethylene (ETFE) valves, connected to the syringes and the microfluidic device, make the automatic fill-in of the syringes feasible, thus allowing a continuous dispensing of reagents. The linkage between Fluorinated ethylene propylene (FEP) tubes and device is carried out through a specially designed connection with Polytetrafluoroethylene (PTFE) connectors. The Flow Focusing behavior on the microchannel is observed using an Optical Fluorescence Microscope (Olympus IX71) with a 4x scanning objective.

Microfluidic Route of production and characterization. Multiple factors influencing the production process of cHANPs through the microfluidic platform have been evaluated in a previous publication [93]. Main steps of this protocol and furthers used in the present work are summarized here:

- Flow Rate Ratio: ratio between Volume Flow Rate Solvent and Volume Flow Rate Non-Solvent (see paragraph 2.4 and Supporting Information);
- Crosslinking strategy: (1) premix of DVS into the middle channel or (2) adding DVS into the side channels (see paragraph 2.5 and Supporting Information);
- Effect of crosslinking agent's concentration, process temperature, type of surfactant, NaOH and NaCl concentration and other parameters have been widely discussed in our previous work [93].

After the nanoparticles' synthesis, further properties of cHANPs are also evaluated:

- Loading capability (see also Supporting Information);

- Stability in water (see also Supporting Information);
- Longitudinal relaxation times, rates and relaxivity (see paragraph 2.9 and Supporting Information);
- Swelling ratio (see also Supporting Information).

Finally, the following hydrogel structural parameters are theoretically computed and their relationships with relaxation parameters are evaluated:

- Crosslink density (see also and Supporting Information);
- Mesh size (see also and Supporting Information).

Preparation of Nanoparticles. Different flow rates are tested and the influence of the Flow Rate Ratio (FR^2), defined as the ratio between Volume Flow Rate Solvent and Volume Flow Rate Non-Solvent, is determined. For the feasibility study, a 5 mL aqueous solution containing HA concentrations ranging from 0.01 to 0.1% w/v is used to examine the effect of the nanoprecipitation by flow-focusing only due to the concentration of the polymer. Higher HA concentrations provide massive precipitation dealing to a strong interference on the Flow Focusing and consequently on the nanoparticle size. Among several tested molecular weights of HA, 42 kDa is selected as the optimal one because it can provide smaller nanoparticles . The initial solution is kept under continuous stirring for at least 4 h and, then, injected through the middle channel. The middle flow rate is ranged from 5 to 100 µL/min. A Non-Solvent, i.e. acetone as suggested elsewhere[47], is injected through the side channels to induce nanoprecipitation by a Flow-Focusing approach. Side flow rates are changed from 50 µL/min to 300 µL/min, with a step of 10 µL/min. Precipitated nanoparticles are collected in a petri glass containing Non-Solvent and kept under continuous stirring. The stirring, conducted over 8 hours, is used to promote the diffusion of DVS and consequently to improve the crosslinking reaction.

Crosslinking reaction by DVS. Crosslinking reaction by Divinyl Sulfone (DVS) is studied in the microfluidic system at a concentration of NaOH and NaCl ranging from 0.1 M to 0.3 M and from 0.02 to 0.2 M, respectively. Acetone, Ethanol and

Isopropanol are tested as Non-Solvent and are introduced in the side micro-channels, as already explained in our previous work [93].

Two crosslinking scenarios are investigated: (1) premix of DVS into the middle channel or (2) adding DVS into the side channels. The crosslinking agent is injected, alternatively, into the side channels or in the middle channel at different concentrations, ranging from 0 to 8 v/v % and from 0 to 20 v/v %, respectively.

Three different surfactants are tested at various reagent concentrations and flow rates. Tween 85 (ranging from 0.5 to 1% w/v), Tween 21 (ranging from 0.5 to 3% w/v), and Span 80 (ranging from 0.5 %w/v to 1.5 %w/v), are mixed to the Non-Solvent or to the aqueous solution. In the first scenario (1), the solvent phase containing also DVS is kept at a constant T of 5 °C to avoid undesired crosslinking effects; the device is instead heated to 35 °C.

Purification, recovery, characterization of nanoparticles. Purification is performed by a solvent gradient dialysis or by ultracentrifugation. Typically, two mL of the produced nanoparticles is collected and used for further analysis and size characterization. A Spectra Por Cellulose Membrane 6 (Molecular Weight Cut Off MWCO 50.000) is used for purification protocol. A typical procedure consists of loading collected samples into dialysis tube and keeping the buffer solution (Phosphate-Buffered Saline, pH 6.8, room temperature; final concentration of 10 mM PO_4^{3-}, 137 mM NaCl, and 2.7 mM KCl) under continuous stirring at 130 rpm to increase the diffusion rate. The first purification step is in Ethanol:

- Purify the sample for 2 hours in 70% Acetone + 30% Ethanol; 2 hours in 50% Acetone + 50% Ethanol; 2 hours in 30% Acetone + 70% Ethanol; 2 hours in 100% Ethanol.

The second purification step is in water:

- Purify the sample for 2 hours in 70% Ethanol + 30% MilliQ water; 2 hours in 50% Ethanol + 50% MilliQ water; 2 hours in 30% Ethanol + 70% MilliQ water; 2 hours in 100% MilliQ water.

The concentration gradient of water is slowly added to the buffer solution to avoid aggregation and diffusion phenomena across the membrane. Dynamic light

scattering is used to determine nanoparticle size. Nanoparticles are concentrated by ultracentrifugation. The recovery is performed at 15°C, at 80000 rpm for 15 minutes. After these treatments, a hundred microliters of purified samples are deposited on a polycarbonate Isopore Membrane Filter (0.05, 0.1 and 0.2 µm) by ultrafiltration vacuum system. The precipitated or deposited particles are gold palladium coated, and a ULTRA PLUS Field Emission Scanning Electron Microscope (FE-SEM Carl Zeiss, Germany) is used to observe particles' morphology. Transmission Electron Microscope (TEM) and Cryo-TEM is also used to characterize the samples. It is worth highlighting that all nanoparticles are purified in Ethanol to remove partially the unreacted reagents and to allow us the SEM characterization deposing the sample on a polycarbonate Isopore Membrane Filter (0.015, 0.05 and 0.1 µm) by ultrafiltration vacuum system.

Loading Capability. Loading Capability is calculated collecting data by Induced Coupled Plasma (ICP-MS). NexION® 350, Perkin Elmer Spectrometer. Nanoparticles are suspended in a solution of deionized (DI) water at a concentration of 250,000 particles/mL. Nanoparticles Tracking Analysis is used to calculate the number of nanoparticles. An acid compound is not added to avoid dissolution of the nanoparticles. All data are collected and processed using the Syngistix Nano Application Module. Gd is measured at m/z 157 using a 100 µs dwell time with no settling time.

The lyophilization of cHANPs is performed using a freeze-dryer Christ, 1-4LSC. Briefly, a Freezing step for 3 hours at -80 °C with a cooling profile of 1 °C/min is applied, sublimation at a shelf temperature of 6 °C and pressure of 0.85mbar for at least 24 h and finally, secondary drying at 25 °C and 0.03 mbar for 5-6 hours. Trehalose or sucrose ranging from 1 to 3% w/v is added as cryoprotector if necessary for re-suspension. Dried particles are also observed by Field Emission-SEM.

Stability and release study of cHANPs. The Gd-DTPA loaded cHANPs are mixed with 150 µL of PBS. The nanoparticles are kept shaking at 100 rpm at 37 °C. The solution is divided into two equal parts at 4, 12, 24, 48, 96 and 172 h post incubation. One-half of the solution is assessed by ICP-MS for the total concentration of Gd^{3+}

ions loaded within the nanoparticles. The other half of the solution is filter-spun using 0.45 μm filter columns at 14,000 rpm for 5 min, and the filtrate is analyzed for Gd^{3+} ions. The two concentrations are compared, and the amount of Gd^{3+} ions released over time is determined. To assess the long stability of the nanoparticles, only conditions that do not produce a swelling behaviour are tested. The release profile of Gd-DTPA is measured at different time points, namely 12, 24, 48 h, both in water and under two physiologically relevant conditions, namely stationary and constant shaking in PBS (pH= 7.4, 37°C).

In vitro relaxivity study. Empty nanoparticles and nanoparticles containing Gd-DTPA at different concentrations are tested by in vitro MRI and results are compared with Magnevist, Gd-DTPA in water as a control. After vigorously stirring, changes in longitudinal relaxation time (T_1) are evaluated at 1.5 T by Minispec Bench Top Relaxometer (Bruker Corporation), adding 300 μL of the sample to a specific tube. Only results about T_1 will be reported. Finally, relaxivity r_1 is calculated using weighted linear regression ($R_1=1/T_1$ s^{-1} relaxation rate plotted against Gd concentration, mM, and r_1, mM^{-1} s^{-1}, is the slope of the fitted curve). Estimation of measurement uncertainty is evaluated using weighted linear regression. Furthermore, the relaxation time distribution was obtained by CONTIN Algorithm. The relaxation spectrum was normalized with respect to the CONTIN processing parameters. The integral of a peak corresponds therefore to the contribution of the species exhibiting this peculiar relaxation to the relaxation time spectrum.

Swelling Ratio and Hydrogel parameters. Swelling Ratio (SR) is calculated with:

$$SR = \frac{d_{H2O}}{d_{eth}}$$

where d_{eth} (in nm) d_{H2O} (in nm) are the nanoparticle's diameters in Ethanol and in water respectively (for further details about the swelling ratio calculation please refer to the Supporting Information at the paragraph "Calculations of the hydrogel network parameters"), measured by Dynamic Light Scattering. A simplified version of the Flory-Rehner equations are used in order to compute the hydrogel structure

parameters ($\overline{Mc}$: molecular weight between crosslinks (g/mol); v_e: effective crosslink density (mol/cm^3); ξ: mesh size (nm). See Supporting Information for detailed calculations of the hydrogel network parameters.

Supporting data, figures and tables.

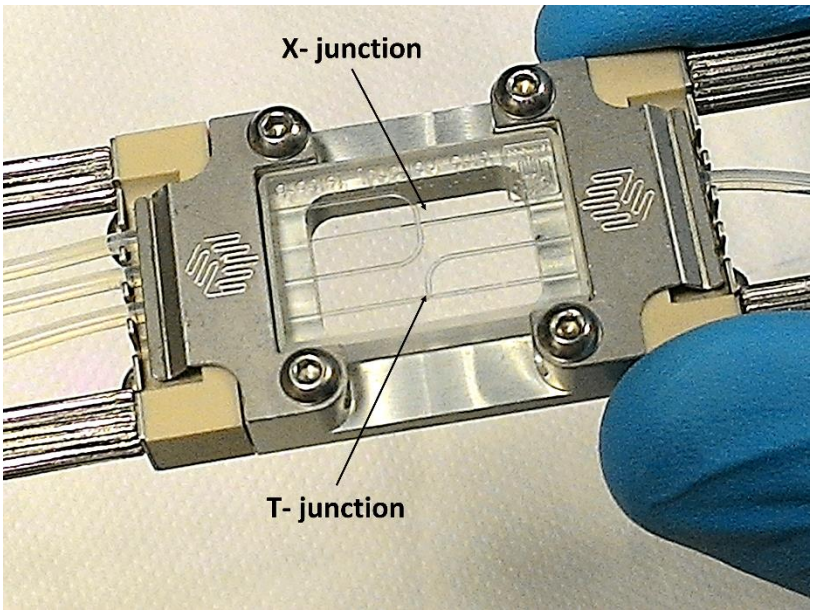

Figure S7. Microfluidic device. "Droplet Junction Chip 190 µm" with two configurations T- and X- junction, which can be used in combination. Droplet Junction Chip is compatible with Chip interface H for fluidic connections.

Table S5. Dynamic Light Scattering. z-Average (nanoparticles diameters) and Standard Deviation (SD) in Ethanol at different Flow Rate Ratio FR[2].

Solvent (S) Flow Rate [µL/min]	**Non-Solvent (NS) Flow Rate [µL/min]**	**Flow Rate Ratio S/NS**	**z-Average [nm]**	
			Mean	*SD*
40	100	0.4	218.2	40.58

	80	0.5	364.6	65.83
	60	0.67	480.8	70.99
	50	0.8	523.2	101.92
	30	1.3	1001.3	144.46
30	100	0.3	35	9
	80	0.37	86.5	19.30
	60	0.5	246	38.46
	50	0.6	341.8	67.74
	40	1	684.4	212.57
	30	1.5	890.1	377.78

A feasibility study was done to obtain a narrow Flow-Focusing that induces Nanoprecipitation Reaction in a continuous flow within our microfluidic device. The presence of precipitate in the mixing channel and the width of hydrodynamic focusing are considered. Optimal conditions provide an absence of a precipitate in the mixing channel and a narrow focusing.

Nanoparticles are formed via a two-stage process: (i) a Nucleation stage, in which seed particles spontaneously precipitate from solution; (ii) a more gradual Growth phase, in which diffusion of solutes from the solution to the seed surface proceeds until the final particles size is attained. As more widely explained in our previous work[1], the increase of the non-solvent Flow Rate and, therefore, the reduction of FR^2 (from 0.5 to 0.3), causes a more stable and narrow hydrodynamic focusing (Figure S8 a). In this situation, the extraction is faster and, therefore, nucleation is favored to the detriment of the growth, obtaining nanoparticles smaller and monodisperse (Figure S8 b). Conversely, higher FR^2 increases the width of the middle stream, requiring a longer time to perform the mixing by diffusion and the non-solvent extraction by means of the nearby streams. This effect results in a larger amount of

solvent in the final mixture possibly causing core swelling, hence the formation of large and polydisperse nanoparticles (Figure S8 c). For these reasons 0.3 is chosen as optimal FR^2.

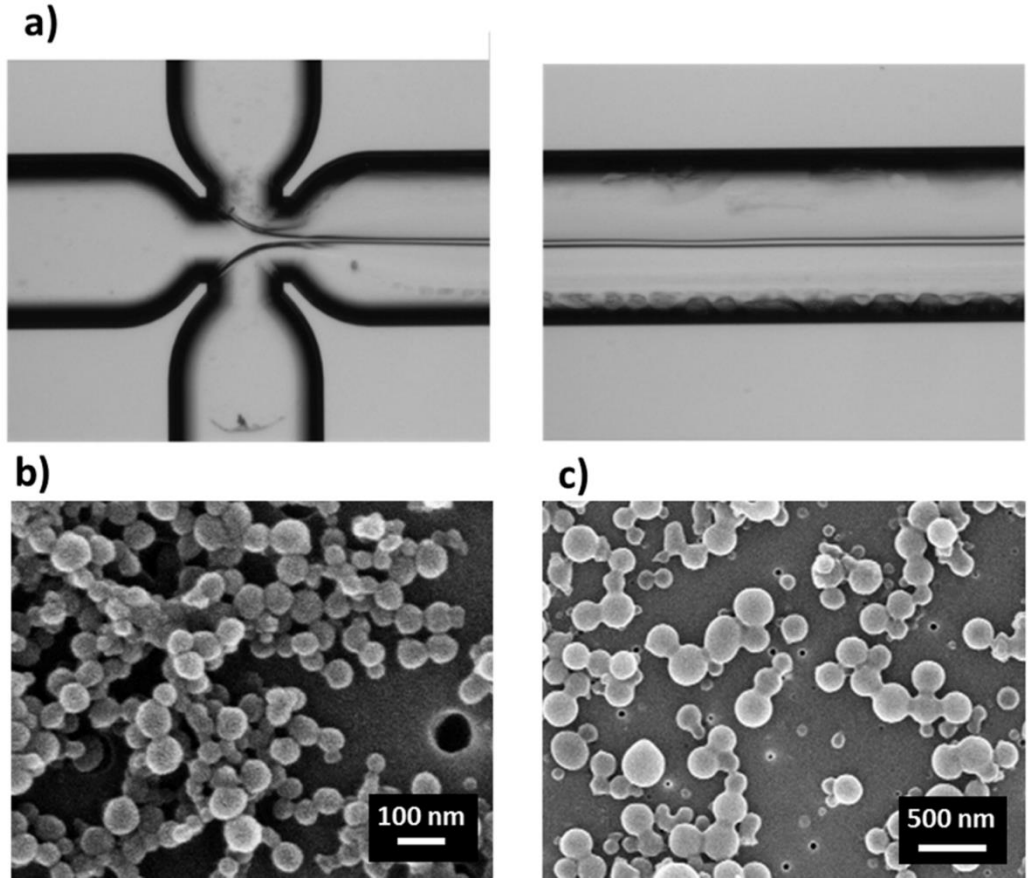

Figure S8. Nanoprecipitation through Flow-Focusing. (a) Representation of microfluidic device consisting of three inlets. Nanoprecipitation is generated by hydrodynamic Flow Focusing with a central stream of polymer solution and two side streams of acetone at standard conditions: FR^2=0.3, HA=0.05% w/v, NaOH=0.2 M, NaCl=0.05 M. FE-SEM images of nanoparticles in Ethanol at standard conditions when (b) FR^2 is 0.3 and (c) FR^2 is 0.5.

Preferred optimal values are selected as "standard conditions", providing the prolonged stability of the hydrodynamic flow focusing, the absence of massive precipitation (Figure S8 a) and a higher yield of nanoparticles collection and

monodispersity (Figure S8 b and c). These optimal microfluidic conditions are used for all experiments.

Encapsulation of Gd-DTPA: Interference of Gd-DTPA on nanoprecipitation. Once selected the best FR^2, the influence of the Gadolinium on nanoprecipitation is also evaluated. The entrapping of $GdCl_3$ or Gd-DTPA by adding the metal complex to the aqueous solution is exploited. Different GdCAs concentrations are tested ranging from 0.005 to 0.1% w/v to investigate relaxometric properties, but a significant interference on Flow-Focusing pattern (Figure S9) and an increasing in size and polydispersity of the nanoparticles is suddenly measured (Table S6 a and b). Although a further lowering of the amount of Gd-DTPA in the process can reduce this strong instability, we keep Gd-DTPA at 0.1% w/v to maximize the final Gd concentration within the collected nanoparticles and, therefore, to perform a reliable study on the relaxometric properties. As far as the results shown in Table S6, it is worth commenting that, despite size distributions of $GdCl_3$ are better compared to the ones of Gd-DTPA, $GdCl_3$ is highly toxic and not approved for clinical development. Therefore, we chose Gd-DTPA as being one of the most clinically used and FDA approved GdCAs.

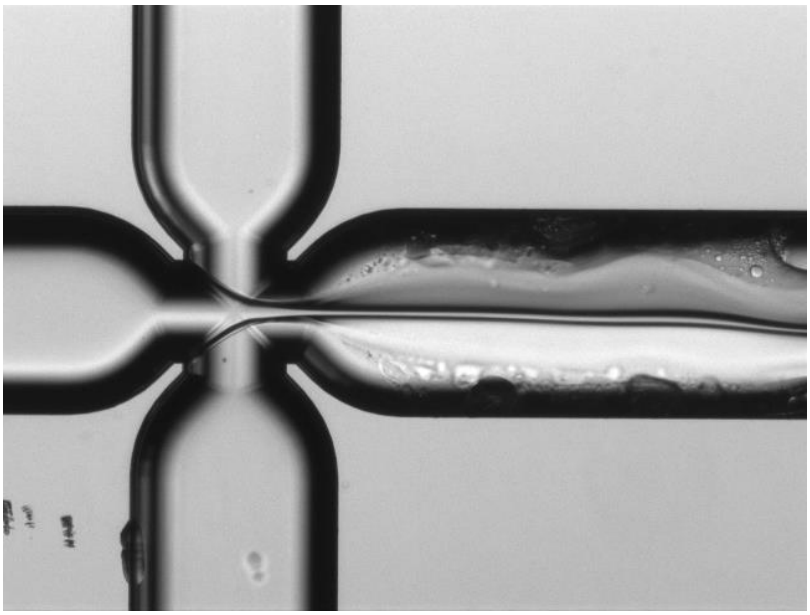

Figure S9. Gd-DTPA interference. Interference on Flow-Focusing pattern in the presence of Gd-DTPA.

Table S6. Nanoparticles size. Increasing in size and polydispersity of nanoparticles at different (a) Gd-DTPA and (b) $GdCl_3$ concentrations. Modal values of the particle size distributions are reported for each Gd-DTPA and $GdCl_3$ concentration.

a)

Gd-DTPA concentration [% w/v]	**Nanoparticles size [nm]**	
	Mean	*SD*
0.005	100	57
0.01	150	60
0.05	200	70

0.1	450	156

b)

$GdCl_3$ concentration [% w/v]	**Nanoparticles size [nm]**	
	Mean	*SD*
0.005	105	40
0.01	110	25
0.05	125	45
0.1	123	10

The interference of Gd-DTPA during polymer precipitation is overcome by finely tuning process parameters and leveraging the use of hydrophilic-lipophilic balance (HLB) of surfactants and pH conditions as discussed in our previous work[1]. At the end, after the optimization, the sizes of all the nanoparticles with Gd-DTPA and DVS will be 35 nm.

Crosslinking reaction by DVS. When DVS is added to the middle channels, optimal conditions regarding the stability of the MFF are only reached at DVS concentrations ranging between 0.6 and 1.2% v/v and by injecting Span80 at 0.5% v/v in the side phase. At higher concentration, spherical morphologies are not observed, and a massive precipitation is detected (Figure S10, a and b). Morphologies obtained for optimal conditions are already displayed in Figure 1 d and e of the main manuscript.

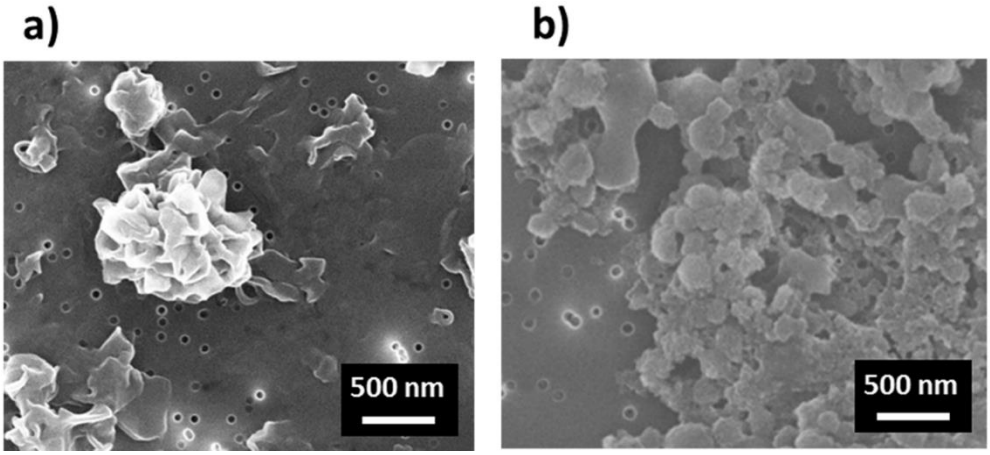

Figure S10. Crosslinking reaction. FE-SEM images of morphologies obtained by adding a high concentration of DVS (a) in middle channel and (b) in side channels. Images show that the massive precipitation along the main channel of the microfluidic device causes the formation of large aggregates.

Loading Capability. We considered loading capability for both crosslinking strategies (Table S7) using the following equation:

$$\% \, \boldsymbol{LC} = \boldsymbol{C_i V_i / m_{np_s}}$$

Table S7. Loading Capability. Loading Capability (LC) of Gd-DTPA loaded cHANPs for both crosslinking reaction strategies at standard conditions. The table shows how the LC increases when DVS is added in the middle channel.

	DVS concentration [% v/v]	**Loading Capability [%]**
DVS middle channel	from 0.6 to 1	from 22 to 59
DVS side channels	from 4 to 4.5	from 26 to 35

The proposed formulations also affect the Gd-DTPA Loading Capability (LC), as reported in Table S7. Furthermore, release behavior under shaking conditions is also

evaluated with respect to the *in vitro* MRI signal. Even if more stable nanoparticles, obtained by adding DVS in the side channels, preserve their spherical shape beyond 96 h under shaking conditions, the lowering of the MRI signal reveals a partially reduced payload of metal compounds after 96 h. The experimental evidence clearly reports that the nanoparticles size, morphology and swelling behavior are highly sensitive to the proposed strategies. Differences between nanoparticles stability obtained through both formulations can be attributed to the diverse reaction-diffusion pathways of DVS and the barrier effect of Span80. In the first strategy, the formation of the crosslinked hydrogel structures is probably favored by the premixing of DVS in the aqueous environment promoting the fastness of the reaction at the nozzle section. Additionally, Span80 reduces the water extraction delaying the precipitation and, at the same time, increasing the water and Gd content in the nanoparticles. We could hypothesize that this phenomenon preserves a high hydration level within the hydrogel structure responsible of the faster swelling and probably promoting a faster hydrolytic degradation of the cHANPs. Therefore, we have next investigated the impact of these findings on the relaxivity.

Swelling Ratio. Swelling Ratio (SR) is calculated with Eq. 1:

$$SR = \frac{d_{H2O}}{d_{eth}} \qquad (1)$$

where d_{eth} (in nm) d_{H2O} (in nm) are the nanoparticle's diameters in Ethanol and in water respectively, measured by Dynamic Light Scattering.

Results clearly show that nanoparticles do not exhibit a swelling behavior until 48 h (Figure S11 a) when produced at the above-reported range of conditions, while a significant increase in size is reported for longer time. In particular, smaller nanoparticles of 70 nm measured in water are only produced at DVS of 0.8% v/v and an increase in size to 168 nm is detected starting from 96 h to 1 week. The second scenario (2) is performed without the support of temperature and surfactants. Indeed, results show that pH conditions play the key role in adjusting the stability. Stable MFF in the presence of Gd-DTPA is always obtained at strict pH conditions ranging from 11.7 to 12.6 and in a wider DVS concentration range (0-4.5% v/v). However, swelling in water is avoided at the above rep orted pH conditions and exclusively at

DVS concentrations varying from 4 to 4.5% v/v. Swelling behavior along the time for loaded-cHANPs obtained outside the optimal range is reported in Figure S11 b. A mean nanoparticle diameter of 40 nm is measured at pH of 12.3 and DVS of 4% v/v; swelling is observed after 96 h. As far as the pH conditions, it is worth highlighting that high pH values (from 11.7 to 12.6) are used to promote nanoprecipitation and crosslinking reaction only during the production process; after the purification phase, the final pH value of cHANPs in water ranges from 6 to 8. Nanoparticle sizes for all the proposed conditions in both scenarios are reported in Table S8 a and b. Furthermore, the amount of Gd^{3+}-ions released over time is found to be below the detection limit (0.1 ppb) of ICP-MS, even after 48 h and for both strategies.

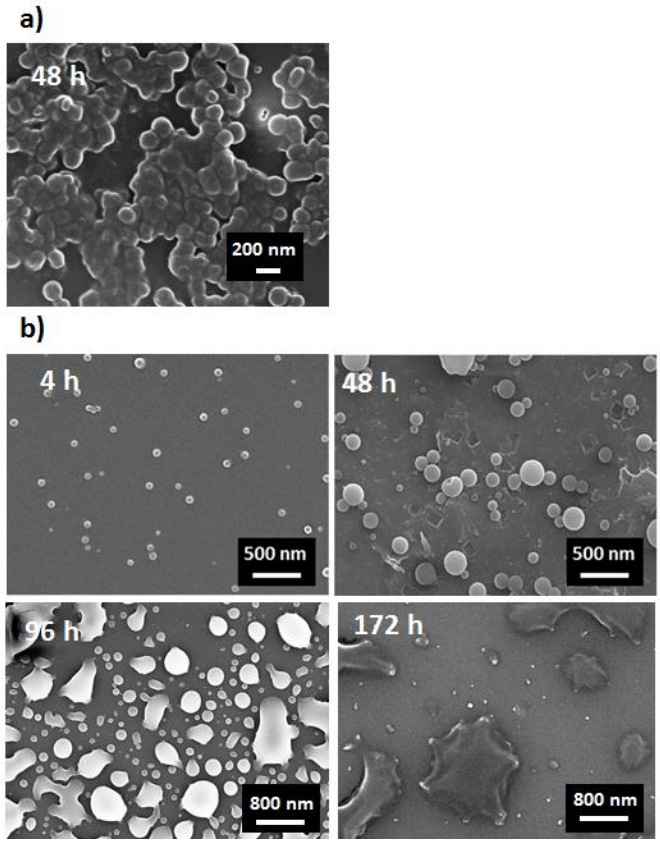

Figure S11. Swelling behaviour. FE-SEM images of cHANPs at very low concentrations of DVS injected (a) in the middle channel and (b) in the side channels at different hours.

Table S8. Size evolution of the nanoparticles. Evolution of nanoparticles size at different hours from 4 to 172 hours with respect to their size in Ethanol by adding DVS (a) in the middle channel and (b) in the side channels.

a)

	DVS 0.4 % v/v		**DVS 0.6 % v/v**		**DVS 0.8 % v/v**		**DVS 1 % v/v**		**DVS 1.2 % v/v**		**DVS 1.6 % v/v**	
Time [h]	Size [nm]	SD [nm]	Size [nm]	SD [nm]	Size [nm]	SD [nm]	Size [nm]	SD [nm]	Size [nm]	SD [nm]	Size [nm]	SD [nm]
EtOH	35	2	35	2	35	2	35	2	35	2	35	2
4	155	22	105	16	71	10	71	10	74	13	734	164
12	178	35	128	23	72	12	72	3	75	14	767	183
24	200	40	137	25	70	11	70	12	78	16	860	223
48	210	47	140	24	71	12	71	13	77	14	900	206
96	324	58	143	29	85	15	85	15	87	16	1256	344
172	420	115	170	34	125	25	89	16	89	15	2420	685

b)

	DVS 1 % v/v		**DVS 2 % v/v**		**DVS 2.5 % v/v**		**DVS 3 % v/v**		**DVS 4 % v/v**		**DVS 4.5 % v/v**	
Time [h]	Size [nm]	SD [nm]	Size [nm]	SD [nm]	Size [nm]	SD [nm]	Size [nm]	SD [nm]	Size [nm]	SD [nm]	Size [nm]	SD [nm]
EtOH	35	2	35	2	35	2	35	2	35	2	35	2
4	156	22	105	16	115	18	95	13	40	9	54	9

12	182	35	128	23	122	21	112	5	53	13	55	11
24	239	48	147	26	143	23	123	20	51	14	51	10
48	358	80	162	28	162	27	152	26	52	12	53	9
96	450	82	273	55	273	53	273	47	54	15	75	14
172	1234	338	680	136	630	126	610	110	115	33	201	35

Stability and release study of cHANPs. Additionally, the stability of cHANPs in water under shaking conditions is reported and discussed with respect to release properties and degradation phenomena. These studies are performed to assess the ability of nanoparticles to carry and retain the CAs. Observations are made starting from previously reported optimal conditions for both strategies (0.8% v/v of DVS in the middle channel and 4 % v/v of DVS in the side channels). Indeed, it appears obvious that, even if swelling is not observed, the presence of Gd-DTPA within the nanoparticles is not predictable.

For cHANPs kept on a rotary shaker operating at 100 rpm under *simulated physiological conditions* (*PBS* 9.5 mM, pH 7.4, 37 °C), a correlation between crosslinking strategy and release and degradation behaviors is also detected. Indeed, under shaking, cHANPs of 70 nm obtained when DVS is added to the middle channel show a noticeable change in shape or prominent hydrolytic degradation just after 72 h (Figure S12 a and b).

Furthermore, for 40 nm nanoparticles, obtained by adding DVS in the side channels at the conditions previously reported, degradation and release are not observed even up to 96 h. Figure S12 c shows a slight degradation of nanoparticles observed only after 172 hours under shaking conditions, when DVS is added in the side channels. As far as the release is concerned, relaxation time and ICP-MS measurements have been carried out and already reported in our previous work[1].

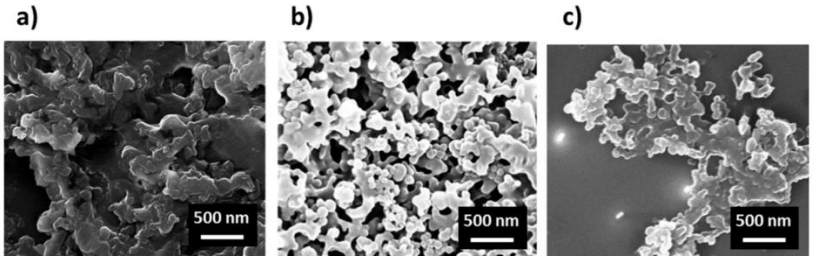

Figure S12. Degradation of cHANPs. (a), (b) FE-SEM images of cHANPs prepared by adding 0.8% v/v of DVS in the middle channel, showing a slight change in shape or hydrolytic degradation just after 72 hours under shaking conditions. (c) FE-SEM images of cHANPs prepared by adding 4% v/v of DVS showing a slight degradation only after 172 hours under shaking conditions.

Loading of Gd-DTPA by sorption: In vitro relaxivity study. Loaded cHANPs are also prepared by sorption of Gd-DTPA to compare the relaxometric effects obtained with both strategies (Figure S7). Relaxivity r_1 is calculated using weighted linear regression ($R_1=1/T_1$ s^{-1} relaxation rate plotted against Gd concentration, mM, and r_1, mM^{-1} s^{-1}, is the slope of the fitted curve). Estimation of measurement uncertainty is evaluated using weighted linear regression[2]. Briefly, a solution of Gd-DTPA 91 μM is dissolved in the same volume of cHANPs solution and the suspension is placed on a wheel for 48 h in order to get maximum sorption of Gd-DTPA on NPs mainly through diffusion. In detail, the groups of HA interact with the COO- groups of Gd-DTPA, which could facilitate the sorption. The small Gd-DTPA molecules, which were not adsorbed, are removed by dialysis.

Then, the sample is dialyzed against water in dialysis membrane tube of 50000 MCWO for 12 h. The concentration of Gd-DTPA from the exterior medium of dialysis bag, treated by evaporator (Buchi® R-215 Rotavapor®), is calculated by T_1 value measured at 37°C on Bruker Minispec mq60 instrument using standard inversion-recovery pulse sequence. Later the content of gadolinium adsorbed on NPs is calculated by subtracting the amount of gadolinium in the external medium from the total amount of Gd-DTPA was previously added to the system. In this study, the release of Gd-DTPA is very fast and there is no enhancement in MRI signal at the same concentration of Gd-DTPA in water. Furthermore, the adding of GdDTPA alters the morphology of formed cHANPs. However, after the sorption, no enhanced

relaxivity is observed compared to the free Gd-DTPA, but partial release of the Gd^{3+} ions is observed even after 12 h.

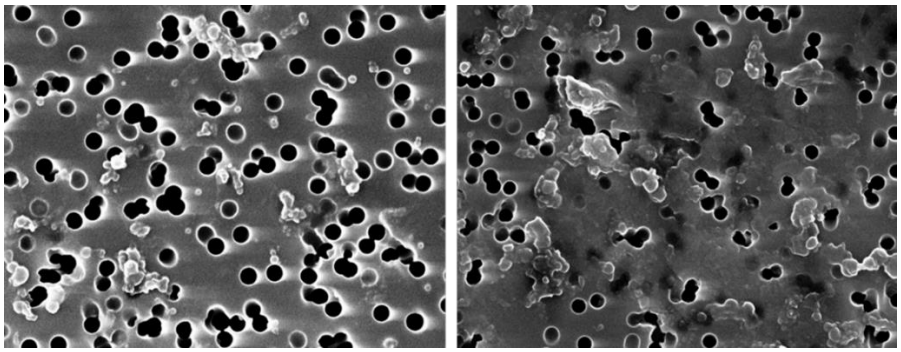

Figure S13. Sorption of Gd-DTPA. FE-SEM images of cHANPs treated by sorption of Gd-DTPA after the production through nanoprecipitation in hydrodynamic Flow-Focusing.

Contribution of the unloaded cHANPs to the relaxivity.

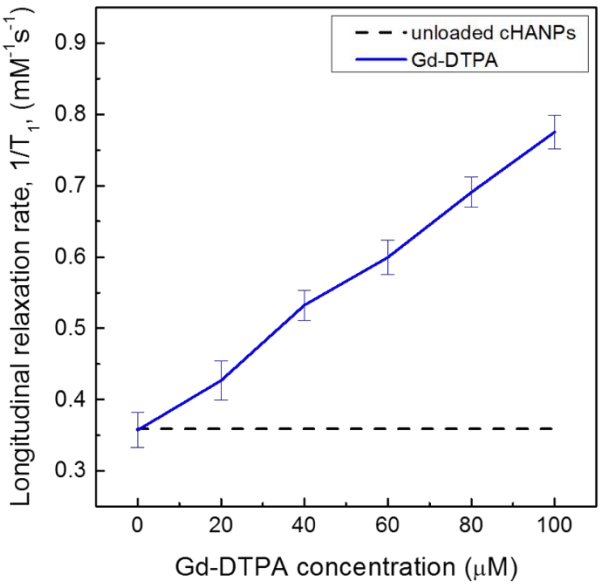

Figure S14. Relaxometric properties of unloaded cHANPs. The relaxation time measurements versus Gd-DTPA concentration show that the unloaded cHANPs do not contribute to the enhancement of MRI signal.

Nanoparticles tracking analysis (NTA). NTA is a powerful characterization technique that complements DLS and is particularly valuable for analyzing polydisperse nanosized particles and their concentration. NTA measurements are performed with a NanoSight (NanoSight, Malvern), equipped with a sample chamber with a 640-nm laser and a Viton fluoroelastomer O-ring. The samples are injected in the sample chamber with a sterile syringe until the liquid reached the tip of the nozzle. All measurements are performed at room temperature. The samples are measured for 40s with manual shutter and gain adjustments. Three measurements of the same sample are performed for all samples. The mean size and SD values obtained by the NTA software correspond to the arithmetic values calculated with the size of the nanoparticles analyzed by the software (Figure S15 a), b), c)).

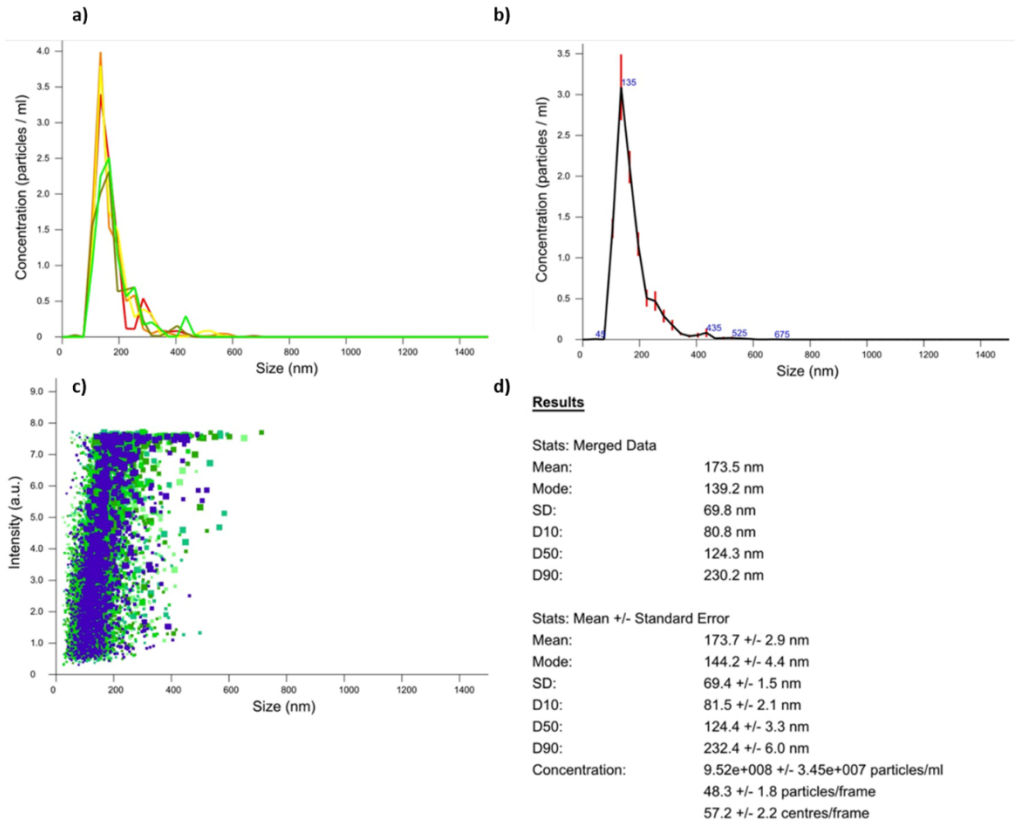

Figure S15. Nanoparticles Tracking Analysis. Size distribution of cHANPs obtained through Nanoparticles Tracking Analysis. (a), (b) Concentration (particles/mL) versus size; (c) intensity (arbitrary unit) versus size; (d) summarized results.

Calculations of the hydrogel network parameters. As previously described, studies on the swelling behavior of the nanoparticles are conducted in water at room temperature and the obtained results, in terms of swelling ratio (see Eq. 1), are used to estimate the following hydrogel structural parameters of the cHANPs:

- $\overline{Mc}$: molecular weight between crosslinks (g/mol);
- v_e: effective crosslink density (mol/cm^3);
- ξ: mesh size (nm).

In order to compute the above mentioned parameters, a simplified version of the Flory-Rehner equations are used[2, 3].

Firstly, the average molecular weight between crosslinks ($\overline{Mc}$) are computed using the following equation:

$$Q_v{}^{5/3} = \frac{\overline{v}\ \overline{Mc}}{\mathrm{V_1}} \left(\frac{1}{2} - \chi\right) \qquad (2)$$

where Q_v is the volumetric swelling ratio, $\overline{v}$ is specific volume of polymer (0.814 cm^3/g for HA)[3], V_1 is molar volume of solvent (18 mol/cm^3 for water)[4], χ is polymer-solvent interaction parameter (0.473 for HA)[5]. The volumetric swelling ratio, Q_v, is estimated based on the approximate diameter ratio (see Eq. 1), determined experimentally by comparing the diameters of the swelled cHANPs with the cHANPs' diameters in Ethanol, i.e. before the hydration of the nanoparticles in water.

Differently from the previous works[4-6], in which the volumetric swelling ratio is estimated from the mass swelling ratio by dividing the sample mass after swelling by the dry sample mass, no dehydration of the nanoparticles is performed in order to keep unchanged the structure and the shape of the Gd-DTPA loaded cHANPs. Therefore, the nanoparticles' diameter measured in Ethanol is used as the reference value to compute the volumetric swelling ratio. This allows us to avoid the alteration

of the Gado-Mesh network and the release of the entrapped Gd-DTPA caused by the dehydration process, making us able to properly investigate the relationship between the cHANPS' hydrogel structure and the relaxivity values, which strictly rely on the encapsulation of the contrast agent and on the hydrogel parameters.

After $\overline{Mc}$ is estimated, the effective crosslink density, v_e, is determined from the following equation:

$$v_e = \frac{\rho_p}{\overline{M_c}} \qquad (3)$$

where ρ_p is the density of polymer (1.229 g/cm^3 for HA)[6].

The water swollen hydrogels mesh size, ξ, is calculated by the following equation:

$$\xi = {Q_v}^{1/3} \sqrt{\overline{r_o}^2} \qquad (4)$$

where $\sqrt{\overline{r_o}^2}$ is the root-mean square distance between crosslinks, specifically reported for HA by Collins et al. [5] as follows:

$$\sqrt{\left(\frac{\overline{r_o}^2}{2n}\right)} \cong 2.4\ (nm) \qquad (5)$$

where n is the number of monomer units for HA. For HA with a molecular weight (M_n) of ~ 4*10^5, n is ~100, which gives the following estimation of $\sqrt{\overline{r_o}^2}$:

$$\sqrt{\overline{r_o}^2} = 0.035 \sqrt{M_n} \qquad (6)$$

Finally, the mesh size can be calculated by combining equations (4) and (6) as follows:

$$\xi = 0.035 \sqrt{\overline{M_c}}\, {Q_v}^{1/3} \qquad (7)$$

Estimated values of all swelling study parameters, Q_v, $\overline{Mc}$, v_e and ξ should be considered as approximate values on account of certain assumptions considered in Flory-Rehner calculations and for our specific systems. However, these values can

be used for making comparisons between various network features of different hydrogel nanoparticles.

The following tables report all the computed values for swelled cHANPs after 48h:

Table S9. cHANPs network parameters. Hydrogel network parameters of cHANPs after 48 h of swelling, obtained by adding DVS a) in the side channel and b) in the middle channels.

a)

	Volumetric swelling ratio		**Molecular mass between two crosslinked points [*10^3 g/mol]**		**Effective crosslink density [*10^{-5} mol/cm^3]**		**Mesh size [nm]**	
DVS [% v/v]	Q_V		$\bar{M}_C$		v_e		ξ	
	mean	*SD*	*mean*	*SD*	*mean*	*SD*	*mean*	*SD*
0.00	9.00	0	31.9	0	3.85	0	13.00	0
1.00	10.23	2.87	39.5	18.5	3.11	1.46	15.09	4.94
2.00	4.63	1.06	10.5	4.04	11.7	4.47	5.99	1.61
2.50	4.63	1.04	10.5	3.93	11.7	4.35	5.99	1.56
3.00	4.34	0.99	9.47	3.60	13.0	4.94	5.56	1.48
4.00	1.49	0.43	1.58	0.760	77.6	37.2	1.59	0.53
4.50	1.51	0.34	1.64	0.619	75.1	28.4	1.63	0.43

b)

	Volumetric swelling ratio	**Molecular mass between two crosslinked points [*10^3 g/mol]**	**Effective crosslink density [*10^{-5} mol/cm^3]**	**Mesh size [nm]**
DVS [% v/v]	Q_V	$\bar{M}_C$	v_e	ξ

	mean	*SD*	*mean*	*SD*	*mean*	*SD*	*mean*	*SD*
0.00	9.00	0	31.9	0	3.85	0	13.00	0
0.40	6.00	1.69	16.2	7.60	7.57	3.55	8.10	2.66
0.60	4.00	0.91	8.26	3.14	14.9	5.67	5.05	1.35
0.80	2.03	0.46	2.66	1.00	46.2	17.4	2.29	0.60
1.00	2.03	0.49	2.66	1.07	46.2	18.5	2.29	0.64
1.20	2.20	0.53	3.05	1.21	40.3	16.1	2.51	0.70
1.60	25.71	7.36	183	87.5	0.670	0.319	44.25	14.77

A.4. MICROFLUIDIC FLOW FOCUSING APPROACH TO PRODUCE COACERVATED CHITOSAN-HYALURONIC ACID NANOPARTICLES BASED ON HYDRODENTICITY

Materials. Hyaluronic acid (HA) with a molecular weight of 50000 Da is purchased from CreativePEGWorks (USA). Chitosan with a low molecular weight of 50000 Da and sodium tripolyphosphate (TPP) with a MW of 367,86 Da produced by Sigma-Aldrich are chosen in this study. Acetone (Sigma-Aldrich) is used for collection and dialysis while ethanol (Carlo Erba, Italy) is employed in the successive step to change sample collection from acetone to water. Milli-Q water is used to prepare solutions and dialysis.

Microfluidic platform. Microfluidic platform is composed by a system of three syringes (SETonic, 5 mL PTFE PEEK tubing connector) pushes fluids within tubes. Each single syringe is controlled by a low-pressure syringe pump (Low Pressure Syringe Pump neMESYS 290N by CETONI) that doses with high precision emitted fluid unit. Syringe is connected, through a ferrule, to the first segment of PTFE tubing (Dolomite, 0,8 x 1,6 mm) that, on the other side, is joined with a 2-way in-line valve. Thereafter, there is a second segment of PTFE tubing (Dolomite, 0,8 x 0,25 mm) that leads fluid to chip. Connection between tubes and chip is easily allowed by a linear

connector 7- way. All reactions and processes are conducted in the main body of a custom-made chip, purchased from the Dolomite center ltd designed to obtain a meeting point such as to promote flow focusing generation, that is locked in a H interface 7 way between two linear connectors 7 way. It is made up of quartz and its dimensions are 22.5mm long x 15mm wide x 4mm thick. Chip consists of 5 parallel inlets converging at a junction, followed by a straight output channel to the opposite edge. All channels have the same cross-section of 160 x 150 μm. Finally, a tube of outlet, that starts from the second connector, is employed to collect fluid in a glass Petri containing water or acetone.

Nanoparticles production. Middle and side streams include two different polymers that leads to NPs formation through an ionotropic gelation via CS-TPP crosslinking followed by HA-CS complex coacervation. The starting step consists in the preparation of polycationic and polyanionic solutions. Components are withdrawn from previously prepared stocks at 0,1 % w/v. The first one is obtained by mixing CS (concentration range from 0,00625 to 0,2 % w/v) at an acetic acid buffer (1%) while the second one is obtained dissolving HA (concentration range from 0,002 to 0,008 w/v) and TPP (concentration range from 0,003 to 0,012 % w/v) in water. Both solutions are stirred at 300 rpm for 30 min. Each syringe is connected to ferrule according to chip pattern: polycationic solution will be pushed in the middle channel while polyanionic solution in the two side channels. Holders are used to lock each syringe with piston and support in order to avoid their movement during fluid push. Before experiment launch, flow rates are set on PC software. Start button is pressed and fluids begin to flow in tubes but valves remain closed for few minutes to allow first tubing segment total filler and promote the compression of the small air bubbles, if present. Therefore, middle valve is opened and, after about 30 seconds, even side valve. Flow focusing is established at chip junction and can be modified changing flow rate on PC. Sample is collected in Petri dishes with acetone inside covered by aluminium foil to limit solvent evaporation. Experiment stops when syringes have pushed all solution volume within them or when precipitation is so high that main channel is occluded or macroaggregates are formed and so flow focusing is not more stable. Sample is moved in a vial by using Gilson pipetman and chip is partially cleaned with MilliQ water charged into plastic syringe. Possible matter residual

within chip are removed by immersing chip in a *piranha solution* composed of ¼ nitric acid and ¾ sulfuric acid for one day.

Nanoparticles characterization. NPs morphological and structural surface features are analyzed with a scanning electron microscope (Carl Zeiss UltraPlus Field Emission Scanning Electron Microscope). Examined samples are dropped on glass directly from microfluidic platform outlet or filtered, after collection and dialyses, on membrane of 50 nm pore size. Nanoparticles are coated with 5,5 nm Au or Pt/Pd prior observation. Another characterization is carried out with a TEM (Tecnai FEI® transmission electron microscope) that allow to examine NPs internal features. Samples are collected on Formvar/Carbon 200 mesh Cu Agar® small net from platform outlet or dropping off 20-50 μL of solution from collection on it, before or after various dialyses.

Minispec benchtop relaxometer. Relaxation times are measured on a Bruker Minispec (mq 60) benchtop relaxometer operating at 60 MHz for protons (magnetic field strength: 1.41 T). The acquisitions are performed at 37°C and, before each measurement, the sample is placed into the NMR probe for about 15 min for thermal equilibration. Longitudinal relaxation times, T_1, are determined by both saturation and inversion recovery pulse sequences while transversal relaxation time T_2 is determined by Carr-Purcell pulse sequence. The relaxation recovery curves are fitted using a multi-exponential model and then they are represented using OriginPro software. Relaxivity is evaluated through eq (1) and it is the slope of the straight line.

Supporting data, figures and tables.

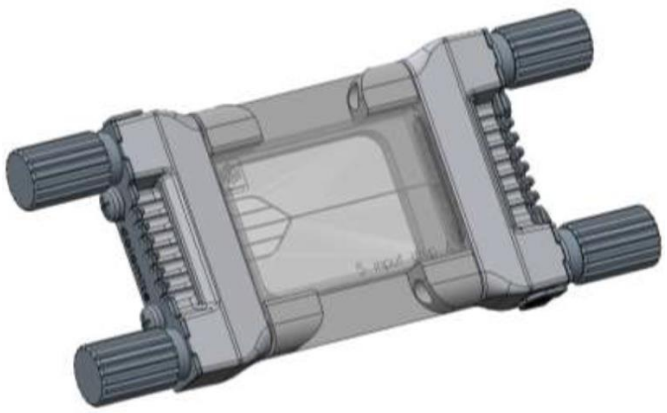

Figure S16. Microfluidic chip within H interface 7 way and locked between two linear connectors 7 way.

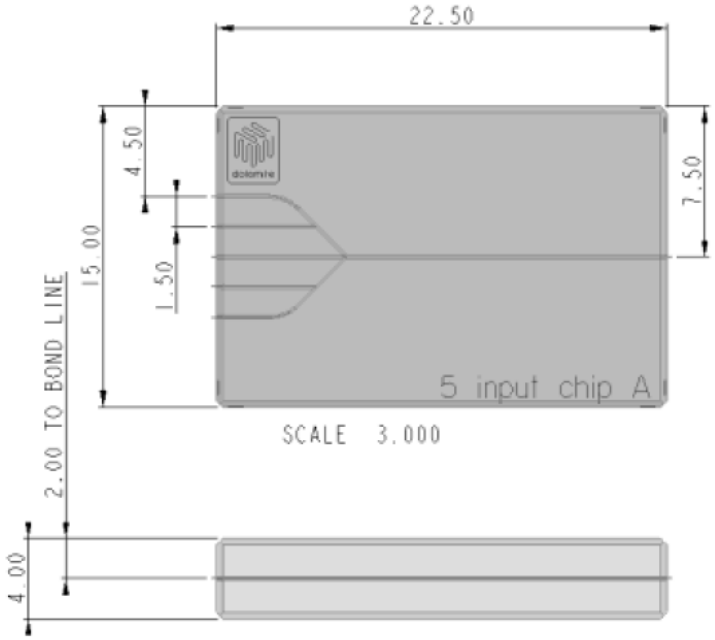

Figure S2. Chip features

Table S10. Dimensionless numbers in microfluidic device (ρ, fluid density; *v*, average flow velocity; *d*, characteristic channel dimension; *η*, fluid viscosity; *σ*, interfacial force; *g*, gravity

acceleration constant; β, coefficient of expansion; ΔT, temperature difference; a, sound speed; λ, mean free path;

Dimensionless numbers	Definition	Equations
Reynolds number (Re)	Inertial force/viscous force	$\rho v d/\eta$
Capillary number (Ca)	Viscous force/interfacial force	$\eta v/\sigma$
Bond number (Gr)	Gravity/interfacial force	$\rho g d^{2/}\sigma$
Grashof number (Gr)	Buoyancy/viscous force	$d^3\rho^2 g\beta\Delta T/\eta^2$
Mach number (Ma)	Inertial force/elastic force	v/a
Kn number (Kn)	Free path/flow dimension	λ/d

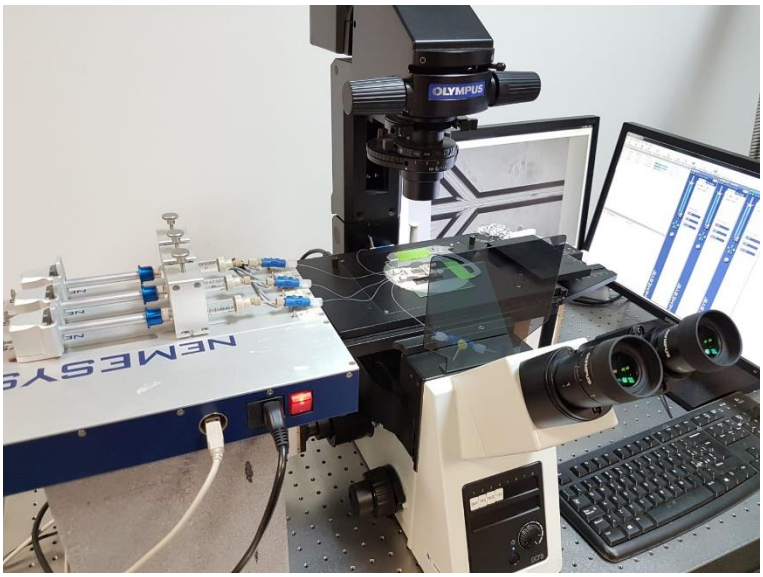

Figure S17. Microfluidic platform photo

Table S11. Investigated parameters during the experiments design

Test #	HA (%w/v)	TPP (%w/v)	CS (%w/v)	Flow rate middle channel (µL/min)	Flow rate side channel (µL/min)	Flow Rate Ratio	CS:HA (g/g)
1	0.008	0.012	0.025	20	100	0.2	0.3125
2	0.008	0.012	0.025	20	100	0.2	0.3125
3	0.008	0.012	0.025	0.75	5	0.15	0.234375
4	0.004	0.006	0.0125	0.75	5	0.15	0.234375
5	0.004	0.006	0.0125	20	100	0.2	0.3125
6	0.002	0.003	0.00625	20	100	0.2	0.3125
7	0.002	0.003	0.00625	0.75	5	0.15	0.234375
8	0.002	0.003	0.00625	20	100	0.2	0.3125
9	0.002	0.003	0.00625	20	100	0.2	0.3125
10	0.002	0.003	0.00625	20	100	0.2	0.3125
11	0.002	0.003	0.00625	0.75	5	0.15	0.234375
12	0.002	0.003	0.00625	20	100	0.2	0.3125
13	0.002	0.003	0.00625	0.75	5	0.15	0.234375
14	0.002	0.003	0.00625	3 (CH) - 9 (HA)	90		
15	0.002	0.003	0.00625	20	100	0.2	0.3125
16	0.002	0.003	0.00625	3 (CH) - 9 (HA)	90		
17	0.002	0.003	0.00625	0.3	4	0.075	0.117188
18	0.002	0.003	0.00625	0.2	4	0.05	0.078125
19	0.002	0	0.00625	20	100	0.2	0.3125
20	0.004	0.006	0.0125	0.15	2.5	0.06	0.09375
21	0.002	0.003	0.00625	0.2	4	0.05	0.078125

22	0.002	0.003	0.00625	0.2	4	0.05	0.078125
23	0.002	0.003	0.00625	0.2	4	0.05	0.078125
24	0.002	0.003	0.00625	0.2	4	0.05	0.078125
25	0.002	0.003	0.00625	0.2	1	0.2	0.3125
26	0.002	0.003	0.00625	0.2	1	0.2	0.3125
27	0.002	0.003	0.00625	0.2	1	0.2	0.3125
28	0.002	0.003	0.00625	0.2	0.5	0.4	0.625
29	0.002	0.012	0.00625	0.2	1	0.2	0.3125
30	0.002	0.012	0.00625	10	25	0.4	0.625
31	0.002	0.012	0.00625	0.2	4	0.05	0.078125
32	0.002	0.012	0.00625	0.2	0.5	0.4	0.625
33	0.002	0.003	0.00625	10	25	0.4	0.625
34	0.002	0.012	0.00625	0.2	1	0.2	0.3125
35	0.002	0.003	0.00625	0.2	0.5	0.4	0.625
36	0.002	0.003	0.00625	0.2	1	0.2	0.3125
37	0.002	0.012	0.00625	10	25	0.4	0.625
38	0.002	0.012	0.00625	2	5	0.4	0.625
39	0.008	0.012	0.2	0.3	0.6	0.5	6.25
40	0.004	0.006	0.1	0.3	0.6	0.5	6.25
41	0.002	0.003	0.05	0.3	0.6	0.5	6.25
42	0.008	0.012	0.05	0.3	0.6	0.5	1.5625
43	0.008	0.012	0.1	0.3	0.6	0.5	3.125
44	0.002	0.003	0.0125	0.3	0.6	0.5	1.5625
45	0.002	0.003	0.0125	3	6	0.5	1.5625
46	0.008	0.012	0.1	3	6	0.5	3.125
47	0.008	0.012	0.1	3	6	0.5	3.125
48	0.008	0.012	0.1	0.3	0.6	0.5	3.125
49	0.002	0.003	0.025	3	6	0.5	3.125

Table S12. Summary of all the trials carried out with Gd-DTPA

Test #	HA (%w/v)	TPP (%w/v)	CS (%w/v)	Gd (mg)	Gd (%w/v)	Flow rate Middle channel (µL/min)	Flow rate Side channel (µL/min)	Collection (mL)	Flow Rate Ratio	CS:HA (g/g)	total ug collected	µg Gd collected
Gd1	0,008	0,012	0,1	8	0,1	3	6	15 (acetone)	0,5	3,125	37,8	21
Gd2	0,008	0,012	0,1	8	0,1	3	6	15 (acetone)	0,5	3,125	37,8	21
Gd3	0,002	0,003	0,05	4	0,05	3	6	8 (acetone)	0,5	6,25	126	180
Gd4	0,002	0,003	0,05	4	0,05	3	6	8 (acetone)	0,5	6,25	73,5	105
Gd5	0,008	0,012	0,1	8	0,1	3	6	8 (water)	0,5	3,125	43,2	24
Gd6	0,008	0,012	0,1	8	0,1	3	6	8 (water)	0,5	3,125	43,2	24
Gd7	0,008	0,012	0,1	8	0,1	3	6	10 (acetone)	0,5	3,125	54	30
Gd8	0,008	0,012	0,1	8	0,1	3	6	1 (water in eppendorf)	0,5	3,125	54	30
Gd9	0,008	0,012	0,1	8	0,1	3	6	1 (etoh in eppendorf)	0,5	3,125	27	15
Gd10	0,008	0,012	0,1	8	0,1	3	6	1 (water in eppendorf)	0,5	3,125	32,4	18
Gd11	0,008	0,012	0,1	8	0,1	3	6	1 (etoh in eppendorf)	0,5	3,125	32,4	18
Gd12	0,008	0,012	0,1	8	0,1	3	6	1 (water in eppendorf)	0,5	3,125	37,8	21
Gd13	0,008	0,012	0,1	8	0,1	3	6	8 (acetone)	0,5	3,125	37,8	21
Gd14	0,008	0,012	0,1	8	0,1	3	6	8 (acetone)	0,5	3,125	37,8	21

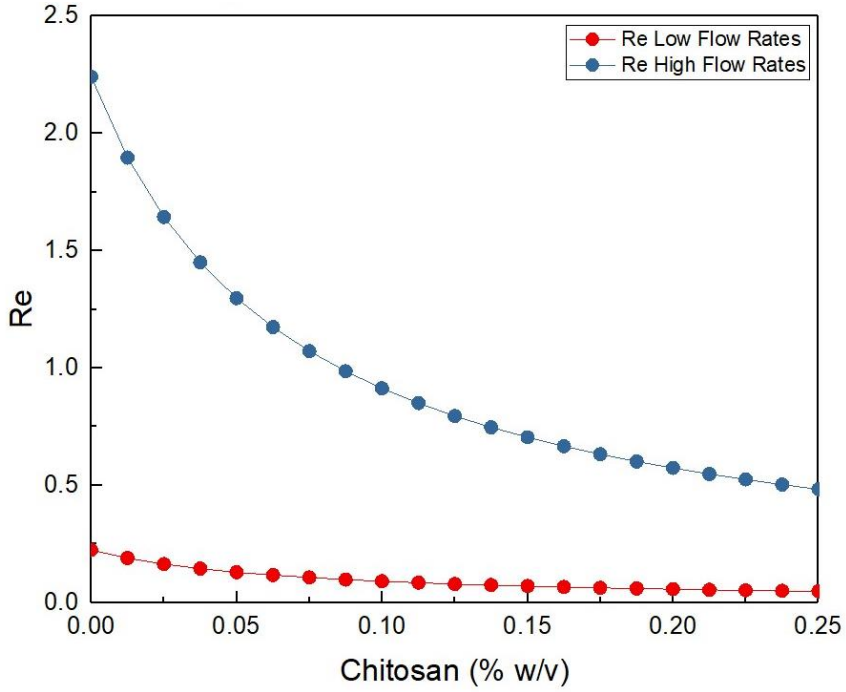

Figure S18. Graphic trend of Reynolds number within microfluidic channels, distinguished in high and low flow rate regime, based only on the chitosan concentration due to its high intrinsic viscosity

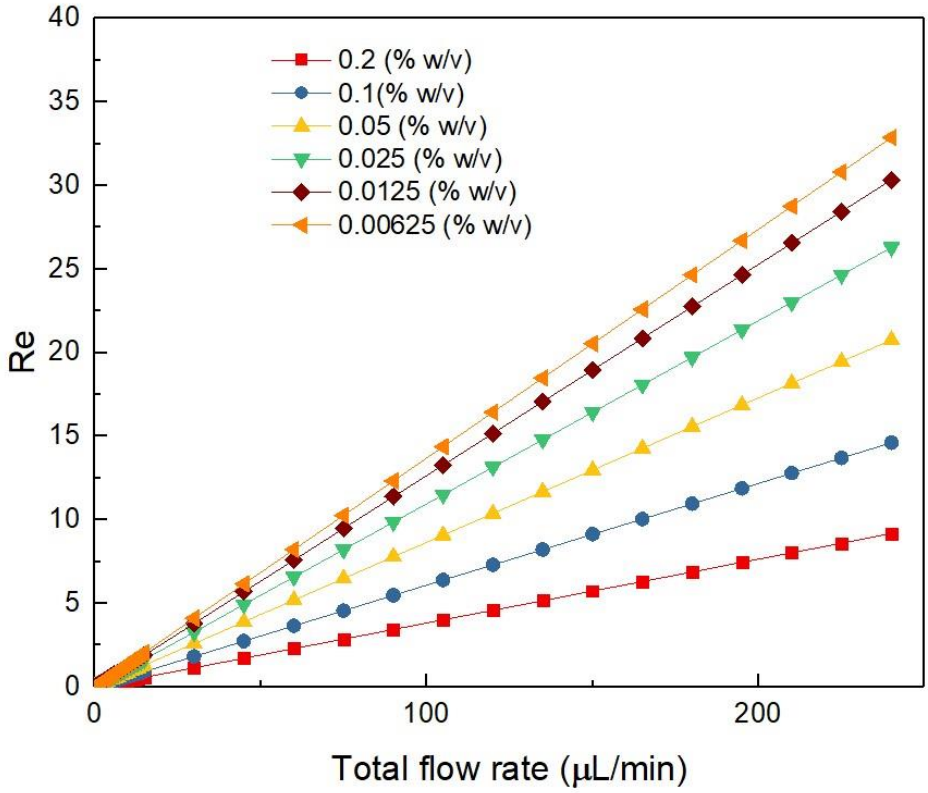

Figure S19. Reynolds number trend at different chitosan concentrations depending on the total flow rate

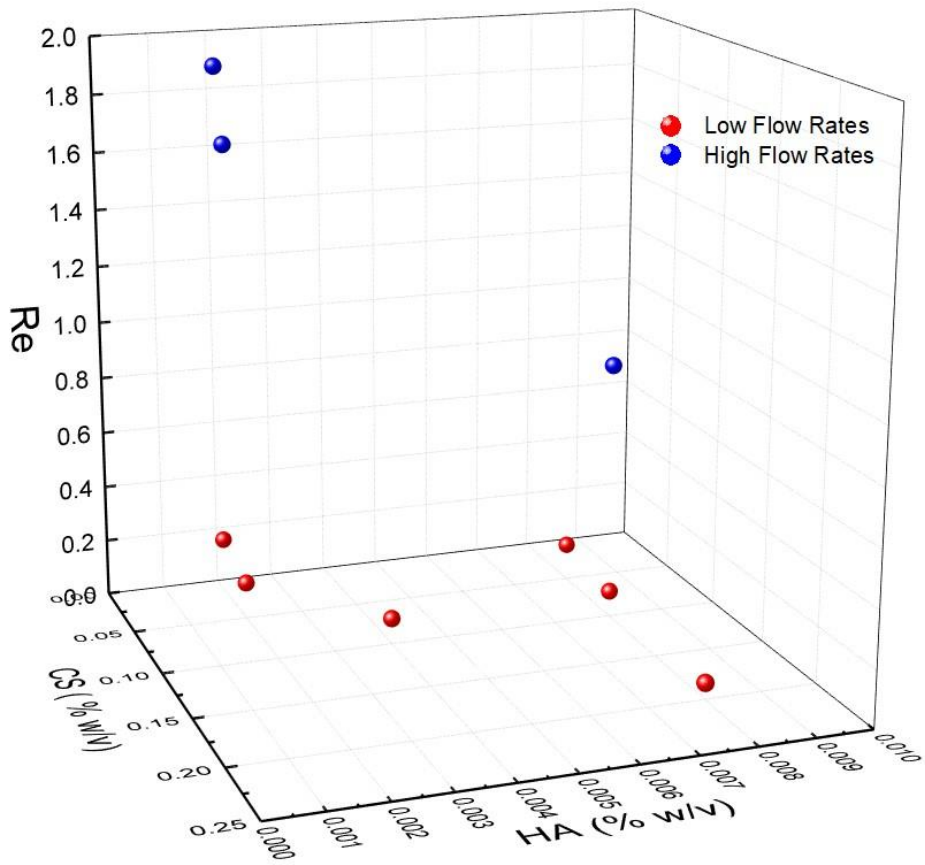

Figure S20. Reynolds number value depending on chitosan and hyaluronic acid concentration calculated at low (0.6 – 0.3 – 0.6 μL/min) and high (6 – 3 – 6 μL/min) flow rates

A.5. MICROFLUIDIC FLOW FOCUSING APPROACH TO PRODUCE CHITOSAN-LOADED LIPOSOME NANOSTRUCTURES BASED ON HYDRODENTICITY

Materials. As lipids, we used phosphatidylcholine get from soybean (lyophilized powder; storage temperature −20°C; average molecular weight of approximately 776 g/mol) and cholesterol derived from sheep wool (Empirical Formula C27H46O;

molecular weight 386.65 g/mol; storage temperature −20°C) that we bought both from Sigma Aldrich. As polymer, we used chitosan (low molecular weight: 50,000-190,000 Da; soluble in dilute aqueous acid) that we bought from Sigma Aldrich too. As solvents, we used acetic acid (absolute), ethanol (puriss. p.a., absolute, ≥99.8%GC; MW: 46.07 g/mol) and filtered MilliQ water for all the experiments and purification steps (dialysis).

Preparation of stock solution. Preparation of lipids stocks solutions (PC:Ch – 4:1):

- PC: 80mg in 10 ml (8 mg/ml);
- Ch: 10 mg in 10 ml (1 mg/ml).

At each trial ratio of cholesterol to phosphatidylcholine was 1:4, respectively.

Solubility tests. At first we prepared solution of lipids and ethanol, and then step by step we was adding 1% acetic acid in water (2.92ml water + 0.08 ml acetic acid), solution was stirring all time (300x) at temp. 25 ^{o}C. Starting concentration of lipids in ethanol was 2.25 mg/ml after addition 3 ml of 1% acetic acid precipitation occur (1.28 mg/ml lipids concentration).

Solubility of lipids in ethanol and acetic acid was checked. Starting lipids concentration was 1,6 mg/ml in ethanol. Then step by step acetic acid was added until 7.41% of acetic acid when precipitation occur. Precipitation disappear after decreasing acid percentage to 6%. In this way we checked solubility of lipids in presence of acetic acid (final lipids concentration 1.2 mg/ml). With starting concentration of lipids 0.1125 mg/ml, 10% of acetic acid was obtained without precipitation. in the same solution solubility of chitosan was checked in concentration 0.25 mg/ml, 24h stirring, solution not transparent. Water was added (33.3%) to the solution step by step, after next 24h solution become transparent (lipids 0.00375 mg/ml; acetic acid 6.66%; ethanol 58.5 %; chitosan 0.166%; water 33.33%).

Next one test was solubility of chitosan in absolute acetic acid. Starting point was 5 mg/ml of chitosan in acetic acid; final concentration was 1 mg/ml, but solution was

not transparent. For this reason water was added, after 24h solution was transparent (final concentrations: acetic acid 77%; chitosan 0.77 mg/ml; water 23%).

The last one solubility test checked mixing of lipids solution (lipids: 0.072 mg/ml; ethanol 64.3%; water 35.7%) with chitosan solution (acetic acid 77 %; water 23%; 0.77 mg/ml). Chitosan solution was adding step by step every 15 min to the lipids solution until following concentrations: lipids 0.05305mg/ml; chitosan 0.203 mg/ml; ethanol 45%; water 35%; acetic acid 20%.

Experiments on microfluidic platform. Microfluidic devices enable the manipulation of microquantities of liquid solutions, where mixing and demixing processes can be controlled to improve the efficiency of chemical reactions. In particular, the mixing that occurs within these devices happens on the order of a few milliseconds and provides the needed control over efficient and homogeneous mass transfer to achieve monodisperse nanostructure formulations. This has been widely used for applications in pharmacy, biotechnology, and chemical industries for years. The control of morphology, surface texture, size and polydispersity as well as of the system complexity through the variation of process parameters make the microfluidics one of the most promising approach in the reproducible and reliable design of micro- and nano-structures. In addition, the recent advancements in the fabrication of microfluidic devices for large-scaled production and direct clinical applications will rapidly drive the microfluidics technology to the industrial and medical arena.

Each trial on microfluidic platform was performed. Microfluidic platform is composed by various components that work simultaneously: computer, microscope, NeMESYS device. The last one is a system of three syringes (SETonic, 2.5 mL PTFE PEEK tubing connector) that pushes fluids within tubes. Each single syringe is controlled by a low-pressure syringe pump (Low Pressure Syringe Pump neMESYS 290N by CETONI). NeMESYS device can be controlled by PC software, thanks to that flow rate and volume can be monitored and changed. Syringe is connected and holding by the neMESYS through a ferrule and on the other side, is joined with a 2-way valve. Thereafter, there is a second segment of PTFE tubing that lead fluid to chip. Fluid from the chip can be collected thanks to the tubing on other site of the

chip. All reactions and processes are conducted in the proposed chip design is 22.5mm long x 15mm wide x 4mm thick and fabricated in Quartz, designed to obtain a meeting point to promote flow focusing. Chip consists of 5 parallel inputs and one output. In ours experiments Chip A (the Dolomite center ltd.) was used. All channels have the same cross-section of 160 x 150 μm, approximately circular as shown below.

Further details concerning the experiment design can be found in the Supporting Information.

Characterizations of samples. Characterization was performed on transmission electron microscope by FEI® in DRY and CRYO modes and Field Emission Scanning Electron Microscope (FE-SEM) by Zeiss. Samples for TEM characterization was stained in some cases with phosphotungstic acid (phosphotungstic acid 2%) on formvar carbon film 300 mesh. Regular samples on TEM was collected on Carbon Films on 300 Mesh Grids Copper. SIze of nanoparticles and Z-potential was analyzed by dynamic light scattering (DLS). Relaxation times are measured on a Bruker Minispec (mq 60) benchtop relaxometer operating at 60 MHz for protons (magnetic field strength: 1.41 T). The acquisitions are performed at 37°C and, before each measurement, the sample is placed into the NMR probe for 15 min for thermal equilibration.

Supporting data, figures and tables.

Table S13. Summary of all the trials carried out

Trial	Lipids total (mg/ml)	Chitosan (mg/ml)	Acetic acid (%)	Etoh-lipids (%)	Water-lipids (%)	Gd-DTPA (mg/ml)	Middle/Side	Flow rate middle (uL/min)	Flow rate side (uL/min)
1	1,68	0	0	63,6	36,4	0	water/lipids	21	41
2	1,68	0	0	63,6	36,4	0	water/lipids	7	41
3	1,63	0	0	100	0	0	lipids/water	7	41
4	1,63	0	0	100	0	0	lipids/water	21	41
5	0,072	0,375	1	65	35	0	polymer/lipids	21	41
6	0,072	0	1	65	35	0	ater+acid/lipic	21	41
7	0,05	0	0	65	35	0	lipids/water	21	41
8	0,05	0	20	50	30	0	pids+acid/wate	21	41
9	0,05	0,2	20	45	35	0	pids+acid/wate	21	41
10	0,072	0,1	1	65	35	0	polymer/lipids	21	41
11	0,072	0,1	20	45	35	0	er+lipids+acid/	21	41
12	0,072	0	0	65	35	0	water/lipids	21	41
13	0,072	0	10	65	35	0	ater+acid/lipic	21	41
14	0,072	0,1	10	65	35	0	polymer/lipids	21	41
15	0,072	0	0	80	20	0	water/lipids	21	41
16	0,072	0	0	80	20	0	water/lipids	7	41
17	0,072	0	10	80	20	0	ater+acid/lipic	21	41
18	0,072	0	10	80	20	0	ater+acid/lipic	7	41
19	0,072	0,1	1	65	35	0	polymer/lipids	3	41
20	0,072	0,1	1	65	35	0	polymer/lipids	7	41
21	0,072	0,1	1	65	35	0	polymer/lipids	14	41
22	0,072	0,1	1	65	35	0	polymer/lipids	28	41
23	0,072	0,1	1	65	35	0	polymer/lipids	1	41
24	0,072	0,1	1	65	35	0	polymer/lipids	3	41
25	0,072	0,1	1	65	35	0	polymer/lipids	1	41
26	0,072	0,1	1	65	35	0	polymer/lipids	3	41
27	0	0,1	1	65	35	0	ymer/water+e	3	41
28	0,072	0,1	1	65	35	0	polymer/lipids	1	41
29	0,072	0,1	1	65	35	0	polymer/lipids	3	41
30	0,072	0,1	1	65	35	0	polymer/lipids	1	41
31	0,072	0,1	1	65	35	0	polymer/lipids	3	41
32	0,072	0,1	1	65	35	0	polymer/lipids	3	41
33	0,072	0,1	1	65	35	4	polymer/lipids	3	41
34	0,072	0,1	1	65	35	4	polymer/lipids	3	41
35	0,072	0,1	1	65	35	4	polymer/lipids	1	41
36	0,072	0,1	1	65	35	4	polymer/lipids	3	41

A.6. REFERENCES OF THE APPENDIX

1. M. Russo, P. Bevilacqua, P. A. Netti and E. Torino, *Sci. Rep.*, 2016, **6**.
2. D. R. Messroghli, A. Rudolph, H. Abdel-Aty, R. Wassmuth, T. Kuhne, R. Dietz and J. Schulz-Menger, *BMC medical imaging*, 2010, **10**, 16-16.
3. L. A. Wells, S. Furukawa and H. Sheardown, *Biomacromolecules*, 2011, **12**, 923-932.
4. J. B. Leach, K. A. Bivens, C. W. Patrick and C. E. Schmidt, *Biotechnol. Bioeng.*, 2003, **82**, 578-589.
5. M. N. Collins and C. Birkinshaw, *Journal of Applied Polymer Science*, 2008, **109**, 923-931.
6. A. G. P. Kottapalli, M. Bora, M. Asadnia, J. Miao, S. S. Venkatraman and M. Triantafyllou, *Sci. Rep.*, 2016, **6**.